REPORT DOCUMENTATION PAGE

AFRL-SR-BL-TR-99-

0345

1. AGENCY USE ONLY *(Leave blank)*	2. REPORT DATE	3. REPORT TYPE AND DATES COVERED
	28 mAY 98 99	Final Technical Report 15 Sep 95 to 14 Jun 98

4. TITLE AND SUBTITLE
The Application of High Resolution Dynamical-Numerical Models as a Tool to Infer Climate Statistics: January Simulations

5. FUNDING NUMBERS
F49620-95-1-0523

6. AUTHOR(S)
Dr. Charles E. Graves

7. PERFORMING ORGANIZATION NAME(S) AND ADDRESS(ES)
Earth and Atomospheric Sciences
Saint Louis University
3507 Laclede Ave
St. Louis, MO 63103

8. PERFORMING ORGANIZATION REPORT NUMBER

9. SPONSORING/MONITORING AGENCY NAME(S) AND ADDRESS(ES)
AFOSR/NM
801 N. Randolph Street, Rm 732
Arlington, VA 22203-1977

10. SPONSORING/MONITORING AGENCY REPORT NUMBER
F49620-95-1-0523

11. SUPPLEMENTARY NOTES

12a. DISTRIBUTION AVAILABILITY STATEMENT
Approved for Public Release; Distribution Unlimited.

12b. DISTRIBUTION CODE

13. ABSTRACT *(Maximum 200 words)*

Overall, the model was able to reproduce the long term means and variability. A slight bias in pressure has lead to a re-evaluation of the initialization fields to ensure proper mass balances (which should remove the bias). Also the semi diurnal tide in pressure was missing but further research found that this effect could be included by a post-processing procedure. The 40km temperature and dew point fields generally showed diurnal trends closer to observed. This is likely due to the "assimilation" of observed temperatures into the 40km simulations but not the 10 km simulations. As expected, variability is generally more accurately reproduced in the 10 km simulations. However, the fields dominated by large scale variability (i.e. pressure arid temperature) showed on minimal improvements. The most notable improvements in capturing the observed variability were associated with the wind field. Often the 40 km simulations only capture a small portion of the total variability of the wind field (typically 30%), whereas the 10 km simulations captured nearly half of the observed variability. Within the model resolution the shape of the frequency distributions was generally well represented by the model. However some discrepancies in temperature and dew point temperature has lead to further investigations of the model's moist thermodynamic processes.

14. SUBJECT TERMS

15. NUMBER OF PAGES
95

16. PRICE CODE

17. SECURITY CLASSIFICATION OF REPORT	18. SECURITY CLASSIFICATION OF THIS PAGE	19. SECURITY CLASSIFICATION OF ABSTRACT	20. LIMITATION OF ABSTRACT
Unclassified	Unclassified	Unclassified	UL

Technical Report
Saint Louis University
Department of Earth and Atmospheric Sciences

The Application of High Resolution Dynamical-Numerical Models as a Tool to Infer Climate Statistics: January Simulations

Charles E. Graves
Earth and Atmospheric Sciences
Saint Louis University

John Zack
MESO Inc.
Troy, NY

May 28, 1998

This research was sponsored by Air Force Office of Scientific Research
Grant: F49620-95-1-0523

Executive Summary

The AFOSR project *The Application of High Resolution Dynamical-Numerical Models as a Tool to Infer Climate Statistics* is designed to determine the feasibility of producing mesoscale climates statistics from a mesoscale model. Mesoscale models are typically used for short-term weather forecasting and have not been tested on long-term integrations. This pilot study was designed to incorporate only a limited amount of observational data to also examine the its feasibility in data sparse or data denied areas.

The project considers the Upstate New York area as a test-bed and two months, January and July, were chosen. For each of these months, 10 years of statistics were generated from mesoscale model simulations. The data for the simulations were from the years 1985-1994. This report deals specifically with the simulations for January. The July simulations will be represented in another report.

The January results show discernible skill at reproducing climate statistics, both for the average of meteorological fields and their variability. Besides establishing this approach for obtain climate statistics, refinements to the numerical simulation strategy and subsequent analysis have been made.

Overall, the model was able to reproduce the long term means and variability. A slight bias in pressure has lead to a re-evaluation of the initialization fields to ensure proper mass balances (which should remove the bias). Also the semi diurnal tide in pressure was missing but further research found that this effect could be included by a post-processing procedure. The 40 km temperature and dew point fields generally showed diurnal trends closer to observed. This is likely due to the "assimilation" of observed temperatures into the 40 km simulations but not the 10 km simulations.

As expected, variability is generally more accurately reproduced in the 10 km simulations. However, the fields dominated by large scale variability (i.e. pressure and temperature) showed only minimal improvements. The most notable improvements in capturing the observed variability were associated with the wind field. Often the 40 km simulations only capture a small portion of the total variability of the wind field (typically 30%), whereas the 10 km simulations captured nearly half of the observed variability. Within the model resolution the shape of the frequency distributions was generally well

represented by the model. However some discrepancies in temperature and dew point temperature has lead to further investigations of the model's moist thermodynamic processes.

Also revealed in this research is the effect of simulation strategies on the results. The direct incorporation of observational data during the simulation (i.e. data assimilation) has both positive and negative effects on the simulation statistics. With assimilation the observed means are generally closer but at "assimilation" times the statistics contain "kinks" rather than a smooth progression (from the sudden shock of adjustment to observed values). Consequently a new scheme is being considered for the July runs which should minimize the shock to the simulation when observational data are assimilated.

Contents

1. Background

This report documents the results for the January simulations for the AFOSR research project *The Application of High Resolution Dynamical-Numerical Models as a Tool to Infer Climate Statistics.* In this project, a mesoscale model was run in a nested manner to generate statistics that would capture the mesoscale climate variability. This particular report documents the results from the 10 years of simulations (1985-1994) of Upstate New York for January.

The model simulations and procedure for assessing the model statistics were developed as part of the research project. As with any project, the procedures continually evolved. The simulation strategy and analysis procedure for the 10 year January simulations are described below. The recommendations concerning the simulation and assessment strategies are discussed in later chapters.

1.1 Model Simulation Strategies

The model was run at two resolutions, one at 40 km and one at 10 km, for the Upstate New York area. Each resolution has the same grid point domain; 60 by 60 points in the horizontal directions and 20 vertical levels. The 40 km domain (the large box shown in Fig. 1.1) covers much of the eastern United States. This model domain was designed to provide a bridge between the high resolution 10 km simulations and the coarse resolution of the initialization data (i.e. global optimal interpolation data with $2.5° \times 2.5°$ resolution). The 40 km model included diagnostic moisture physics (rather than prognostic) to speed up the integrations. Every 24 hours (at 00 UTC) the 40 km model was re-initialized incorporating upper-air data. No surface data was incorporated. The hourly output from this model provided the lateral boundary conditions for the smaller 10 km model simulations.

The 10 km domain (the small box shown in Fig. 1.1) was considered to be the "best" data, designed to provide the resolution and accuracy necessary for

Figure 1.1: The spatial domain of the 40 km and 10 km simulations. The crosses indicate locations of possible surface observation sites for assessing the climate statistics.

this project. The model configuration in this domain contained full moisture physics (excluding the formation of hail) but did not directly incorporate any observational data. The only data incorporated into this 10 km model was from the lateral boundary conditions generated by the 40 km model. A summary of the simulation strategy for both the 10 and 40 km domains is shown in Fig. 1.2. Detailed information on both model configurations is presented in Appendix II and a summary of the simulation strategies for both the 10 and 40 km domains is shown in Fig. 1.2.

Each simulation began on 00 UTC January 1 and ran through 23 UTC January 31 for each year (1985-1994). The hourly output from both the 40 km and 10 km simulations were archived. From these hourly grids, simulated station observations were obtained by interpolating from the grid points to the station locations. The eight station locations analyzed extensively in this study are shown in Fig. 1.3. These stations are the main source of model assessment.

Only a minimal amount of observational data was assimilated into the model to provide a stringent test of the model's abilities. As documented

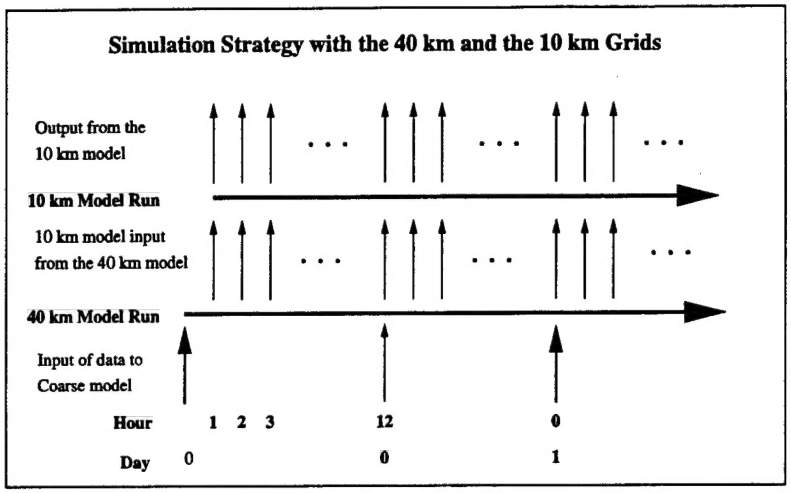

Figure 1.2: The simulation strategy for the 40 km and 10 km domains. The arrows indicate the timing of lateral (and sounding data) supplied to the simulation. The thick arrows indicate the timing (i.e. daily) of the assimilation of sounding data

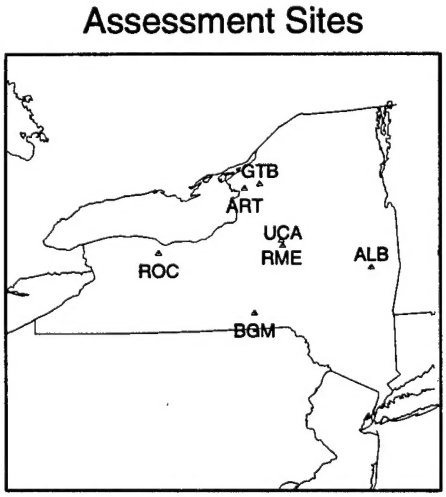

Figure 1.3: Locations in the Upstate New York area which are the focus of the assessment of climate statistics.

in later sections, the assimilation of data has advantages and disadvantages. The consequences of the current assimilation package is discussed in the conclusions.

1.2 Assessment Procedures

The assessment of the model results were based on the statistics generated from the simulations at the locations of the surface stations. The assessment of individual events or spatial characterizations were not considered. The model statistics were examined through a comparison with observational data in two specific ways. First, model and observed averages were compared, and then the variabilities were compared.

Through a comparison of averages, large biases can be identified as well as general trends. The comparison of variability can identify conditional problems, for example, errors that only occur in very cold temperatures. Using these two procedures, the model climate statistics can be assessed and guidelines established for proper usage of the data.

The comparison of the model and observational variability is complicated by the model's inability to capture all of the variability of the observations. This inability stems from the finite model resolution and does not necessarily indicate errors, but simply unresolvable variability. Thus to properly assess the model, the observations need to be adjusted to reflect the resolution restrictions of the model. The analysis of variability in this framework provides two pieces of information:

1. The accuracy of the model's statistics at the model resolution, and

2. The amount of variability not captured by the model.

Both of these are necessary to properly evaluate the model statistics.

The complete procedure for assessing the stations' variability is fully described in Appendix I; only an overview is presented in this section. The model output can be envisioned as filtered data (due to the model finite resolution). This filtering changes the shape of the distribution. From the central limit theorem, with "enough" averaging the shape of the distribution will become Gaussian. By using the techniques from geostatistics (Journel

and Huijbergts, 1978), we can describe the distribution resulting from any amount of filtering of the data. Consequently, the shape of the observed distribution, which is consistent with the resolution of the model, can be determined. In other words, we can transform the observed distributions into distributions which represent the "true" distributions when smoothed to the model resolution. The only parameter required for this technique is an estimate of the true model-scale variance.

With two distributions, one representing the "true" model scale distribution obtained from the transformed observations and the other from the model generated distributions, a "goodness-of-fit" measure is applied to numerically quantify the differences between the two distributions. When the two distributions are close the model is faithfully representing the variability at the scales resolvable by the model. The amount of adjusting to match the observed and model generated variance is a measure of the variability missing from the model simulations.

Experience has shown that no one "goodness-of-fit" measure completely describes the differences between the observed and model distributions. Consequently, we chose three measures which together provide a reasonable description of the quality of the model distributions as compared to the observed distributions. In particular, these "goodness-of-fit" measures are:

1. The χ^2 test, which uses the statistic:

$$\chi^2 = \sum_{i=1}^{N} \frac{(Model_i - Obs_i)^2}{Obs_i}$$

   where $Model_i$ is the frequency of occurrence of model value i and Obs_i is the frequency of occurrence of observed value i. For example, when comparing temperature distributions, i would represent a particular temperature. The summation is therefore over all observed temperatures. The χ^2 value is nearly a mean square difference between the observation and model distributions.

2. The Percentile Root Mean Square Difference (PRMSD), which computes the deviation of the percentiles between the model and observed distributions. In particular, it determines:

$$PRMSD = \left\langle (C_{model}(p) - C_{Obs}(p))^2 \right\rangle$$

Variable	Good Fit	Poor Fit
Pressure (mb)	< 0.11	> 0.20
Temp (F)	< 0.40	> 1.00
Dew Point (F)	< 0.30	> 0.60
Wind Speed (knt)	< 0.10	> 0.17

Table 1.1: The suggested values for the PRMSD measure to determine the quality of the fit

where $C_{model}(p)$ is the value of the pth percentile of the model data and $C_{Obs}(p)$ is the value of the pth percentile of the observational data. The average $\langle\ \rangle$ is evaluated using the percentiles from 2% to 98% in 2% increments. The value of $PRMSD$ is a measure of the expected difference in the percentile values determined from the model data. For example, when comparing temperature distributions, a value of $PRMSD = 2.5$ would indicate that an expected error in any percentile computed from model statistics would be ± 2.5°F (e.g. the 90th percentile would be 38 ± 2.5°F).

3. The Tail Percentile Root Mean Square Difference (TPRMSD), which computes the same quantity as the PRMSD but only for the tails of the distribution. Currently the tail represents the first and last 15% of the distribution. TPRMSD provides a measure of the expected error when only considering the extremes of the distributions.

A smaller value for any of these measures indicates a better fit between the model and the transformed observational distributions. From experience, a value of χ^2 less than 5.0 indicates a good fit, while a value greater than 10.0 indicates a poor fit. In a similar manner, experience has suggested values for PRMSD, but since this measure has units, each variable has its own thresholds. These thresholds are given in Table 1.1.

Finally, all of the measures of variability are determined with the overall bias between the two data sets removed. Therefore the total error must include both the bias and variability error.

2. Analysis

The results for the 8 stations are examined in detail in this chapter. The associated information for these stations is listed in Table 2.1. The figures and tables associated with each station are provided in station appendices. The assessment for each variable is considered individually while the overall assessment is provided in the conclusions.

2.1 Assessment of Long Term Means

The long term means of pressure, temperature, dew point temperature, and wind speed for each of the 8 stations are shown in Figure 2.1. The means for the observations are in green, the 40 km model are in blue and the 10 km model are in red. The following discussions for each of the variables refers to this figure. The actual numerical values for the means and standard deviations are listed in tables in the station appendices.

2.1.1 Pressure

For pressure, the most noticeable difference is nearly a -4 mb bias in the model pressures (both for 10 km and 40 km models). If each mean for the model means are corrected by 3.9 mb, nearly all averages lie within 1 mb of the observed means. The only exceptions are for ALB at 10 km (1.05 mb) and BGM at 40 km (-1.39 mb).

This consistent bias is most likely due to the lateral boundary conditions. The lateral boundary conditions are derived from data which are not mass-balanced. Consequently, the mass imbalance causes a "leak" in the model simulations and a drop in pressure. Currently we are adapting a new algorithm to ensure the lateral boundary conditions are mass-balanced which should eliminate this bias.

Figure 2.1: Long term means of January simulations

Station	Station Lat.	Station Long.	Station Elev.	10 km Elev.	40 km Elev.
ALB - Albany	42.57	-73.80	89.0	114.9	267.6
ART - Watertown	44.00	-76.02	101.0	153.3	194.4
BGM - Binghamton	42.22	-75.98	497.0	378.6	418.7
GTB - Fort Drum	44.05	-75.73	207.0	236.6	248.3
RME - Rome	43.23	-75.40	154.0	208.9	356.9
ROC - Rochester	43.12	-77.67	169.0	189.1	239.3
UCA - Utica	43.15	-75.38	227.0	220.5	366.7
YTR - Trenton	44.12	-77.53	86.0	96.2	226.5

Table 2.1: The stations analyzed in for the January simulations. All stations are in New York except Trenton, Canada. The 10 km and 40 km elevations are the elevations of the stations in those models. (The result of smoothing the terrain.)

2.1.2 Temperature

The temperature comparison reveals several interesting points. First, the 40 km means are closer to the observed than the 10 km means. This is due to the simulation strategy. The 40 km simulations included upperair sounding data which helps to correct any "climate drift" in the model. The 10 km simulations did not contain any data assimilation and consequently were allowed to "drift". The better results of the 40 km simulations is not a consequence of resolution but of simulation strategy.

The second point is the warm bias of the 10 km simulations. Part of this warm bias is the result of the Blackadar Planetary Boundary Layer (PBL) scheme in the model which appears to have a warm bias.

The third point is the uncharacteristically large differences at Rochester (ROC). The large differences for both the 40 km and 10 km simulations are likely related to land/water classification. As shown in the Rochester appendix, the grid points to the north of the station are classified as water even though they occur over land. As a consequence, the water's influence is stronger at Rochester than it should be. This feature will appear again in other variables. The acquisition of higher resolution land/water classification data should minimize this problem.

Finally the height differences between the actual station and the model contributes to the observed differences. The model smooths out the terrain,

raising valleys and lowering hilltops. With compressional warming (expansional cooling) this introduces a bias at each location. (See Table 2.1 for elevation information.) To minimize this effect, station observations could be adjusted (e.g. adiabatically) to the model elevation. The mean temperature at Albany in the 40 km model for example would be 3.15° warmer (27.25°F) which would result in a temperature that is nearly the same as the adjusted 10 km temperatures (26.81°F).

2.1.3 Dew Point Temperature

Similar to the temperatures, the dew point temperatures have a warm bias at all locations and for both model simulations. Again, the model averages at ROC are out of character with the other locations. Consistent with grid point analysis around Rochester (see Appendix Rochester), it appears that Lake Ontario is having too much of an effect on the statistics at Rochester.

The model does not directly predict dew point temperatures, so the simulation accuracy depends on the parameters used to determine the dew point, namely pressure, density, and absolute humidity. When examining absolute humidity or mixing ratio, the relationship shown in Fig 2.1 does not change noticeably.

2.1.4 Wind Speed

Unlike the averages of the other three variables, the wind speed does not show a systematic bias. The stations: ALB, BGM, UCA, and ART have observed wind speeds greater than either the 40 km or 10 km simulations. The stations: GTB, RME, and ROC have observed wind speeds which are less than either 40 km or 10 km simulations. Additionally, YTR has the 40 km wind speeds larger than observed but the 10 km are smaller than observed. This location-dependent bias is probably the result of many factors including both horizontal and vertical model resolutions. At least four particular factors which effect the wind speed can be identified:

1. A coarse model resolution will smooth out surface roughness leading to model wind speeds greater than observed.

2. Shallow inversions which lead to light winds at the surface may not be captured by the model and will lead to model wind speeds greater than observed.

3. Smoothed terrain will reduce the local circulations (e.g. mountain and valley breezes) and will lead to model wind speeds lower than observed.

4. The change in surface conditions like snow cover will change the surface roughness, which if not adjusted in the model will contribute to changes in observed wind speeds which are not found in the model.

An increase in model resolution should minimize most of these effects. However, it is not clear from Fig. 2.1 that the 10 km averages are necessarily better than the 40 km averages. However, the analysis of the variability does suggest the 10 km simulations are providing more information than the 40 km simulations.

2.2 Analysis of Hourly Means

The dominant variability within a single month for most meteorological variables is the diurnal cycle. Consequently, the ability to capture the diurnal cycle is an essential part of this assessment. The figures showing the observed and modeled hourly means are found in the appendices for each station.

In creating the hourly averages, the 00 UTC values represent the 24 hour forecast product only. The initialization and assimilated fields generated at 00 UTC were not included. Consequently 00 UTC represents 24 hours after initialization (and after assimilation), while 01 UTC represent one hour after initialization.

2.2.1 Pressure

Examing the hourly pressure data reveals three major differences between the model simulations and the observations. The first difference was previously identified in the long term means; the very systematic 4 mb bias in the model results. As this was discussed above, no further comments are made here.

The second difference is the semi-diurnal tide found in the observations but not in the model. The cycle is most apparent from 12 UTC to 23 UTC

and is about 0.5 mb in amplitude. The physical mechanism for this tide is associated with the diurnal heating of the stratosphere which is not part of this mesoscale model. Consequently, this feature is not captured by the model. However, from studies (e.g. Chapman and Lindzen 1970) this effect can be included as a post-processing effort with reasonable accuracy (i.e. errors < 0.05 mb).

The third noticeable difference is the "hump" found in the model averages (especially for the 40 km model) from 00 UTC to about 4 UTC. This difference arises from the initialization process at 00 UTC. At re-initialization, the pressure is "corrected" back to observations (or nearly so) and as the simulation proceeds the mass loss from the lateral boundaries shifts the pressure back down to a new equilibrium level about 3 hours later. The value shown at 00 UTC in the plots is the 24 hour forecast and not the initialization so the jump is most noticeable between 00 UTC and 01 UTC. This "assimilation" effect is also found in other variables and has lead to a new strategy for assimilating data which will be discussed in the conclusions.

2.2.2 Temperature

The differences between the model simulations and observations of hourly mean temperature are very small in most situations. The differences are less than 2°F with a warm model bias (as noted in the long term averages). The 40 km model simulations, with the daily assimilation of sounding data, are generally closer to the observed than the higher resolution 10 km data. This result illustrates the usefulness of data assimilation for correcting the drift in the model. In this case the upper air stations (about 2 within the 10 km domain) were enough to adjust the model drift.

Additional tests have suggested that the warm bias would also be in the 40 km model if observational data were not assimilated into the simulations. This warm bias appears to be the result of the Blackadar Planetary Boundary Layer (PBL) scheme. (From preliminary tests another common PBL scheme, Turbulent Kinetic Energy, TKE, appears to have a slight cold bias.)

The two stations with the largest discrepancies are ROC and YTR. Both stations are near the water and have land/water classifications that might be the source of error (See associated appendices).

2.2.3 Dew Point Temperature

There are several notable differences between the observed and simulated hourly dew point temperatures. The most obvious differences occur around 12 UTC which is near sunrise for the New York area. From 00 UTC to 12 UTC the observational dew points drop to a minimum value. This trend toward sunrise is not capture in either model. The model's inability to represent very shallow inversions may account for this error. However, at most stations the model tries to capture the afternoon maximum in dew point temperature.

Again similar to the pressure, the "jump" caused by data assimilation distorts the statistics from 01 UTC to about 03 UTC. Adding to this problem is the dry bias of the assimilated observations leading to some "spin up time" to achieve saturated or near saturated conditions.

The dew point simulations at ART, BGM, and ROC show a warm (wet) bias throughout the day. The bias at ROC is consistent with the water classification of adjacent grid points. However, it is currently unknown why ART and BGM show this same bias.

2.2.4 Wind Speed

The hourly differences in wind speed between model simulations and observations are more noticeable from 00 UTC to 12 UTC. The model generally captures the afternoon wind maximum, however the magnitude is not always correct.

The 10 km hourly means are an improvement over the 40 km hourly means for GTB, RME, and YTR. At these stations the 40 km hourly winds are too strong compared to observations. At ALB, ART, BGM, and UCA the 40 km winds are too light and the 10 km simulations move further away from the observations. The exception to this is at ROC, but as previously mentioned there appears to be a water/land mis-classification which provides too much "water influence" to the Rochester station. It is unclear why there is this dual nature in the modeled wind fields. However, as shown in the next section, a great deal of variability in the winds is not captured by the model simulations. This reduced variability in the models is consistent with the

model's inability to resolve small scales, including irregularities in terrain.

The model results do not show much of a "jump" around the re-initialization time like with pressure and dew point. Even "adjusting" to observed data does not help bring the simulations closer to observed even for a short time suggesting that the initialization data are highly smoothed. The initialization problem may become more prominent if the model resolution is decreased.

2.3 Long Term Variance Analysis

In addition to averages, the variability around that average is also an important assessment tool. The assessment of variability is done in two ways. In the following two sections the standard deviations of the observations and model simulations are compared. In a figure similar to that depicting the long term means, the long term standard deviations are shown in Fig. 2.2. The hourly standard deviations and an examination of the full distributions are examined in later sections.

Because of resolution and smoothing effects within the model, the model standard deviations are expected to be smaller than the observed. The size of the difference is a measure of the unresolvable variability within the model.

2.3.1 Pressure

As expected, the models' standard deviations of pressure are smaller than the observed. The differences between the 40 km model and observations are typically less than 1 mb. Surprisingly, the 10 km model standard deviations are less than the 40 km values. The reason for the drop in variability with an increase in resolution is unknown. One possible cause might be the jump in the statistics which occurs due to the re-initialization at 00 UTC. However, as shown in the next section, the hourly standard deviations for the 40 km simulations are systematically larger than the 10 km simulations throughout the entire day. Thus the adjustment period during and shortly after re-analysis is not solely contributing to the increased variance.

The overall differences are somewhat systematic and are typically around 10%. Realizing that the observations have errors (and possibly spurious values) which increase the variance, these differences are not considered mean-

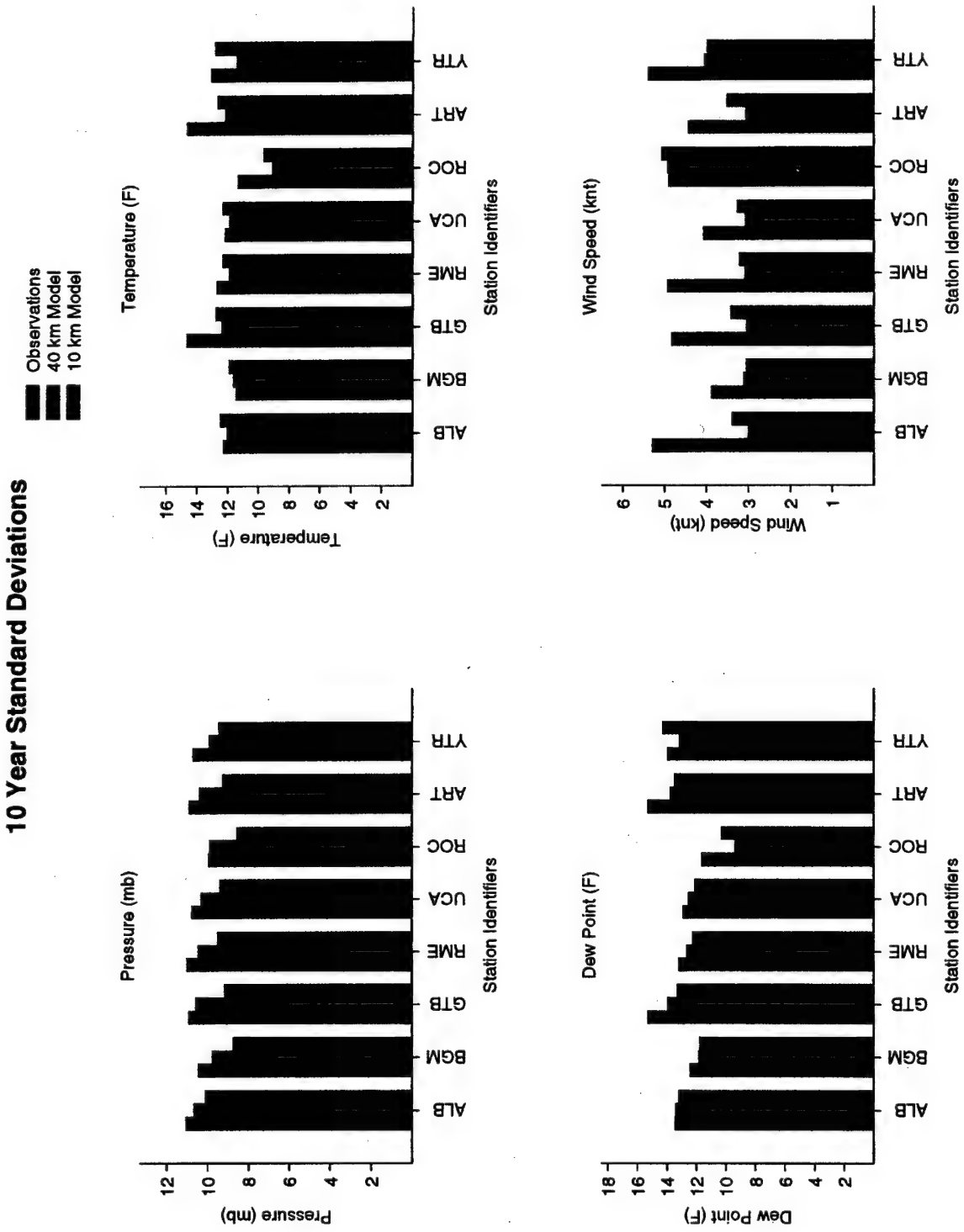

Figure 2.2: The standard deviations for the 8 Upstate New York stations.

ingful.

2.3.2 Temperature

While the pressure differences were systematic, the differences in the standard deviations of temperature are much more chaotic. Here, as expected, the values from the 10 km simulations are closer to the observed than the 40 km data. This is contrary to the long term means in which the 40 km (with data assimilation) were closer to the observed. The higher resolution had a direct positive impact on the temperature variability.

The standard deviation at three stations, ALB, BGM, and UCA actually had slightly higher standard deviations than observed, though the difference was quite small (less than 2%). Three stations: ART, GTB, and ROC, had uncharacteristicly large differences between modeled and observed standard deviations. This suggests that the models had trouble capturing the full extend of the observed variability at ART, GTB, and ROC. Again, coastal regions appear to present potential problems.

2.3.3 Dew Point Temperature

While the station-to-station trend is captured by the models, the 10 km dew point standard deviations are typically smaller than the 40 km standard deviations. Again, the differences are largest for the same three stations: ART, GTB, and ROC, as with temperature. Only at YTR for the 10 km model is the variability greater in the model than in the observations. The reduced variability with increased resolution might be related to unresolved near-surface features (e.g. shallow inversions).

2.3.4 Wind Speed

The observed standard deviations of wind speed are generally much larger than the model standard deviations (typically a factor of two larger). With local circulations caused by local terrain, the large differences are somewhat expected. With the model terrain smoother than observed, the variability is significantly reduced. The 10 km model simulations, having higher terrain resolution, tend to capture more variability than the 40 km simulations. The only exceptions are at YTR and BGM.

Once again the behavior at ROC is different from the rest of the stations. At ROC the model standard deviations are larger than observed. It is unclear why, but as previously mentioned the influence of the water is presumed to have a significant role.

2.4 Hourly Variance Analysis

In addition to the long term standard deviations, an assessment of the hourly variability is done. Again, the figures showing the hourly data are found in the appendices for each station. Since there are fewer points from which to estimate the standard deviation, less meaning should be given to small differences.

2.4.1 Pressure

Consistent with the results from the long term standard deviations, the hourly observations generally have larger variability than the 40 km model data which has larger variability than the 10 km data. The observations typically show a slight peak in variability around 15 UTC while the model and particularly the 10 km model show a nearly flat diurnal pattern. However, the actual differences (less than 2 mb) are quite small in most cases. Also again noticeable are the "jumps" just after 00 UTC, which are most likely associated with the observed data assimilations.

2.4.2 Temperature

The most apparent feature of the observed hourly standard deviations is the maximum around 12 UTC. While this feature is captured by the models, the models generally don't capture the full magnitude. The timing of this maximum suggests this variability maximum is partly the result of occasional very shallow and cold inversions occurring near sunrise. It is possible that the model does not capture this shallow feature and hence misses out on that variability.

The 10 km model appears to have a better handle on the overall magnitude of the temperature variability than the 40 km model. This is interesting

since the 40 km model contained the assimilated observational data and the 10 km model did not.

The model temperature hourly standard deviations at BGM show a second peak around 21 UTC in both simulations. While the 10 km model data match the observed quite well up to 15 UTC, a second peak is found after 15 UTC in the model data (also found in the 40 km data). It is unclear what is responsible for this second peak in the model simulations.

2.4.3 Dew Point Temperature

Like the temperatures, the hourly standard deviations in dew point temperature show a maximum in variability around 12 UTC. Again the models tend to capture this feature, however the magnitude is underestimated and the timing of the peak is often off by 1-2 hours.

Unlike the temperatures, the 10 km simulations do not always capture more variability than the 40 km simulations. The pattern of which model resolution captures the most variability follows the long term standard deviations discussed earlier.

2.4.4 Wind Speed

Unlike the other standard deviations, the wind speed standard deviations do not have strong diurnal cycles. The standard deviation is relatively flat throughout the day.

Present in the 10 km model simulations are some 'jumps" around 00 UTC. Since these jumps are not present in the 40 km model, it is not due to observation data assimilation. However the initialization at 10 km may result is some slight imbalances which can from time to time generate gravity waves. These waves may contribute to spikes in variability shortly after initialization as seen here.

The 10 km simulations generally capture more variability than the 40 km simulations, but even in the 10 km simulations the variability is noticeably smaller than what was observed.

2.5 Distribution Analysis

Examing only the first two moments of the distribution to assess the model results is in many situations incomplete. The observed distributions are often skewed with long tails. Consequently, the mean and variance provide little information on the quality of the tails of the simulated distributions.

Adding to this difficulty is the resolution problems between observations and models. To assess the model's full distribution requires that the observations be transformed to the same resolution as the model. This topic was briefly addressed earlier and the methodology for implementing this transformation is described in Appendix 3.

The following discussions are based on the variability analysis figures found in the station appendices. Since both the the biases and variances have already been discussed, those differences are removed in the figures. Thus the figures are comparing the differences in the shape of the distributions.

Provided with each figure is the observed and modeled long term mean and variance, as well as the bias (model minus observed). In addition the three measures of the quality of the fit discussed earlier are provided. The PRMSD (Percentile Root Mean Square Difference) the TPRMSD (Tail Percentile Root Mean Square Difference) and the χ^2 values are listed on the top left of each figure. The vertical red lines indicate the top and bottom 15% used for the TPRMSD calculations.

2.5.1 Pressure

The model simulations generally capture the observed distributions. This suggests the major problem in simulating pressures is the 4 mb bias discussed earlier. However several other minor differences are noticeable.

First, the model generally fails to capture the smooth fall off at the very large pressures (see for example UCA, BGM, RME). Instead the model distributions contain a "wave" in the tail just below 1040 mb. This would again be consistent with model having difficulty with shallow and cold air masses.

Second, the 10 km distributions are not always better than the 40 km distributions. Often the PRMSD is larger for the 10 km distributions. This suggests improvement in the pressure fields requires more than just an im-

provement in horizontal resolution. Particular suggestions are presented in the conclusions.

2.5.2 Temperature

The temperature distributions are not as good as the pressure distributions. Even though the 40 km mean temperatures were representative of the observational means, there are some differences in the distributions.

First, the models do not capture the slight positive skewness of the observations. A good example is the 40 km model at RME. The 40 km simulations have a slight tendency to generate broad distributions around the average, while the 10 km simulations have a tendency to generate two separate peaks in the distributions near 32°F and 10°F.

The waviness found in the 10 km simulations (see RME for example) is a cause of concern. It suggests "preferred" temperatures which may be the result of the surface energy balance scheme, the vertical resolution, and the moisture physics in the model. With the peak at 32°F, the moisture physics is the main suspect. At some stations there is a slight tendency in the observations for a temperature of 32°F, but not at the frequency that the model generates.

2.5.3 Dew Point Temperature

The distributions in dew point behave in much the same way as the temperatures. However the tendency of the model to generate dew points at 10°F and 32°F is much more pronounced. These peaks in conjunction with the peaks in the temperature distributions suggests problems in the moisture physics of the model.

In spite of those two dew point temperatures, the extremes of the dew point distributions are reproduced very well. In many cases there is significant overlap between the two curves.

2.5.4 Wind Speed

The assessment of wind speed presented some interesting problems. First of all, in the observations any wind speeds less than 3 knots are considered calm. However the model can easily generate wind speeds of less than 3

knots. Including these slow wind speeds in the model distributions resulted in poor agreement at low wind speeds and also introduces biases in the means. Consequently, wind speeds below 3 knots where ignored in the simulations. This lead to an unrepresentative "kink" in the model distributions (see BGM for example). In either case wind speeds below 3 knots are a problem. Further research is suggested to develop a proper assessment procedure for these light winds.

Overall the model distributions are generally too flat and broad. The observed distributions were more peaked. In addition the lack of explained variance indicates a need for better resolution especially to determine the distribution at high wind speeds.

2.6 Precipitation

Precipitation is a more difficult quantity to assess than those above. The infrequent non-zero precipitation values significantly reduces the number of events to examine. Also observational precipitation data are more scare than standard variables. Consequently we only examined daily precipitation amounts and also only analyzed days with precipitation.

Table 2.2 shows the statistics for the 6 stations for which observational precipitation values were found. The table shows both frequency of daily precipitation (fraction of days with precipitation) and the daily average precipitation (for those days with precipitation). Both models do a reasonable job estimating both the frequency and the average. Though not shown here, the diurnal pattern of precipitation frequency contained problems after data assimilation much like the other variables. With precipitation frequency, the "spin-up" after assimilation resulted in a lower frequency of precipitation for several hours.

Found in the station appendices is the variability analysis for daily precipitation. The top figure is the comparison with the 10 km data and the bottom figure is the comparison with the 40 km data. In January in the New York area, the systems generating precipitation are general large, synoptic scale processes (with the exception of lake-effect snows). Therefore the differences in the 40 km and 10 km model results were not expected to be

Station	Frequency (%)			Average (in)		
	Obs.	10 km	40 km	Obs.	10 km	40 km
ALB - Albany	0.204	0.241	0.140	1.762	1.562	1.040
ART - Watertown	0.193	0.132	0.114	0.924	0.722	0.632
BGM - Binghamton	0.132	0.139	0.101	0.965	1.081	0.845
GTB - Fort Drum	0.237	0.133	0.112	0.476	0.722	0.598
RME - Rome	0.181	0.135	0.117	0.613	0.676	0.632
ROC - Rochester	0.090	0.128	0.104	0.661	0.512	0.703

Table 2.2: The daily frequency of precipitation and the average daily precipitation (when precipitation occurs).

significantly different. A more rigorous test of precipitation will be in the July simulations.

The variability analysis shows that generally the observations have more variability than either the 40 km or the 10 km simulations. Although, at model-scale, the general shape of the observed distributions is captured in the simulation distributions. Since precipitation is the non-linear combination of all of the meteorological parameters this result suggests these simulations have great promise.

In the figures, the "negative" precipitation is simply the result of the curve fitting technique which tends to smooth out the sharp drop off to zero precipitation.

3. Conclusions

The simulations generated by the MASS model have much of the same statistical behavior as the surface observations. The model generally captures the spatial character of both the averages and the variances. The model also generally captures the diurnal trends, although the trends in variances are not quite as good as the averages.

The major problems with the simulations are:

1. A relatively large bias in pressure due to the mass imbalance of the lateral boundary conditions,

2. A distortion of the statistics from 00 to 03 UTC due to the shock on the system from data assimilation at 00 UTC,

3. A significant loss in variability in the wind fields,

4. A distortion of statistics in the vicinity of a coast line,

5. An underestimate of the afternoon maximum in the dew point temperature, and

6. Spurious peaks in the dew point temperature distributions near 10°F and 30°F and to a lesser extent in the temperature distributions.

Two changes in simulation strategy have been made to address the first two problems. First, the lateral boundary conditions are checked for mass imbalances. Secondly, the data assimilation has changed to a system known as IAU which incrementally adjusts the data rather than through one sudden shock to the system.

The next three problems appear to mainly be associated with resolution. The largest differences between the 40 km and 10 km simulations were normally found in the wind fields. Generally the 10 km model explained considerably more variability than the 40 km model. Also an increase in horizontal resolution will increase the model's ability to resolve coast lines

and coastal circulations. Likewise, an increase in the vertical resolution will increase the model's ability to resolve shallow temperature inversions which are the leading suspect in the dew point temperature problem.

The last problem is still under investigation. We suspect that these peaks in the distributions are related to the thermodynamics of water (e.g. change of phase). As of yet no general solution has been found.

Finally, as the project proceeded, it became clear that no one parameter could adequately measure the quality of the simulation statistics. In fact the quality of the simulated statistics appear to hinge on three separate factors:

1. the overall bias of the simulations,
2. the amount of variability captured by the simulation, and
3. the distribution of the simulations.

How each of these contribute to the errors of a given statistic depends on the particular statistic (e.g. mean, variance, etc.). However, a reasonable estimate can be made by summing estimates from each of these factors. For example, for the 10 km simulations of temperature for Watertown (ART) we find:

A bias of 1.43°F,

A difference in standard deviation of 1.98°F, and

A PRMSD (typical percentile difference) of 0.90°F.

Thus an average or percentile estimated from the model can be considered to have errors on the order of 4.31°F.

Generally the bias is the largest contributor to this error. The inclusion of observational data has been shown to reduce the bias, consequently this contribution can be minimized. Thus the last two factors represent a reasonable measure of the quality of the simulations. From the material previously presented, neither factor dominates, although the total of these two factors is typically of the same order. The summary of the typical ranges for these two factors, and hence an overall error estimate (excluding bias) is provided in Table 3.1

Parameter	Error Range
Pressure	$0.5 \rightarrow 1.0$ mb
Temperature	$1.5° \rightarrow 2.0°$ F
Dew Point	$1.5° \rightarrow 2.0°$ F
Wind Speed	$1.5 \rightarrow 2.5$ knts

Table 3.1: Typical errors estimated from a difference in standard deviations and from PRMSD for the various parameters. Excluding the bias this is a measure of the typical error associated with statistics calculated from the model simulations.

Appendix I: Distribution Assessment Technique

This study utilized a statistical method developed by Journel and Huijbergts (1978) which was first used in meteorology by Morrissey (1991). At the heart of this technique is the central limit theorem, which states that all distributions of averages approach a standard normal distribution with increasing averaging (Gibra 1973). While the central limit theorem defines the limiting distribution (i.e., Gaussian), it does not provide the path to that Gaussian distribution. The geostatistical techniques of Journel and Huijbergts (1978) provide a quantifiable method for establishing this evolutionary path by allowing estimates of the intermediate distributions.

The model results are filtered due to the finite difference scheme. Consequently model PDFs can be treated as averaged distributions which are expected to be more Gaussian-like than the observations. This procedure can be utilized to determine what the "true" distribution should be if the observations where filtered to the resolution of the model.

This method uses a transform function which expresses a random variable of a known distribution in terms of a standard normal variate, Z. This function which can model any distribution with finite variance is expressed as:

$$\phi(Z) = \sum_{i=0}^{\infty} \frac{\psi_i}{i!} H_i(Z) \tag{3.1}$$

where $H_i(Z)$ are Hermite polynomials (see Appendix B), and ψ_i are the coefficients of the Hermite expansion. Note here that $\phi(Z)$ is a function of a random variable and the principles of functions of random variables apply. Thus $\phi(Z)$ is actually a mapping from the cumulative probability of Gaussian variables to the cumulative probability of the known distribution. An example of determining $\phi(Z)$ is given by Journel and Huijbergts (1978).

From the above expansion series it can be further shown that:

$$\psi_0 = \mu \qquad \sum_{i=1}^{\infty} \frac{\psi_i^2}{i!} = \sigma^2 \tag{3.2}$$

where μ and σ^2 are the mean and variance of the original distribution. Typically, the series is truncated at some level k which adequately explains the distribution. In this study the expansion was carried out to 30 terms.

Once $\phi(Z)$ is determined, the coefficients of the expansion are found in a manner typical with orthogonal functions. Once coefficients are determined from the transform function for the observational data, the series can be transformed to produce a distribution having the mean and variance of the model data (i.e., filtered data). This transformation process assumes a *permanence of distribution*, which states that the point and transformed distributions can be described by the same functions (i.e., a log-normal distribution remains log-normal). The transformed function for the model-scale distribution is written as a modified version of the original Hermite transform function:

$$\phi_s(Z) = \sum_{i=0}^{k} \frac{\psi_i a^i}{i!} H_i(Z) \tag{3.3}$$

where the variance reduction factor, a is chosen so that the variance of the filtered data matches the variance of the transformed distribution. Specifically, a is chosen such that:

$$\sigma_s^2 = \sum_{i=0}^{k} \frac{\psi_i^2 a^{2i}}{i!} = f(a) \tag{3.4}$$

where σ_s^2 is the variance of the true model-scale data, which is determined through independent means. For example, the variance of spatially filtered data can be determined from:

$$\sigma_s^2 = \int s(\vec{k}) w^2(\vec{k}) d\vec{k} \tag{3.5}$$

where $s(\vec{k})$ is the spectral density function, and $w^2(\vec{k})$ is the weighting function (or spectral response ; e.g., North and Nakamoto 1989). Knowing σ_s^2, a, can be determined through Eq. 3.5 (usually found through numerical methods). Once a is determined, ϕ_s represents a function which maps Gaussian variables into variables with the expected distribution of the model-scale variables. This variance correction factor is determined for each field and will be between 0.0 and 1.0, since the filtered data is expected to have less variance than the original data.

Once the function ϕ_s is obtained, the resulting PDF of the model-scale

data is:

$$P_A(x) = P_G(Z)\frac{dZ}{dx} \tag{3.6}$$

where P_G is the Gaussian PDF, $x = \phi_s(Z)$ and $Z = \phi_s^{-1}(x)$. (This result follows from the theory of functions of random variables, Gibra 1973.)

Thus, the steps to applying the technique are:

1. Obtain an observation site which has a consistent data available (enough data is needed to obtain a reasonable representation).
2. Determine the transform function $\phi(Z)$.
3. Calculate of the coefficients of the Hermite expansion.
4. Determination of the model-scale variance.
5. Determine the variance correction factor a so that the observed and model-scale variance agree.
6. Determine the transformed observational distribution and compare to the model distribution.

A major advantage of this technique is that it can be applied to any variable, scale, and model.

3.1 Demonstration of the Technique

The following example is designed to demonstrate the adjustment procedure described in the previous section. A 5×5 grid is generated with each grid point having 500 independent random samples from a gamma distribution. Figure 3.1(a) shows the distribution for a single grid point (histogram), and the corresponding distribution (solid curve) obtained from the expansion given by:

$$\phi(Z) = \sum_{i=0}^{30} \frac{\psi_i}{i!} H_i(Z) \tag{3.7}$$

as discussed in section 3. Next an area-average distribution is obtained from the averaging data from adjacent points on the grid. The transformed PDF is obtained by through the methods discussed in the previous section. Specifically, the variance correction factor a is determined by matching the variance

of the area-averaged distribution with that of the transformed point PDF (see Eqn 3.5). The transformed PDF is found using Eq. 3.6.

The histogram in Fig. 3.1(b) depicts the area-average distribution of the four adjacent points on the grid. The resulting distribution is more Gaussian-like than the point distribution (shown in Fig. 3.1(a)) and the variance has decreased from 1.85 to 0.44. The area-averaged variance is used to calculate the variance reduction factor a (0.53). This value is then used to create the transformed PDF. The transformed PDF is shown in Fig. 3.1(b) by the solid curve.

Figure 3.1(c) is same as Fig. 3.1(b) except that the area-averaged distribution is for the entire 5×5 grid. This distribution is nearly Gaussian (as expected from the central limit theorem). The area-averaged variance in this case is 0.08 and the variance reduction factor is again chosen so that the transformed PDF has the same variance (i.e., $a = 0.23$).

Hence, the three cases from this example show that the transform method for obtaining the filtered distributions correctly reproduces the point distribution (Fig. 3.1(a)) to the limiting distribution (Fig. 3.1(c)) by simply estimating the area-averaged variance.

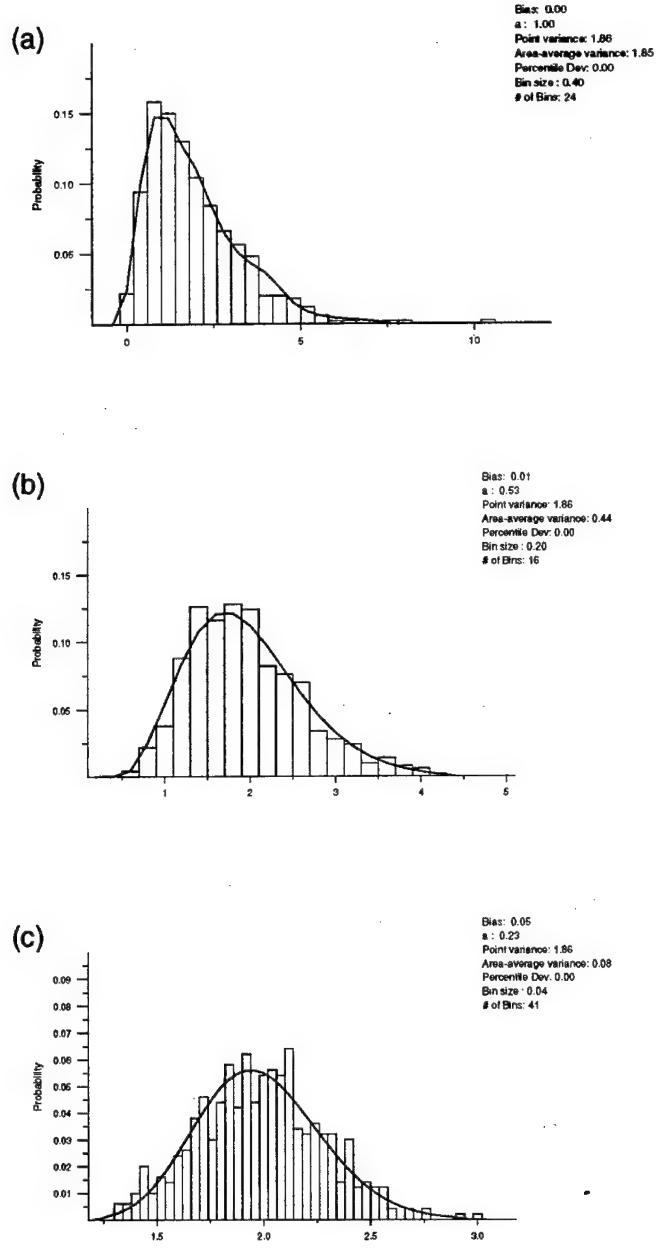

Figure 3.1: The evolutionary path to Gaussian.

Appendix II: Model Configurations

The Mesocale Atmospheric Simulation System (MASS) model is the mesoscale model used for these simulations. Details about the MASS model are provided in Kaplan et al. 1982; MESO 1995; and Manobianco et al. 1996. The model has several configurations. Below the particular configurations are described for both the 40 km and 10 km models.

3.2 10 km Model

The 10 km model is a 60 × 60 × 20 polar stereographic grid with spacing of 11 km at the center gird point, 42.25°, -79.30°. The lower left corner of the grid is 39.82°, -80.40°. The 20 sigma levels in the model are listed in Table 3.2. The top pressure level of the model is 100 mb.

The 10 km model uses a short time step of 20 seconds and a long time step of 60 seconds. This model uses the Kuo-MESO cumulus parameterization scheme and Blackadar planetary boundary layer formulation.

3.3 40 km Model

The 40 km model is a 60 × 60 × 20 polar stereographic grid with spacing of 40 km at the center gird point, 42.25°, -79.30°. The lower left corner of the grid is 31.32°, -90.47°. The 20 sigma levels in the model are the same as those in the 10 km configuration and are listed in Table 3.2. Like the 10 km model, the top pressure level in the 40 km model is 100 mb.

The 40 km model uses a short time step of 72 seconds and a long time step of 144 seconds. The model uses the Kuo-MESO cumulus parameterization scheme and Blackadar planetary boundary layer formulation.

3.4 Configuration File

All options of the MASS model are chosen through a configuration file. The actual configuration file for the 10 km model is provided below.

Level Number	Sigma	Level Number	Sigma
1	1.000	11	0.600
2	0.998	12	0.540
3	0.985	13	0.480
4	0.965	14	0.420
5	0.945	15	0.360
6	0.900	16	0.300
7	0.840	17	0.240
8	0.780	18	0.180
9	0.720	19	0.120
10	0.660	20	0.060

Table 3.2: The 20 sigma levels used in the model simulations

```
=========================================
=========================================
M A S S  NUMERICAL MODEL INPUT PARAMETERS
=========================================
=========================================

=========================================
TIME STEP / GRID SPACING / LENGTH OF RUN
=========================================

 ------
|  72  |  Short time       RULE OF THUMB: TIMESTEP (sec) < 1.8 x DX (km)
 ------   step (seconds)
                            Time steps which are evenly divisible into 1 hour
                           (x = also divisible into 30 min. xx = into 15 min.)
                           -------------------------------------------------
                          ! xx150  144   x120 xx100 xx90   80 xx75 x72 xx60  !
                          ! xx50    48   xx45  x40  xx36 xx30 xx25 x24       !
                          ! xx20  xx18     16 xx15  xx12 xx10 xx9  x8        !
                           -------------------------------------------------

 --
| 2|      Ratio of long timestep to short timestep
 --
*************************************************************
*  -                                                        *
* |1|       Length of run is measured in: (1) hours         *
*  -                                      (2) long timesteps *
*  ---                                                      *
* | 12|     Length of run                                   *
```

```
*  ---                                                                 *
**********************************************************************

 ====================
 DIAG FILE PARAMETERS
 ====================

 -
|1|       Write out DIAG files? (0) No
 -                              (1) Yes
**********************************************************************
*  -                                                                 *
* |1|       Frequency of output is measured in: (1) hours           *
*  -                                             (2) long timesteps *
*  -------                                                           *
* |    1  | Frequency of output to DIAG files.                      *
*  -------                                                           *
**********************************************************************

 III  JJJ
 ---  ---
|  1||  1| Lower left corner of area covered by DIAG files.
 ---  ---
| 60|| 60| Upper right corner of area covered by DIAG files.
 ---  ---


 ====================
 PLOT FILE PARAMETERS
 ====================

**********************************************************************
*  -                                                                 *
* |1|       Frequency of output is measured in: (1) hours           *
*  -                                             (2) long timesteps *
*  -------                                                           *
* |  1    | Frequency of output to plot files.                      *
*  -------                                                           *
**********************************************************************

 III  JJJ
 ---  ---
|  1||  1| Lower left corner of area covered by plot files.
 ---  ---
| 60|| 60| Upper right corner of area covered by plot files.
```

```
--- ---


================
DIAGNOSTIC POINT
================

  III  JJJ
  ---  ---
 | 41|| 32| Location of grid point for which expanded data will be printed.
  ---  ---


====================
DIFFUSION PARAMETERS
====================

 --
| 1|       Frequency of calls to diffusion scheme (long timesteps).
 --        (REQUIRED FREQUENCY: EVERY TIME STEP PENDING IMPROVEMENTS TO CODE)

 ------
| 0.004|   Non-dimensional diffusion coefficient (Range: 0.001 - 0.0075).
 ------
|  8.0 |   Ratio of diffusion at side boundaries to interior of domain.
 ------
|    1 |   Ratio of diffusion at top boundary to interior of domain.
 ------
 --
|21|       Sigma level at which diffusion coefficient begins to increase
 --        to top of domain value.


 ========================
 CUMULUS SCHEME PARAMETERS
 ========================

 --
|30|       Frequency of calls to cumulus scheme (minutes).
 --        (SUGGESTED FREQUENCY: about every 20 to 30 minutes)

 -
|1|        Type of cumulus scheme: (0) None
 -                                (1) Kuo-MESO
                                  (2) Fritsch-Chappell
```

(3) Original Kuo-Anthes

```
**********************
KUO ANTHES PARAMETERS
**********************

 ----------
| 1.0E-05  | Threshold for moist convection.
 ----------
|     0    | Updraft entrainment parameter.
 ----------
|   750    | Downdraft entrainment parameter.
 ----------
|  -1.0    | Ratio of detrainment / entrainment in updraft.
 ----------
|    0.5   | Downdraft mixing parameter
 ----------
|   500    | Downdraft level of initiation parameter
 ----------
|   1001   | RAIN fallout parameter.
 ----------
|   00.85  | RH of downdraft below cloud base.
 ----------
 --
|5 |         Number of sub-intervals to use when
 --          computing Kuo-Anthes scheme microphysics.
 -
|4|          Method of calculating precipitation efficiency.
 -


======================
PBL SCHEME PARAMETERS
======================

 -
|1|          Type of PBL scheme: (1) Blackadar
 -                               (2) TKE

 ====================
 MICROPHYSICS SCHEME
 ====================

 -
|0| Moisture Physics Option: (0) Diagnostic Moisture Physics
```

```
-                              (1) Level 1: Non-mixed Phase
                               (2) Level 2: Mixed Phase w/o Hail
                               (3) Level 3: Mixed Phase w/ Hail
                               (4) No condensation

================
ADVECTION SCHEME
================

-
|2| Advection scheme: (1) Centered Adams Bashford
-                    (2) MPDATA
-
|0| Tracer advection? (0) OFF
-                    (1) ON


==================
BOUNDARY CONDITIONS
==================

-
|1| Temperature           (1) Kreitzberg-Perkey Sponge
|1| Mixing Ratio          (2) Orlanski Radiation
|1| U wind
|1| V wind
|1| Surface pressure
|2| Cloud/rain water
|2| Tracer
-


============
FILE FORMATS
============

-
|U| Input files (INIT and BC)      (U) Unformated
-                                  (F) Formated
|F| Output files (Plot etc.)
-
|U| diag files
-


======================
```

```
TRAJECTORY INFORMATION
======================

---
|  0|        Number of trajectories
---
----------
|          | Name of file in which trajectory information resides
----------


============================
RAWINSONDE NUDGING PARAMETERS
============================

-
|0|        Nudge to rawinsonde data set?              (0) No
|0|        Nudge to rawinsonde temperature?           (1) Yes
|0|        Nudge to rawinsonde winds?
|0|        Nudge to rawinsonde moisture?
|0|        Nudge to rawinsonde data within the PBL?
|0|        Nudge to surface pressure?
-
|0|        Nudging dataset in diag file format?
-

--------
| 3.0E-04| Rawinsonde nudging coefficient (temperature and winds)
--------
| 1.0E-05| Rawinsonde nudging coefficient (mixing ratio)
--------

                                          -----
First rawinsonde nudging data set valid |00.00| hours after initial time
                                          -----
             Rawinsonde nudging starts |08.00| hours after initial time
                                          -----

-----
|12.00|   Time between rawinsonde nudging data sets (hours)
-----
-
|2|        Number of rawinsonde nudging data sets
-

                                     -----
TFULL3D:  Use full weighting within | 2.00| hours of nudging data set
```

```
                                                  -----
                                                 |     |
TTRANS3D: Decrease weighting linearly to 0 within | 2.00| hours of
                    full weighting period         -----

          Note: 2*TFULL3D + TTRANS3D must be less than the time between
             nudging data sets in order for the weighting factor to be <=1.


 ==========================
 SURFACE NUDGING PARAMETERS
 ==========================

 -
 |0|        Nudge to surface data set?                (0) No
 |0|        Nudge to surface temperature?             (1) Yes
 |0|        Nudge to surface winds?
 |0|        Nudge to surface moisture?
 -

 --------
 | 3.0E-04| Surface nudging coefficient
 --------

                                        -----
First surface nudging data set valid   |00.00| hours after initial time
                                        -----
              Surface nudging starts   |08.00| hours after initial time
                                        -----

 -----
 | 1.00|   Time between surface nudging data sets (hours)
 -----
 -
 |04|       Number of surface nudging data sets
 -
                                        -----
TFULL2D:  Use full weighting within    | 0.00| hours of nudging data set
                                        -----
                                                  -----
                                                 |     |
TTRANS2D: Decrease weighting linearly to 0 within | 1.00| hours of
                    full weighting period         -----

          Note: 2*TFULL2D + TTRANS2D must be less than the time between
             nudging data sets in order for the weighting factor to be <=1.
```

```
======================
MDR NUDGING PARAMETERS
======================

-
|0|     Nudge to MDR-derived RH data set?      (0) No
-                                              (1) Yes
-
|0|     Nudge to 4 km hourly precip data set?      (0) No
-                                                   (1) Yes

                        ---------
First data set valid | 0.0      | hours after initial time
                        ---------
For 4 km precip data sets, enter a time that is one hour before the
time in the name of the first file in the series.  (These files are
hourly accumulated precipitation.  The file name is the time at the
end of the hour for which the file is valid).

 -----
|01.00| Time between MDR nudging data sets (hours)
 -----
                        ---------
Last data set valid | 6.0      | hours after initial time
                        ---------

============================
PROFILER NUDGING PARAMETERS
============================

-
|0|        Nudge to profiler data?                                  (0) No
|0|        Nudge to profiler winds?                                 (1) Yes
|0|        Nudge to temperature derived from profiler winds?
-

 --------
| 3.0E-04| Profiler nudging coefficient
 --------

                                          ---------
First profiler nudging data set valid |-0.416667| hours after initial time
                                          ---------
 -----
```

```
|01.00|    Time between profiler nudging data sets (hours)
 -----
 -
|2|        Number of profiler nudging data sets
 -

 ============================================
 INCREMENTAL ANALYSIS UPDATE (IAU) PARAMETERS
 ============================================

 -
|0| Perform IAU?     (0) No
 -                   (1) Yes

 -------
|  6.0  | Duration of IAU period (hours)
 -------

================
SRPH 3-D Options
================


============================
Location of diagnostic points
============================

     i    j        Optional description
    ---  ---   ----------------------------
 1 | 41|| 32| |ALB Albany, NY               |
 2 |   ||   | |Bad Point 2                  |
 3 |   ||   | |Bad Point 3                  |
 4 |   ||   | |Adirondacks                  |
 5 |   ||   | |Maine                        |
    ---  ---   ----------------------------


============================================================

==========================
SRPH Scheme General Options
==========================

======
Timing
```

```
======
 -
|x|     Automatic Timestep Selection?
 -
 -----
| 90.0| SRPH timestep (seconds)
 -----
 -----
|  6.0| Minimum surface energy budget timestep (seconds)
 -----
 -----
|630.0| Radiation timestep (seconds)
 -----
 -----
| 90.0| Hydrology timestep (seconds)
 -----


==============================
Surface Energy Budget Options
==============================
 -
|1| Vegetation canopy physics:  (1) Isothermal soil/canopy
 -                              (2) Separate canopy temperature

=================
Radiation Options
=================
 -
| | RH-based radiation scheme?
 -
 -
|x| Explicit radiation scheme?
 -   -
    | |  Specify cloud fractions?
     -
    |x|  Specify cloud mixing ratios?
     -
    |x|  Use RH method to get cloud
     -    fractions and mixing ratios?

================================
Planetary Boundary Layer Options
================================
```

```
==================
Hydrology Options
==================

================
Diagnostic Flags
================

long deep
  -    -
 |x|  |x|  Surface Energy Budget
  -    -
 |x|  |x|  Radiation
  -    -
 |x|  |x|  Planetary Boundary Layer
  -    -
 |x|  |x|  Hydrology
  -    -

  -
 | |  Print diagnostics to screen as well as to output files?
  -

 ==========
 ==========
 THATS ALL!
 ==========
 ==========
```

Station Appendix: ALB - Albany, NY

	Pressure	Temperature	Dew Point	Wind Speed
	(mb)	(F)	(F)	(knot)
Obs. Mean	**1018.600**	**23.908**	**15.252**	**8.488**
40 km Mean	1014.353	24.099	15.589	7.531
10 km Mean	1013.623	26.360	17.124	6.552
Obs Std Dev.	**11.071**	**12.260**	**13.447**	**5.289**
40 km Std Dev.	10.662	12.030	13.399	3.000
10 km Std Dev.	10.106	12.465	13.201	3.385

Table 3.3: The long term means and standard deviations for the observations, the 10 km and the 40 km simulations at Albany, NY. The observed values are in bold type.

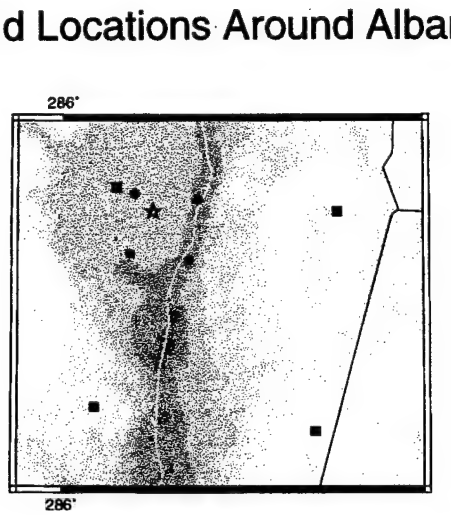

Figure 3.2: Grid point locations around Albany. The squares are the 40 km grid points the circles are the 10 km grid points and the star indicates the station location. Brown grid points are designated as land, while the blue points are designated as water.

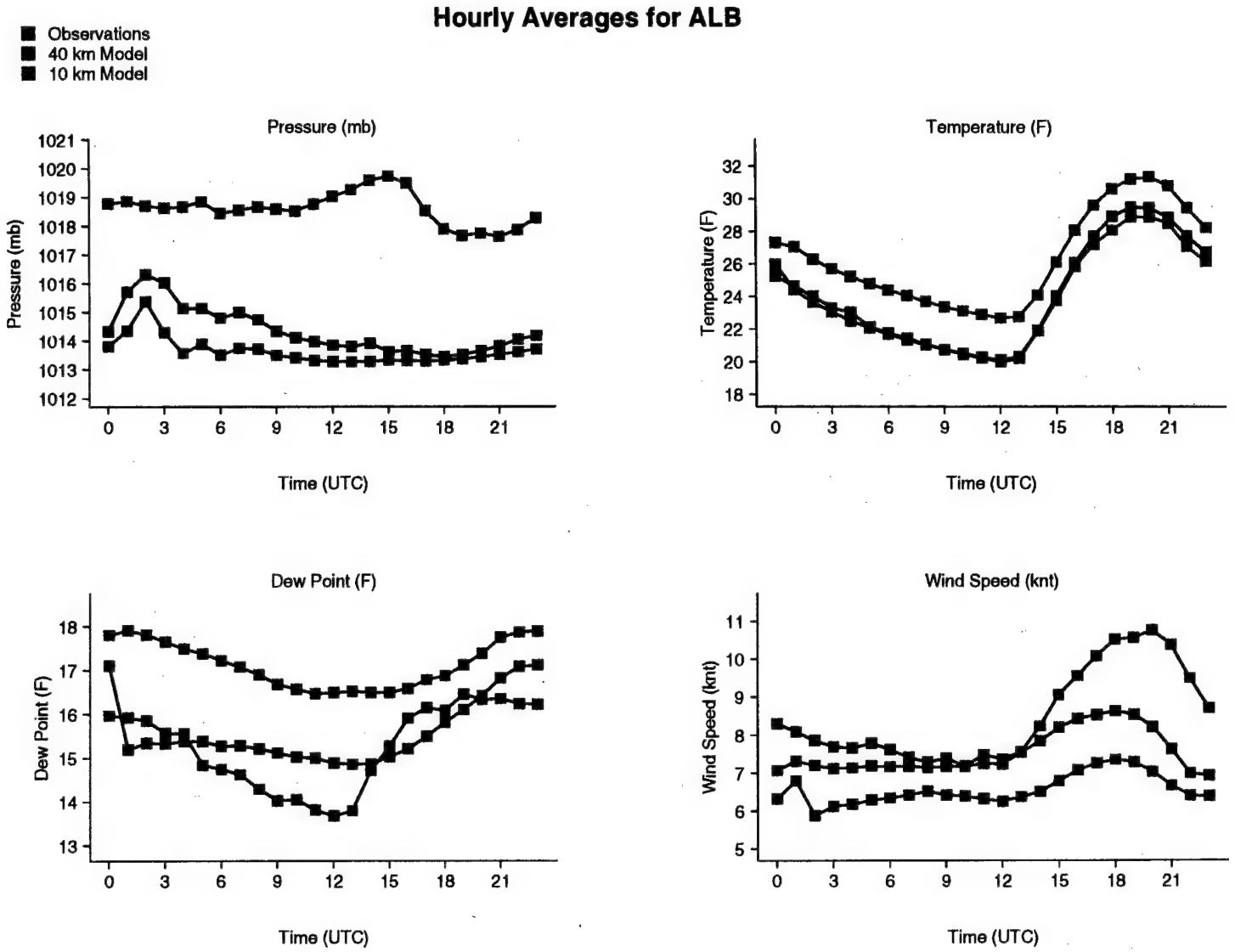

Figure 3.3: The hourly averages for Albany, NY

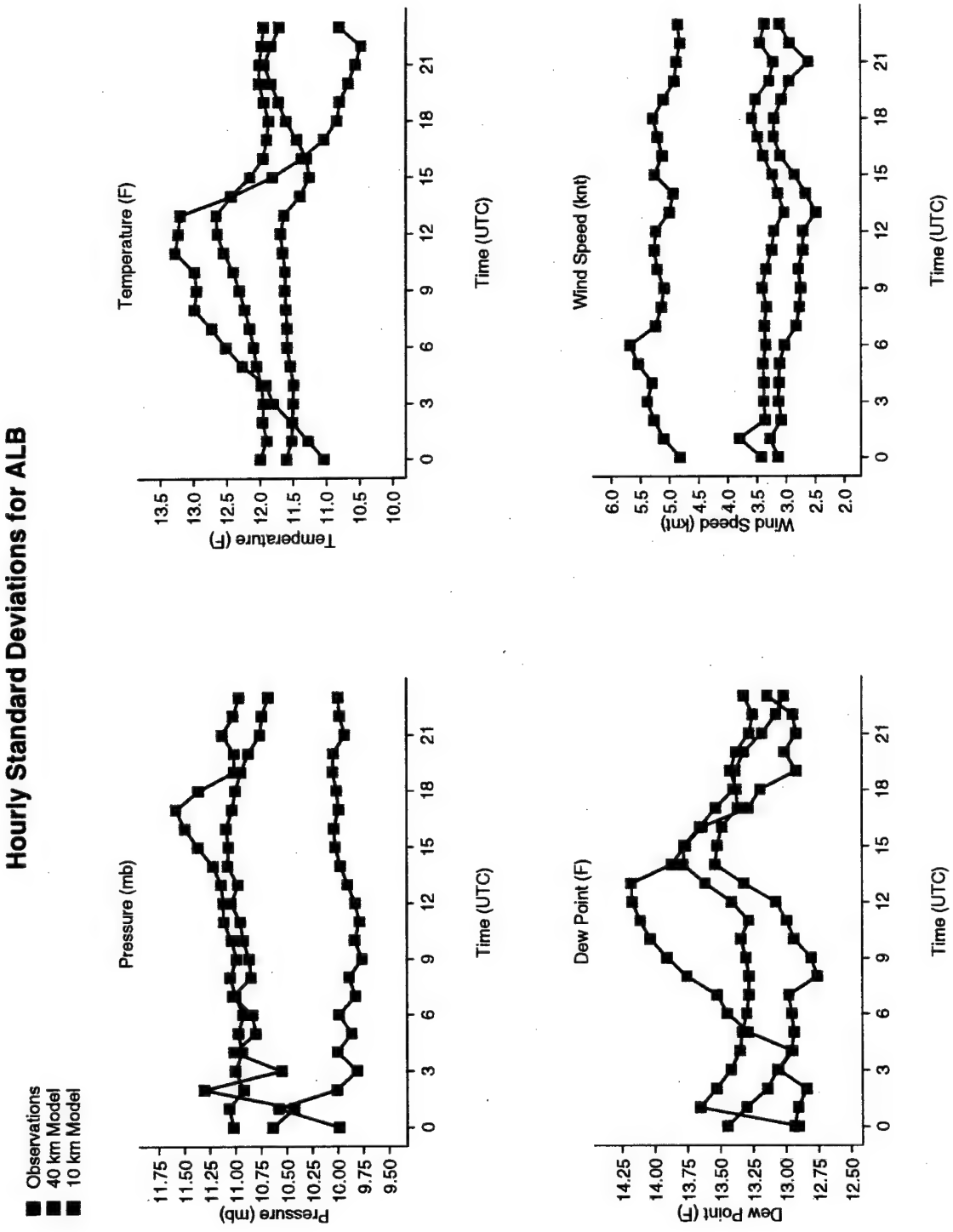

Figure 3.4: The hourly standard deviations for Albany, NY

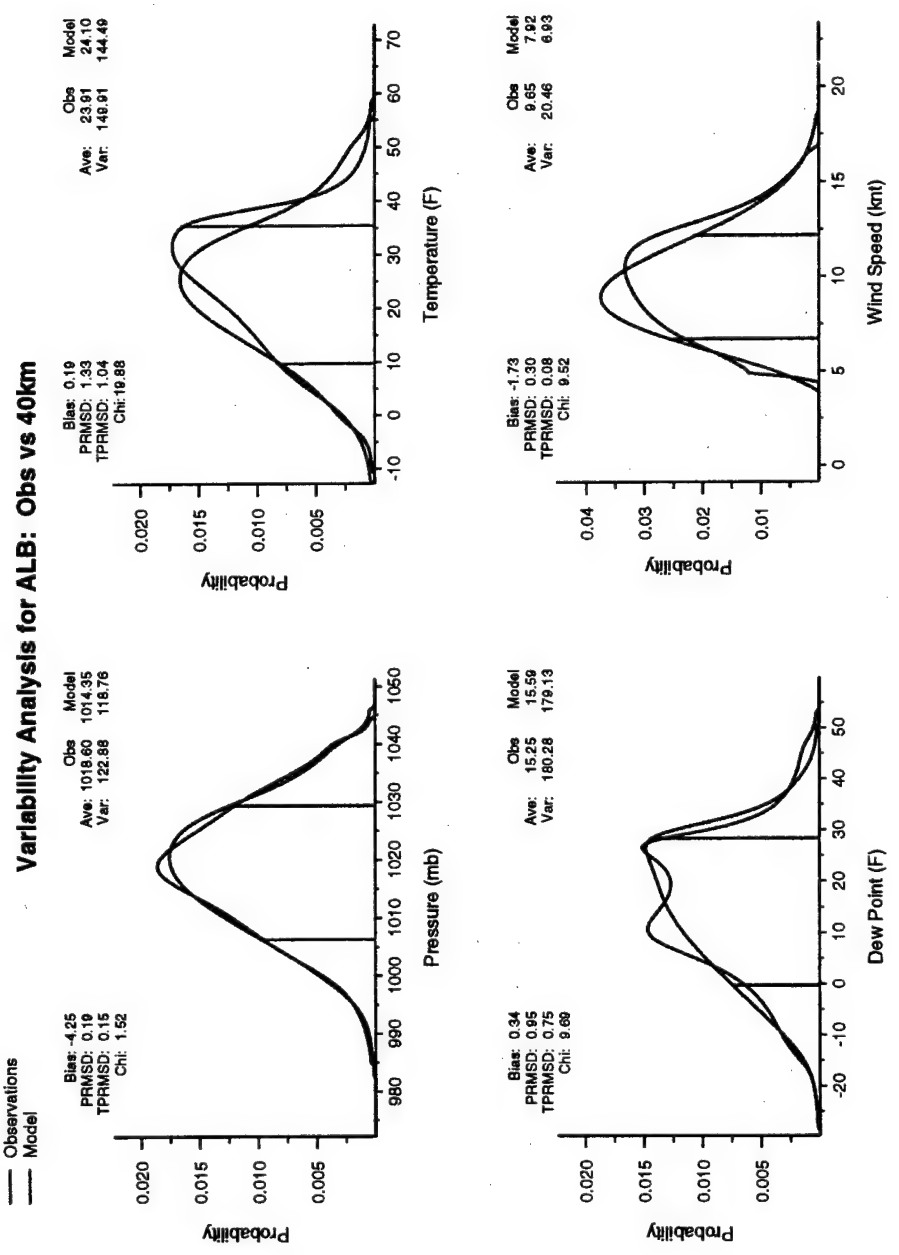

Figure 3.5: The 40 km distribution analysis for Albany, NY

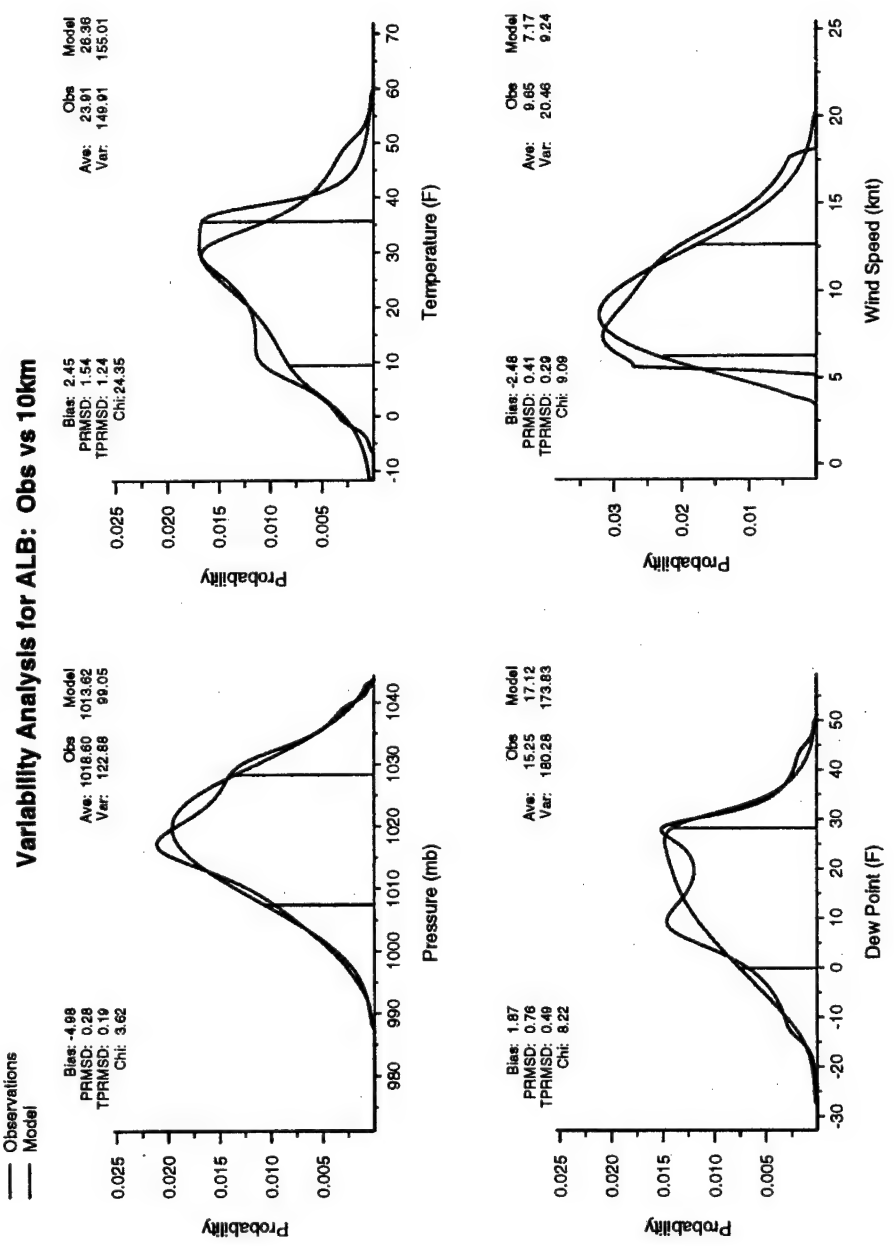

Figure 3.6: The 10 km distribution analysis for Albany, NY

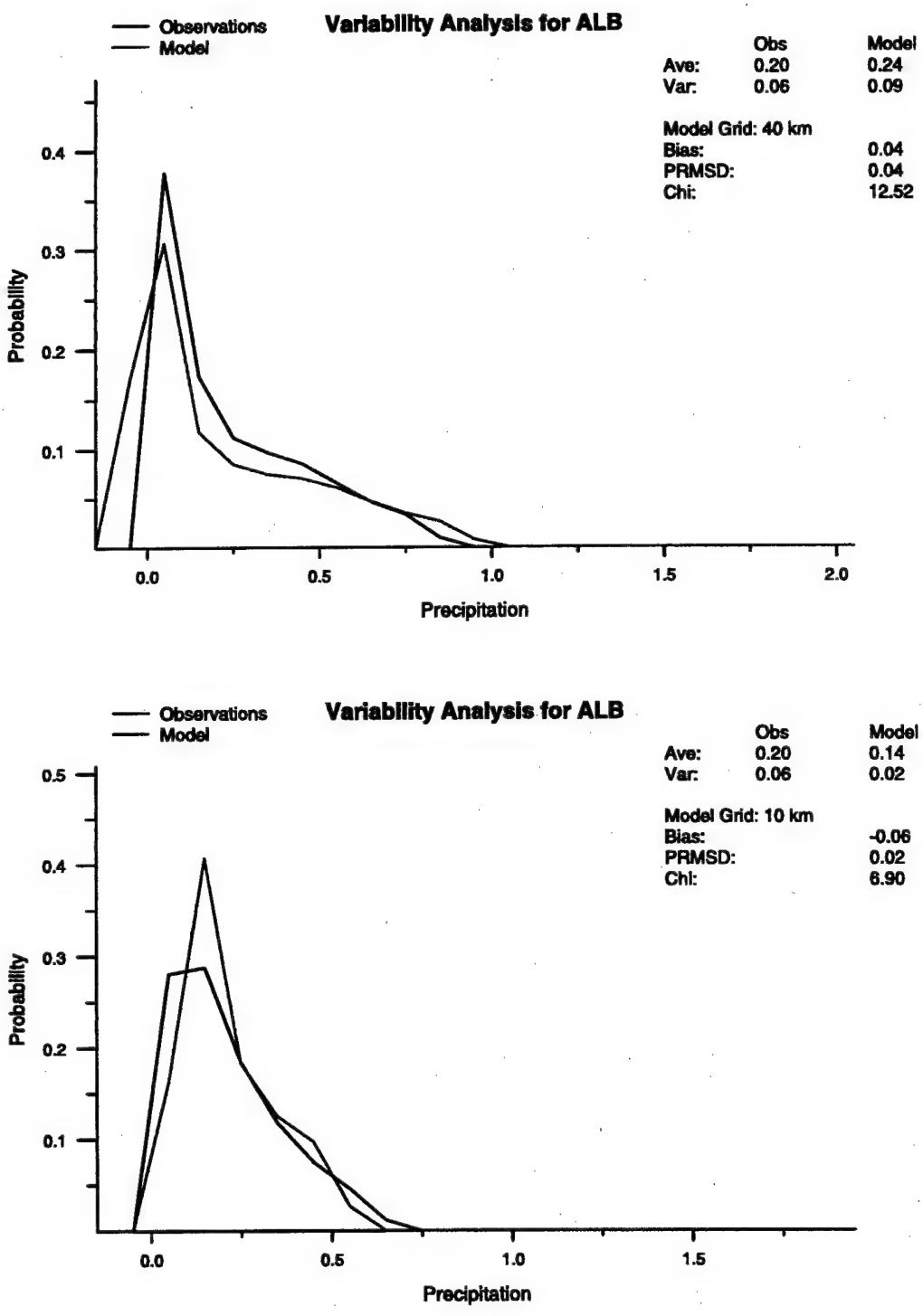

Figure 3.7: The daily precipitation distribution analysis for Albany, NY

Station Appendix: ART - Watertown, NY

	Pressure	Temperature	Dew Point	Wind Speed
	(mb)	(F)	(F)	(knot)
Obs. Mean	**1017.389**	**21.363**	**13.692**	**9.335**
40 km Mean	1013.854	21.290	15.628	7.951
10 km Mean	1013.493	22.790	15.314	7.600
Obs Std Dev.	**10.906**	**14.676**	**13.785**	**4.438**
40 km Std Dev.	10.392	12.179	13.785	3.069
10 km Std Dev.	9.287	12.683	13.483	3.516

Table 3.4: The long term means and standard deviations for the observations, the 10 km and the 40 km simulations at Watertown, NY. The observed values are in bold type.

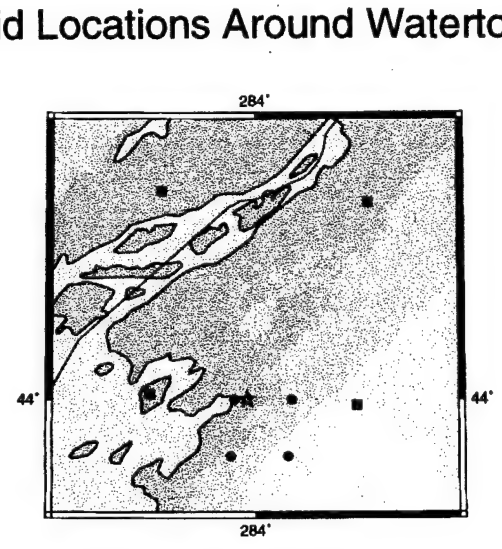

Figure 3.8: Grid point locations around Watertown. The squares are the 40 km grid points the circles are the 10 km grid points and the star indicates the station location. Brown grid points are designated as land, while the blue points are designated as water.

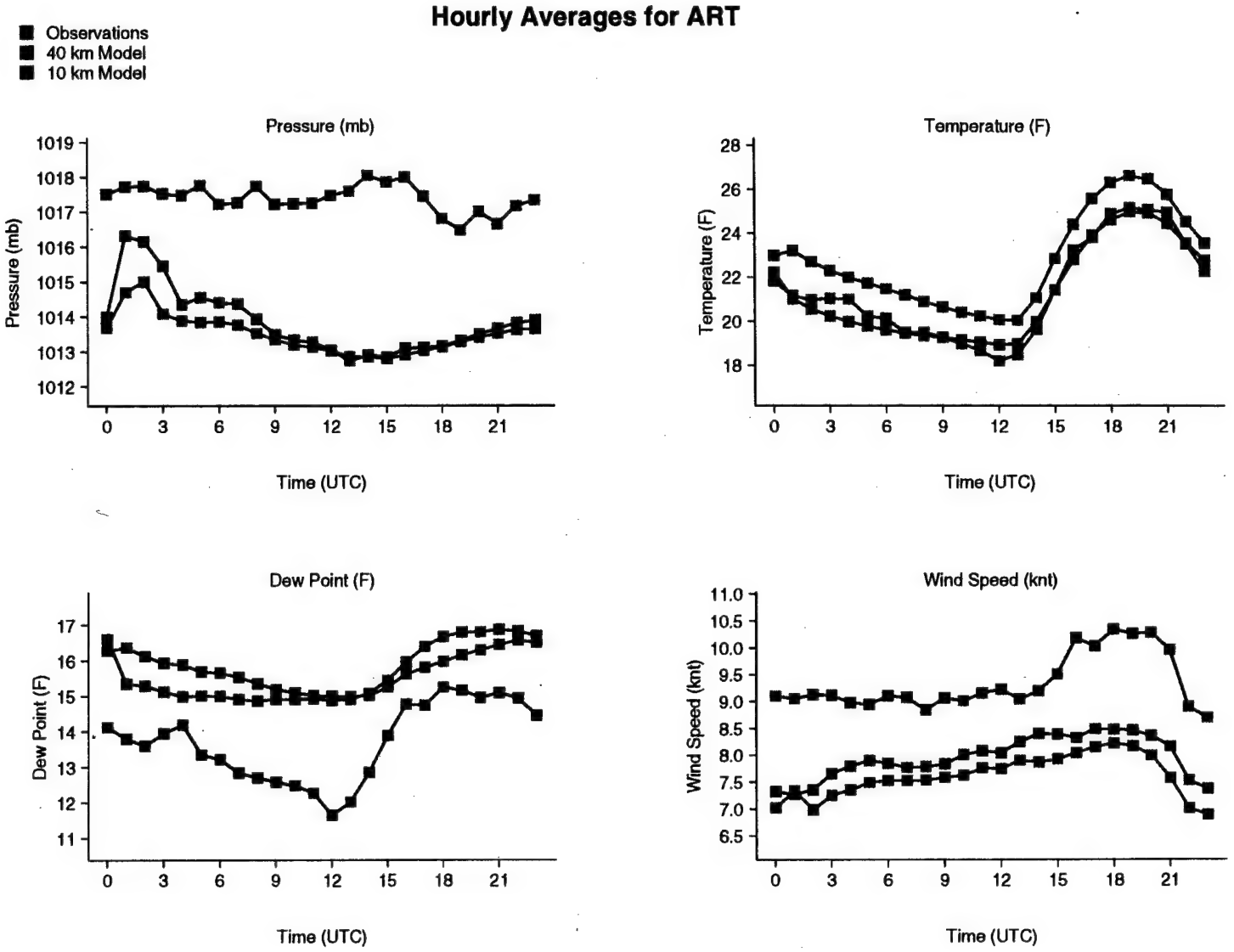

Figure 3.9: The hourly averages for Watertown, NY

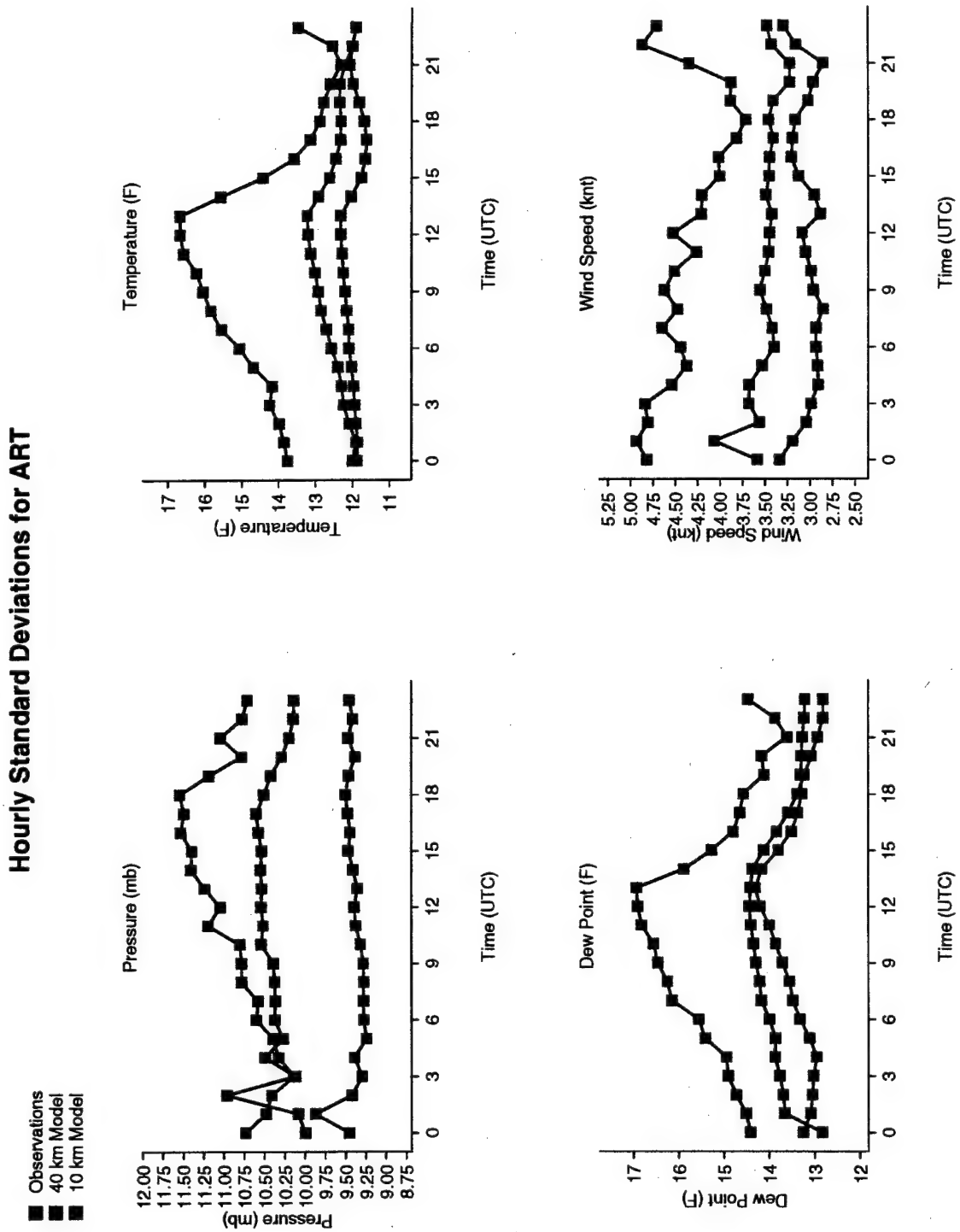

Figure 3.10: The hourly standard deviations for Watertown, NY

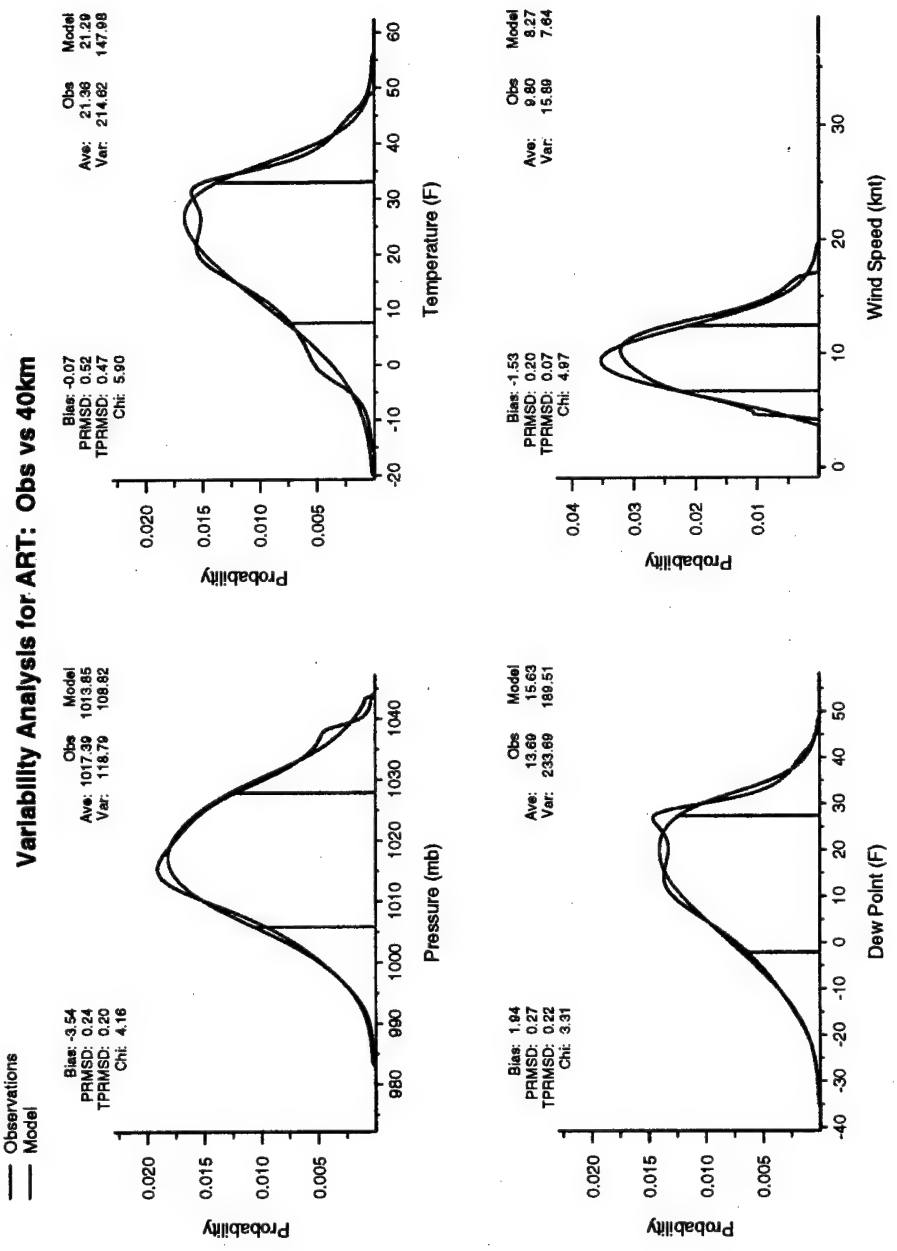

Figure 3.11: The 40 km distribution analysis for Watertown, NY

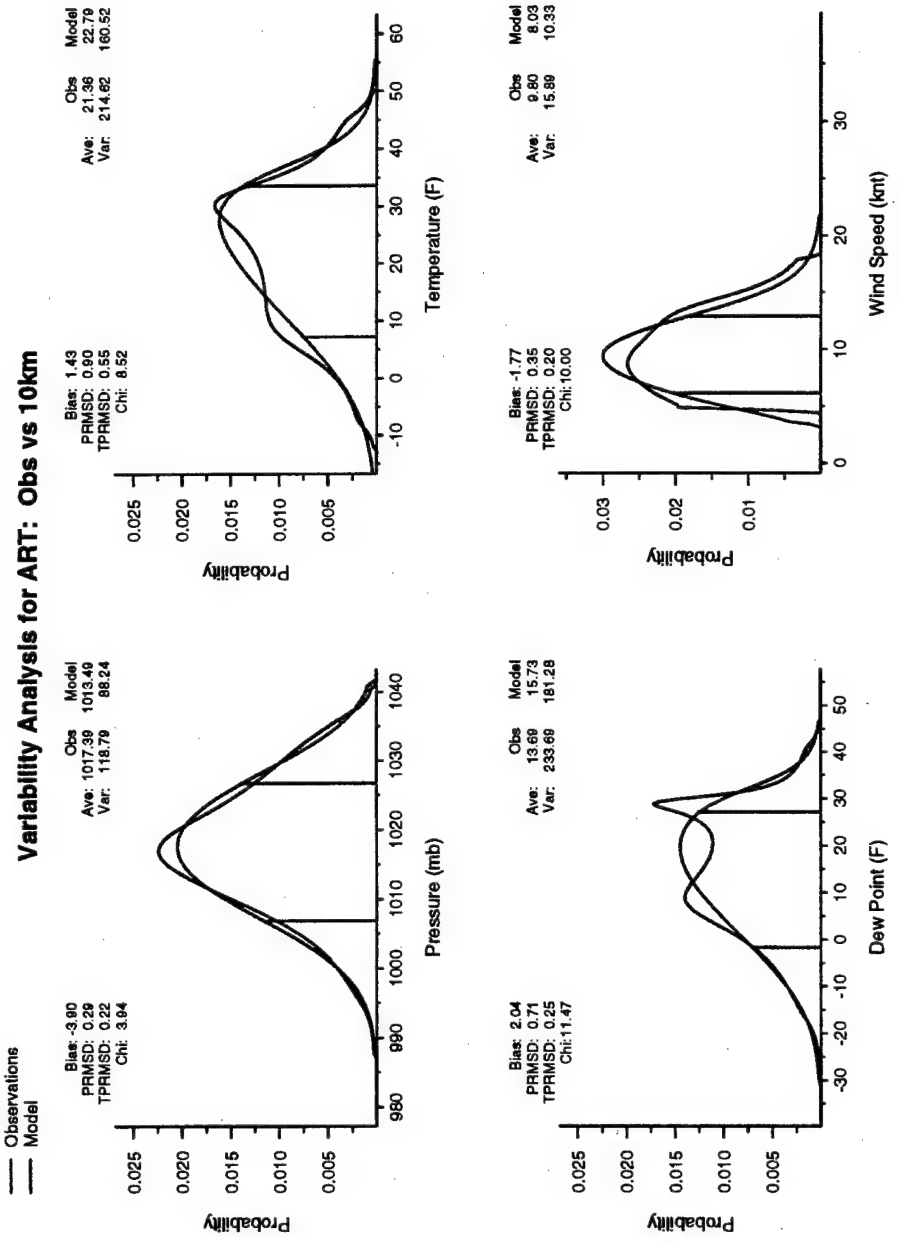

Figure 3.12: The 10 km distribution analysis for Watertown, NY

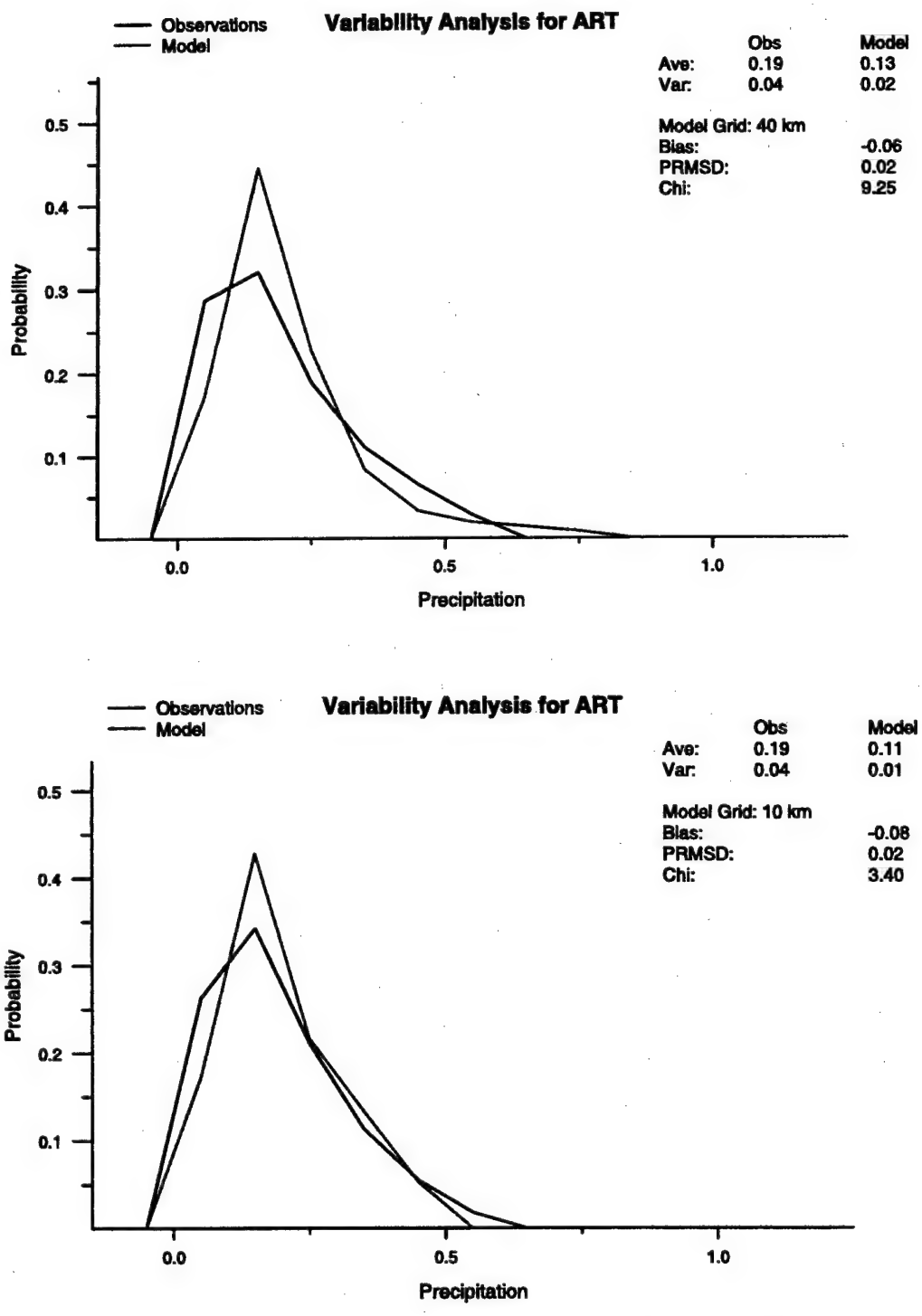

Figure 3.13: The daily precipitation distribution analysis for Watertown, NY

Station Appendix: BGM - Binghamton, NY

	Pressure	Temperature	Dew Point	Wind Speed
	(mb)	(F)	(F)	(knot)
Obs. Mean	**1017.409**	**23.578**	**16.151**	**9.601**
40 km Mean	1014.875	24.185	17.671	8.015
10 km Mean	1013.800	26.770	18.117	7.223
Obs Std Dev.	**10.455**	**11.464**	**12.425**	**3.891**
40 km Std Dev.	9.782	11.648	11.853	3.126
10 km Std Dev.	8.746	11.919	11.777	3.062

Table 3.5: The long term means and standard deviations for the observations, the 10 km and the 40 km simulations at Binghamton, NY. The observed values are in bold type.

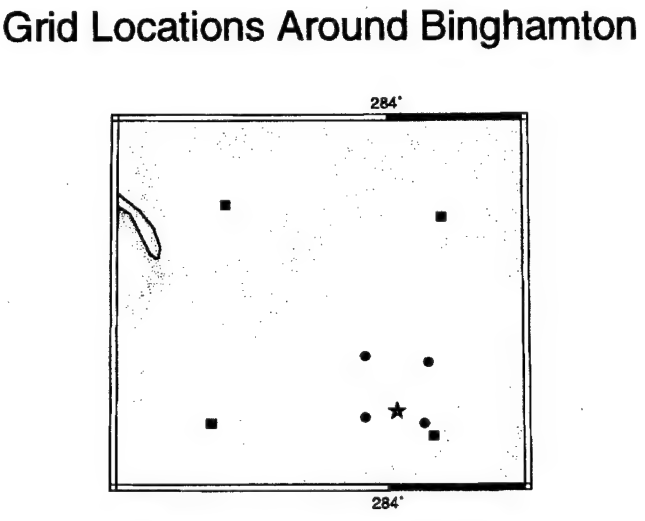

Figure 3.14: Grid point locations around Binghamton. The squares are the 40 km grid points the circles are the 10 km grid points and the star indicates the station location. Brown grid points are designated as land while the blue points are designated as water.

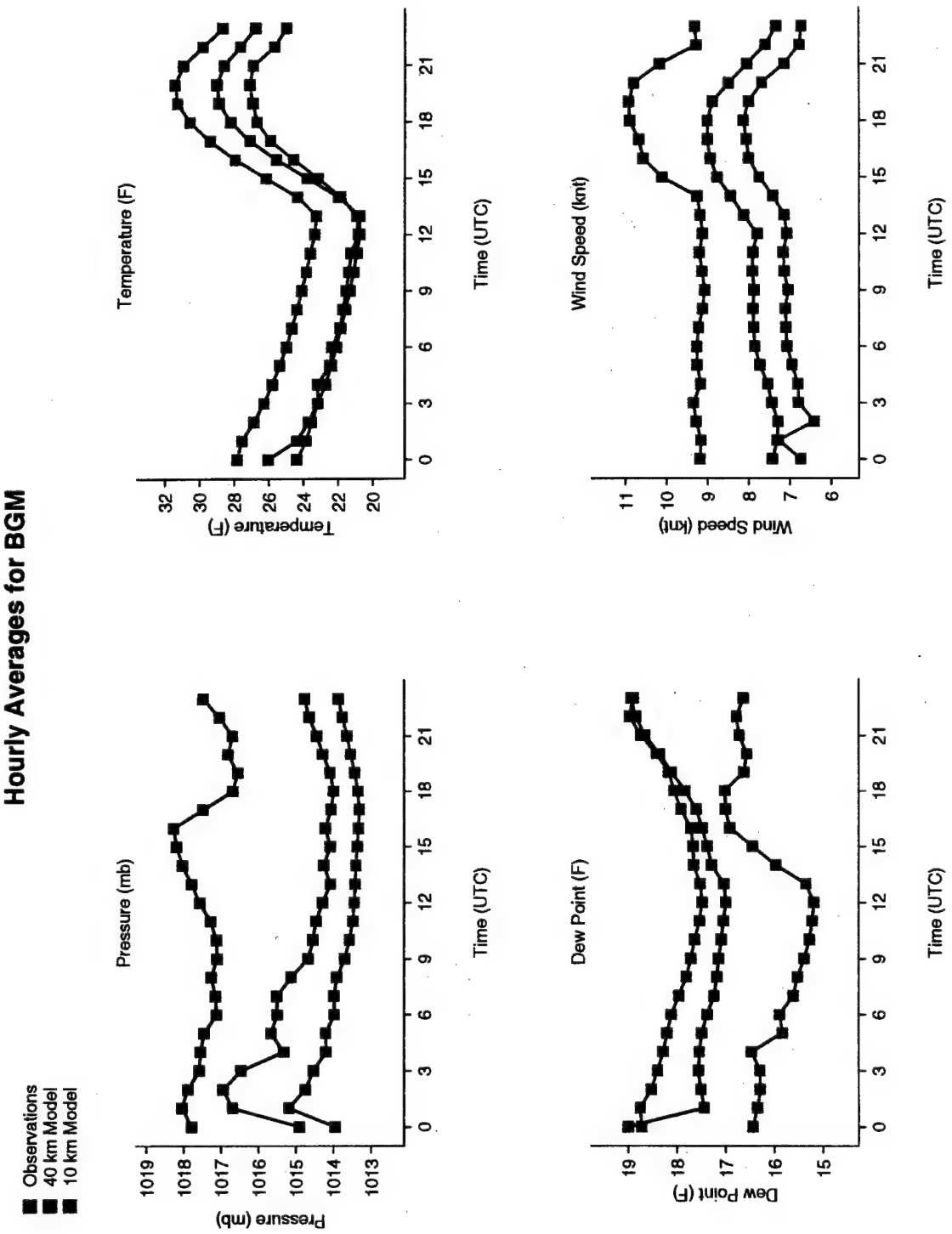

Figure 3.15: The hourly averages for Binghamton, NY

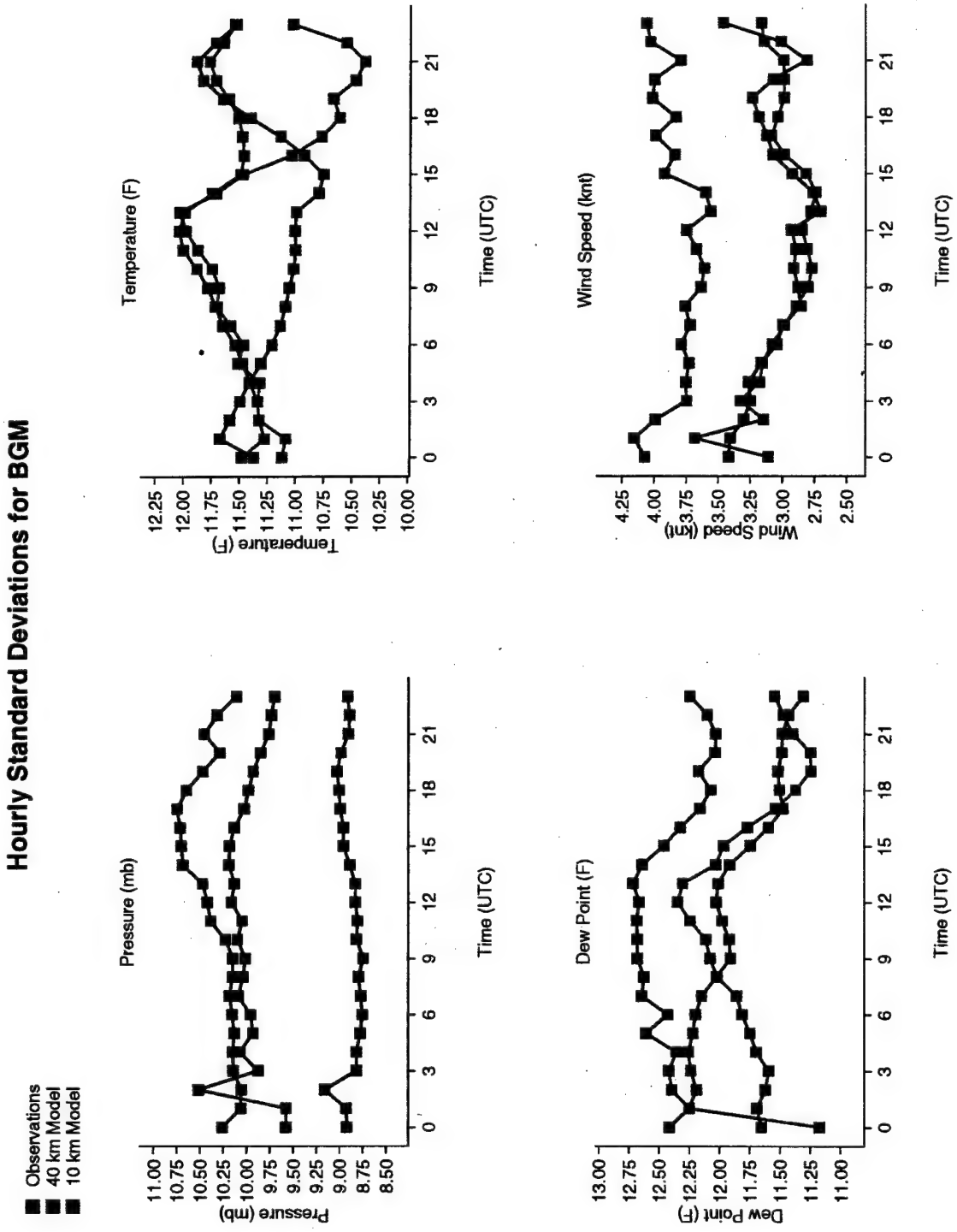

Figure 3.16: The hourly standard deviations for Binghamton, NY

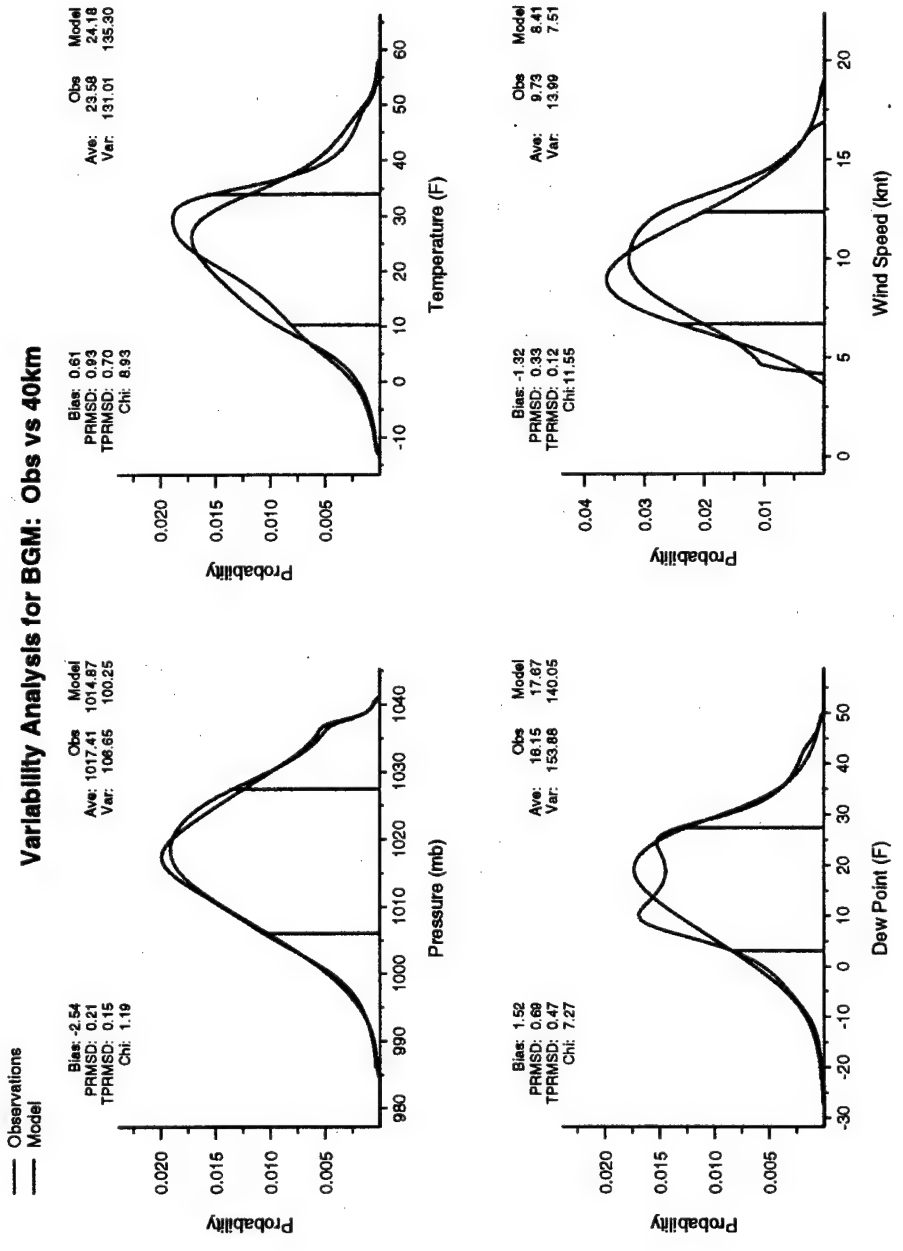

Figure 3.17: The 40 km distribution analysis for Binghamton, NY

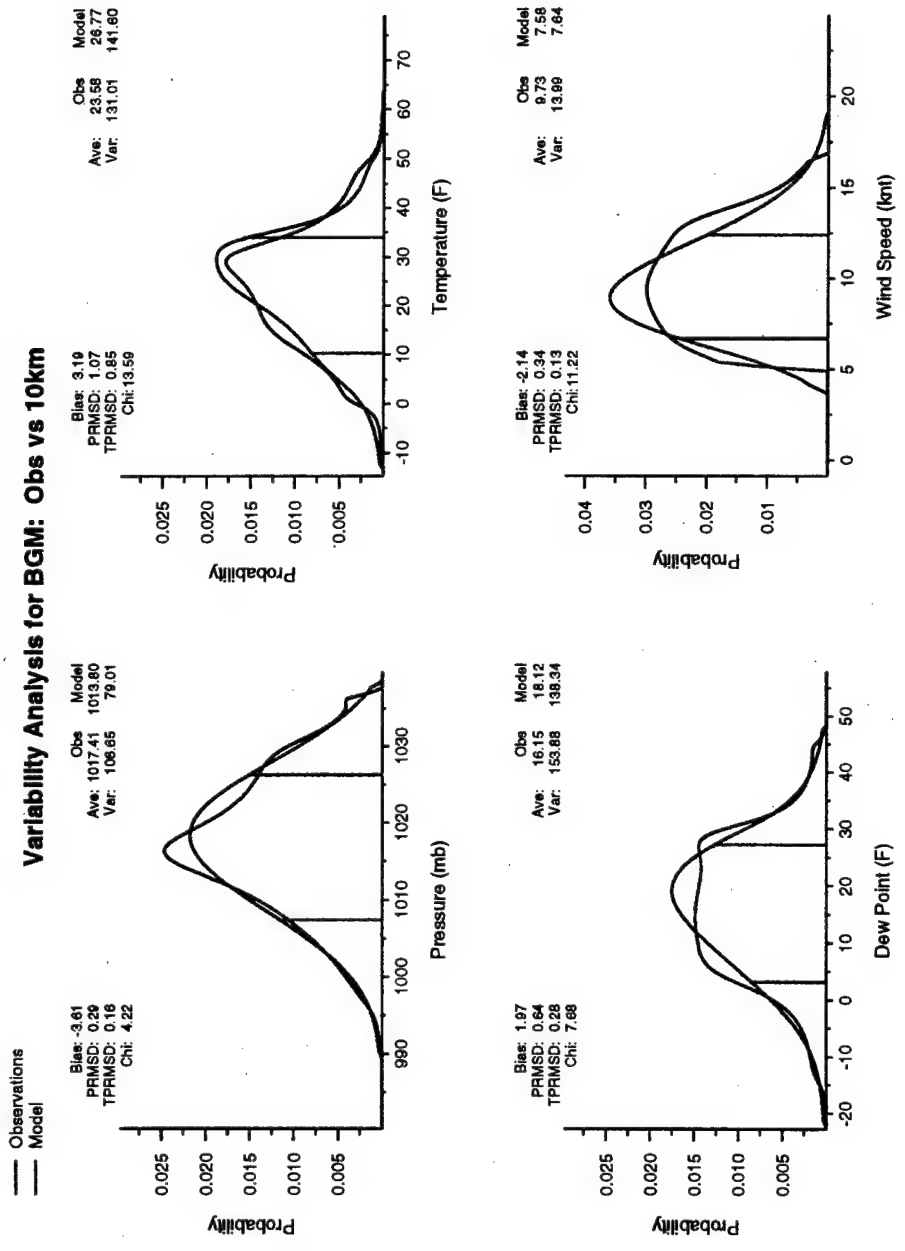

Figure 3.18: The 10 km distribution analysis for Binghamton, NY

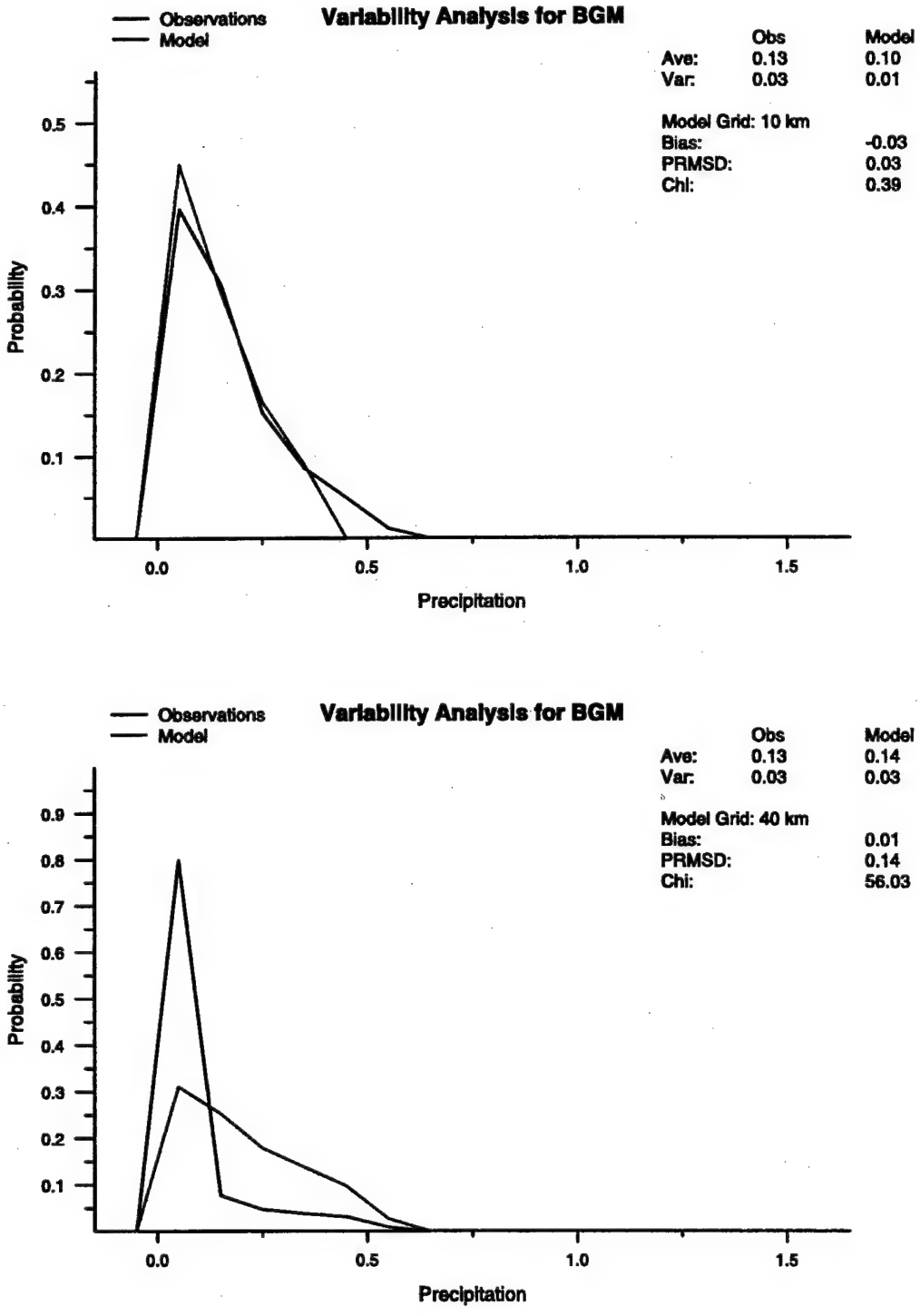

Figure 3.19: The daily precipitation distribution analysis for Binghamton, NY

Station Appendix: GTB - Fort Drum, NY

	Pressure	Temperature	Dew Point	Wind Speed
	(mb)	(F)	(F)	(knot)
Obs. Mean	**1017.643**	**19.886**	**14.382**	**7.560**
40 km Mean	1013.848	20.252	14.782	8.060
10 km Mean	1013.335	21.580	15.061	7.673
Obs Std Dev.	**10.929**	**14.668**	**15.306**	**4.828**
40 km Std Dev.	10.577	12.419	13.959	3.055
10 km Std Dev.	9.175	12.773	13.320	3.425

Table 3.6: The long term means and standard deviations for the observations, the 10 km and the 40 km simulations at Fort Drum, NY. The observed values are in bold type.

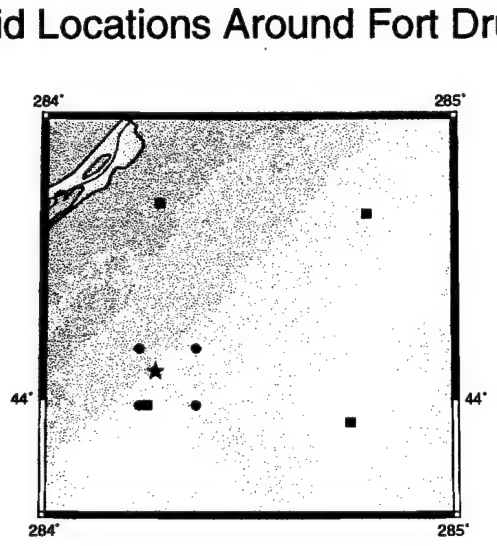

Figure 3.20: Grid point locations around Fort Drum. The squares are the 40 km grid points the circles are the 10 km grid points and the star indicates the station location. Brown grid points are designated as land while the blue points aredesignated as water.

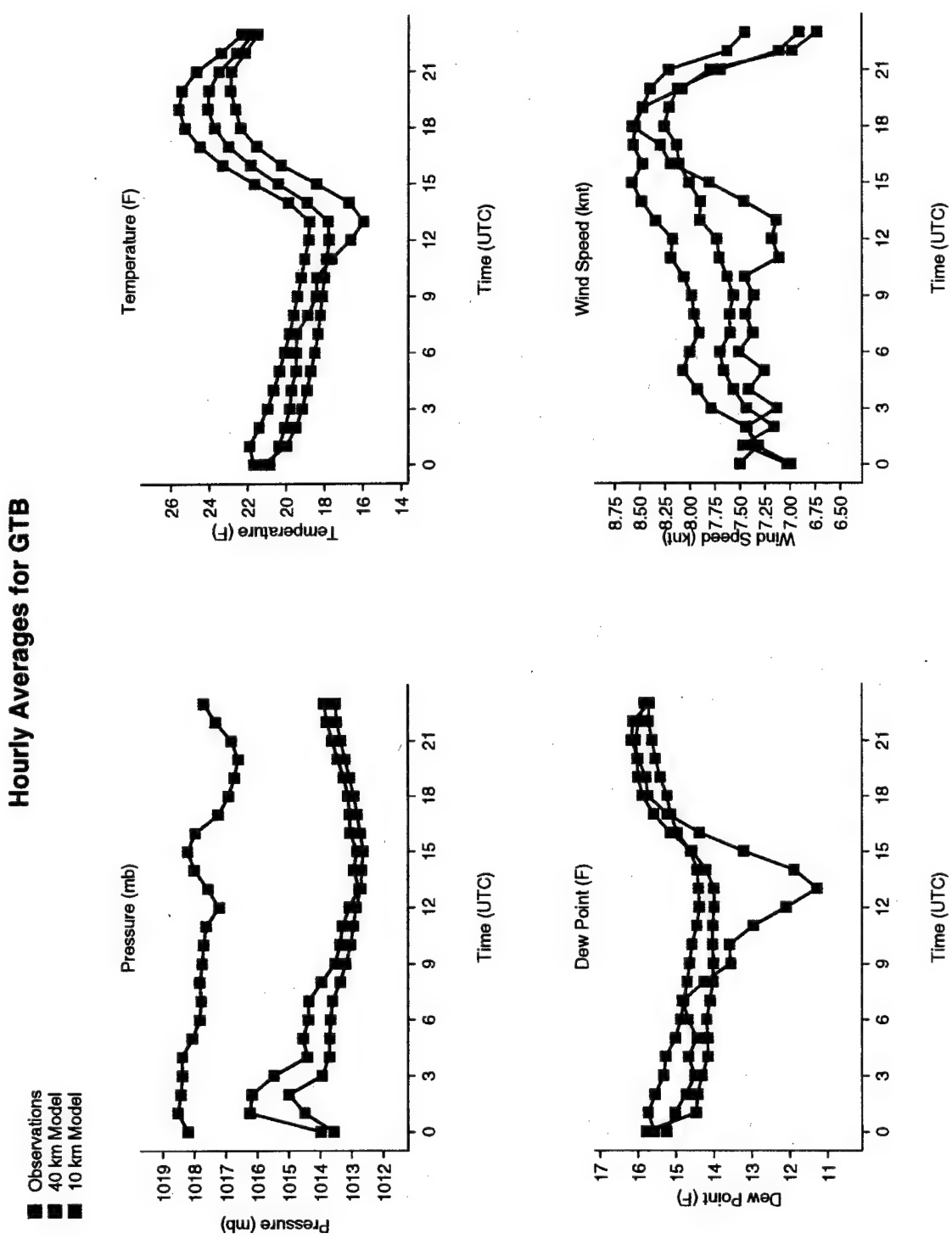

Figure 3.21: The hourly averages for Fort Drum, NY

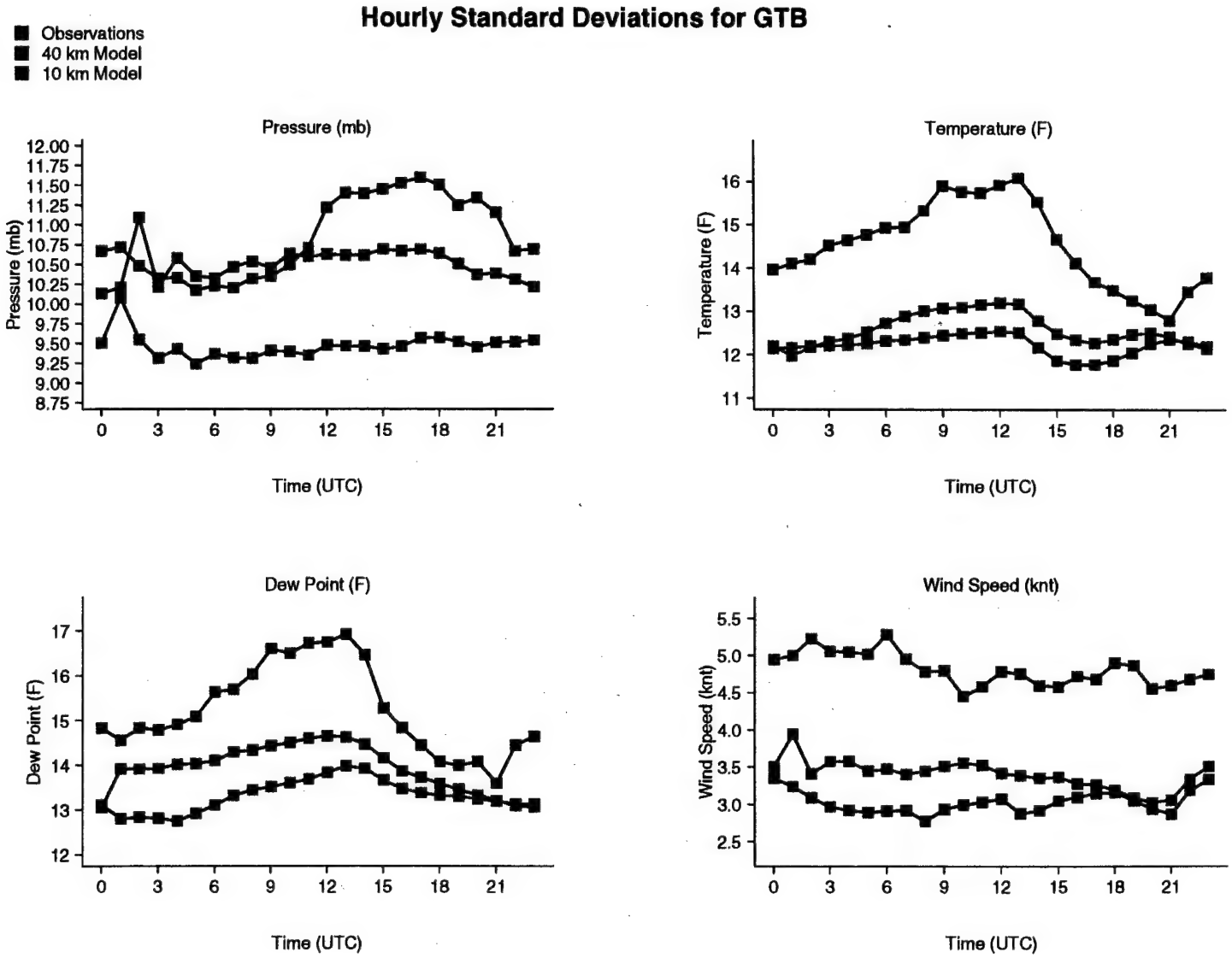

Figure 3.22: The hourly standard deviations for Fort Drum, NY

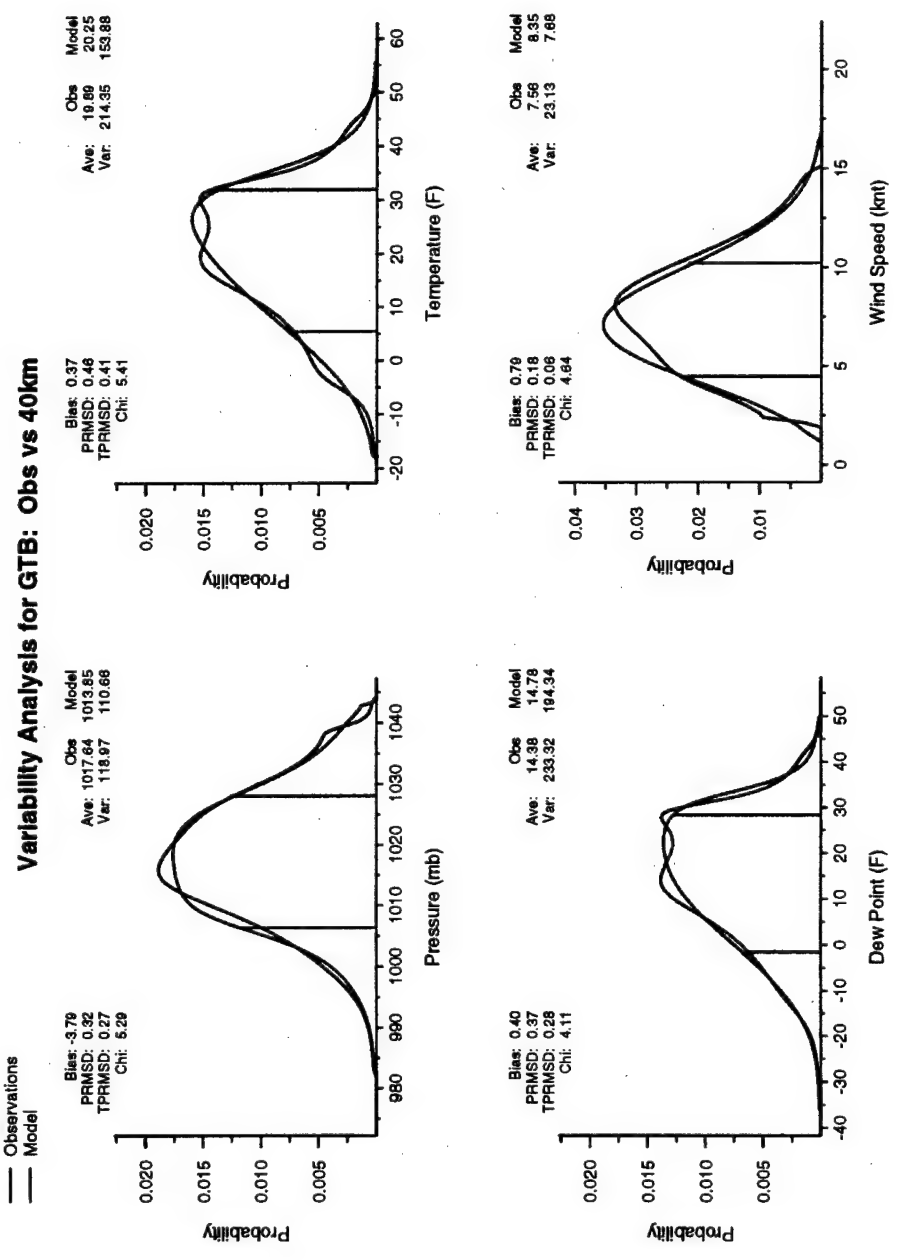

Figure 3.23: The 40 km distribution analysis for Fort Drum, NY

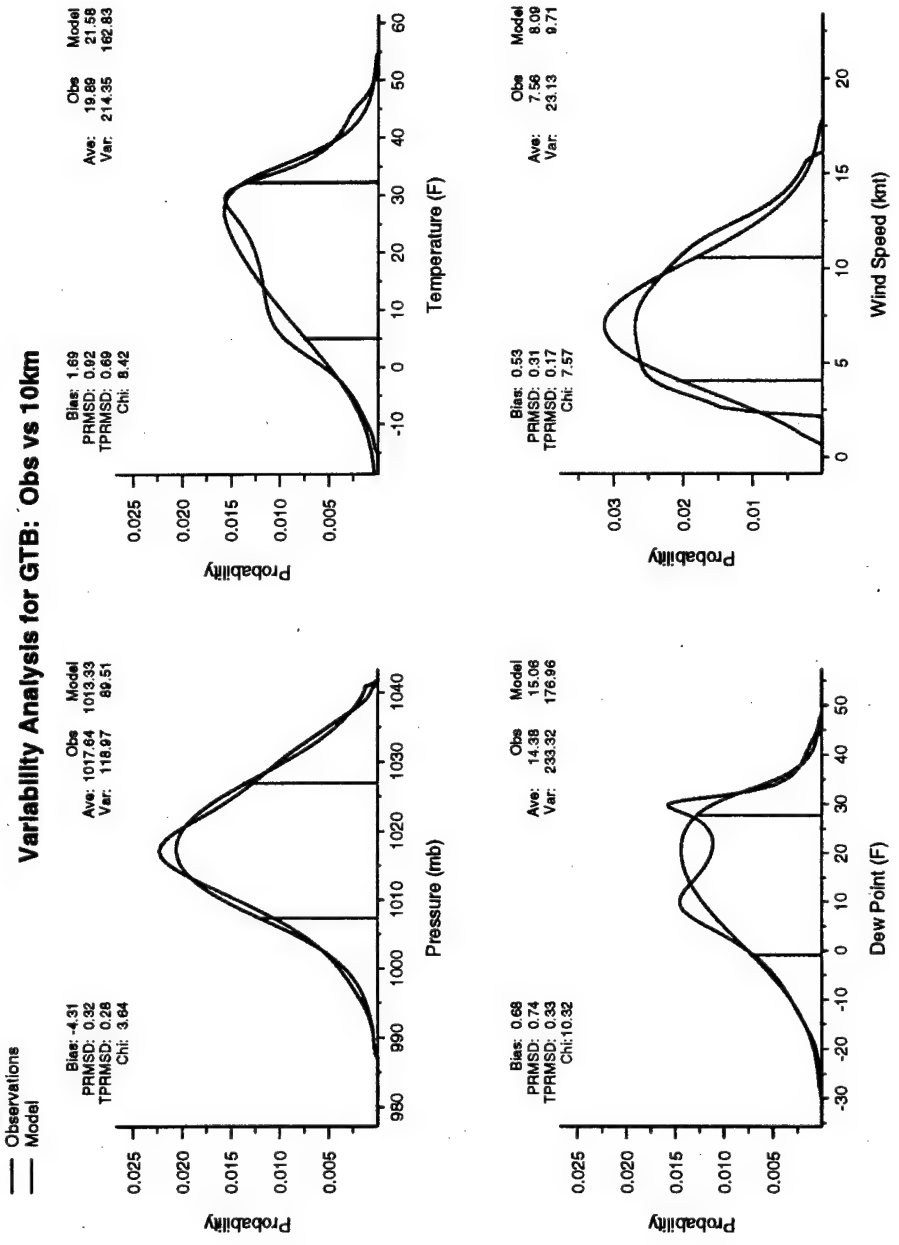

Figure 3.24: The 10 km distribution analysis for Fort Drum, NY

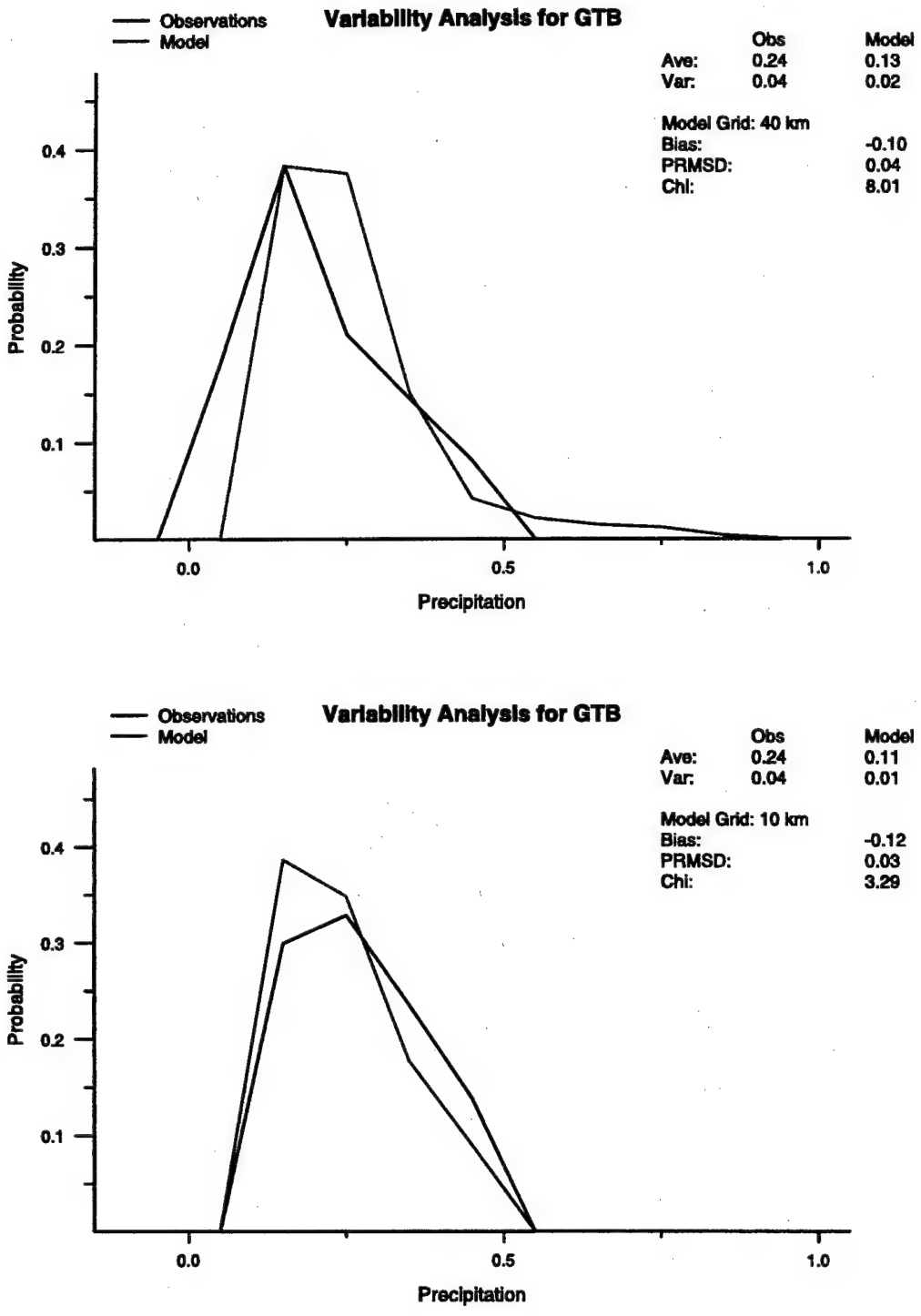

Figure 3.25: The daily precipitation distribution analysis for Fort Drum, NY

Station Appendix: RME - Rome, NY

	Pressure	Temperature	Dew Point	Wind Speed
	(mb)	(F)	(F)	(knot)
Obs. Mean	**1017.830**	**22.646**	**15.833**	**6.557**
40 km Mean	1014.238	21.438	16.122	8.028
10 km Mean	1013.345	24.233	16.995	6.608
Obs Std Dev.	**11.020**	**12.715**	**13.186**	**4.940**
40 km Std Dev.	10.467	11.927	12.659	3.099
10 km Std Dev.	9.507	12.343	12.240	3.226

Table 3.7: The long term means and standard deviations for the observations, the 10 km and the 40 km simulations at Rome, NY. The observed values are in bold type.

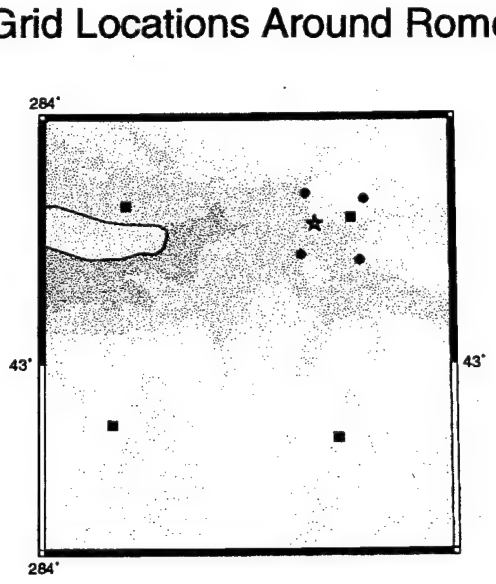

Figure 3.26: Grid point locations around Rome. The squares are the 40 km grid points the circles are the 10 km grid points and the star indicates the station location. Brown grid points are designated as land while the blue points are designated as water.

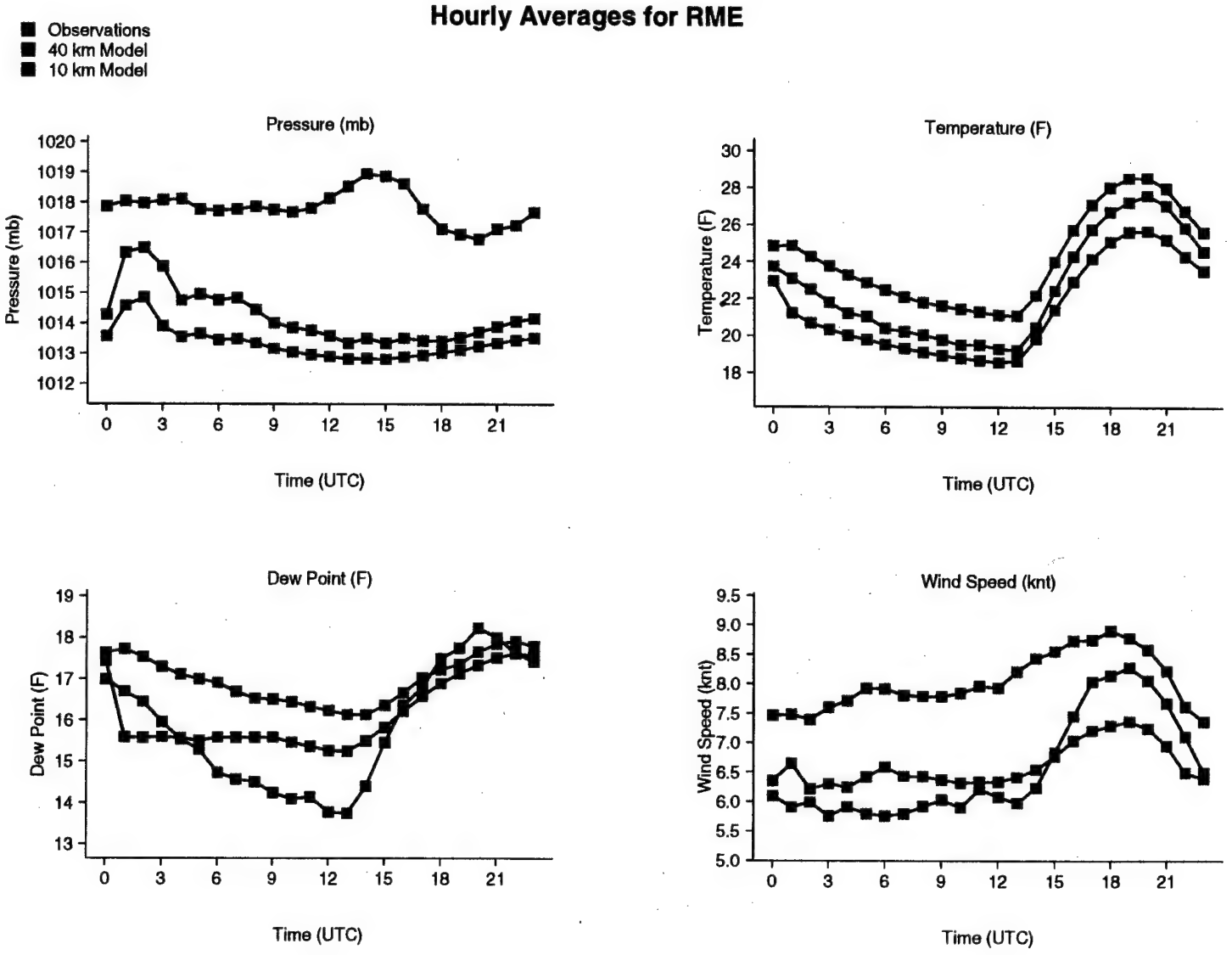

Figure 3.27: The hourly averages for Rome, NY

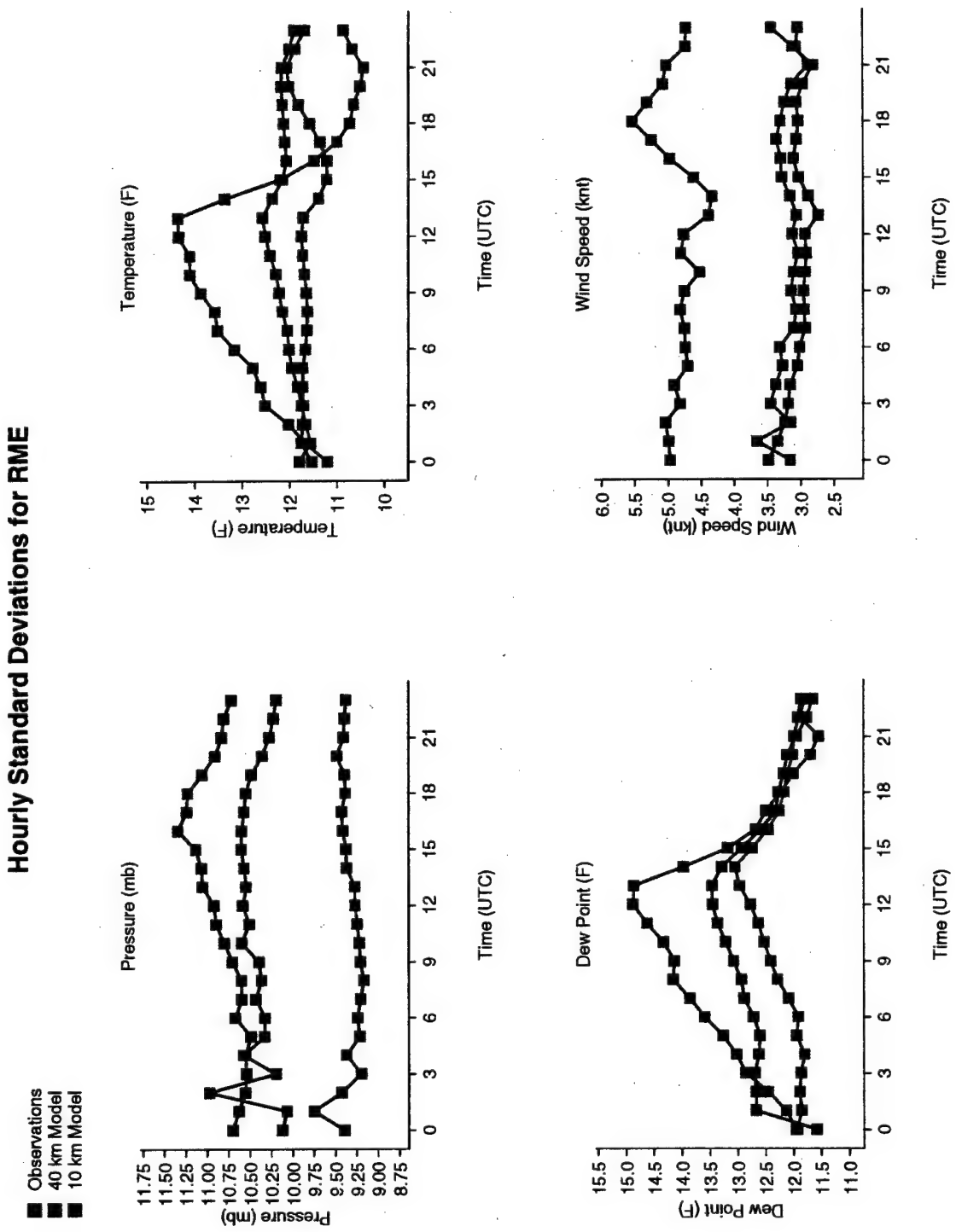

Figure 3.28: The hourly standard deviations for Rome, NY

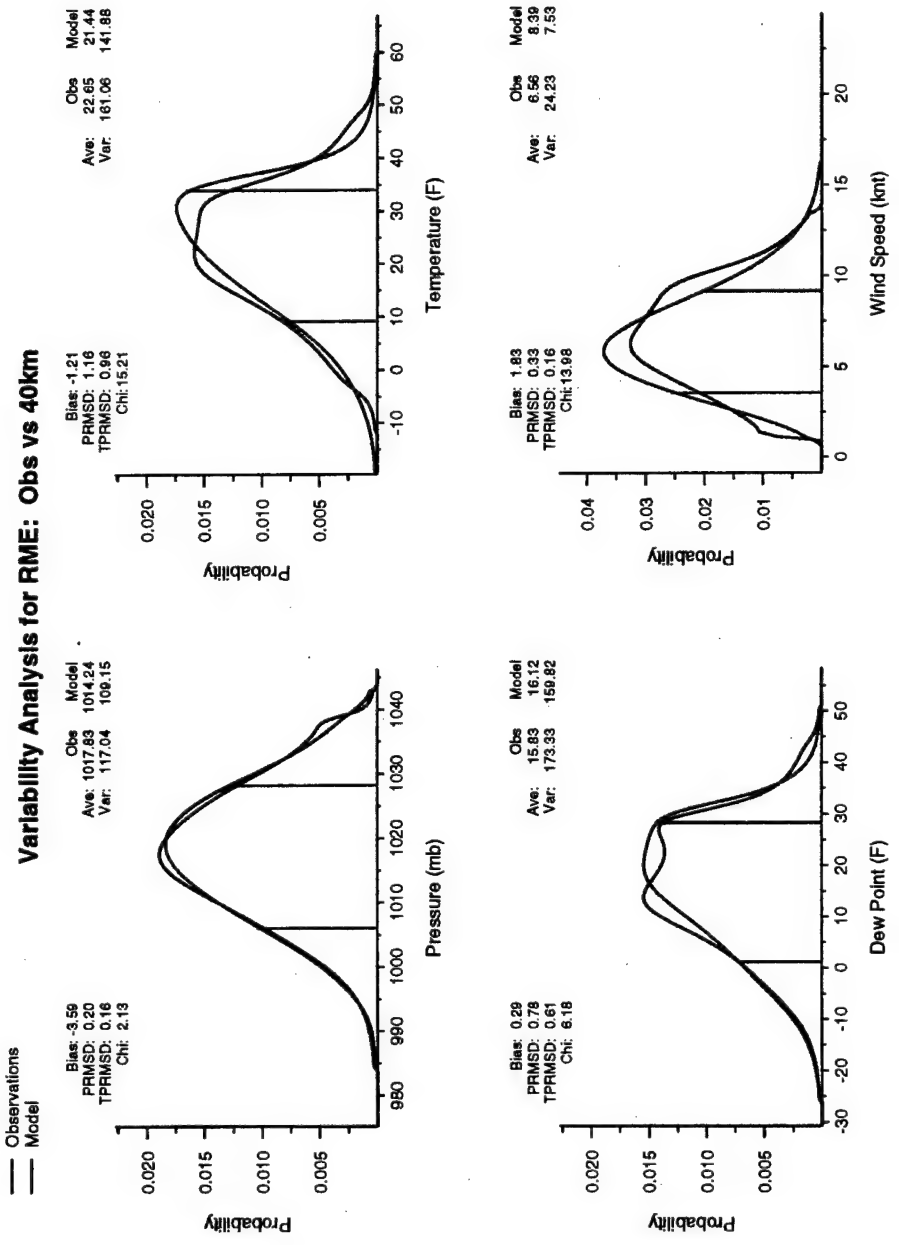

Figure 3.29: The 40 km distribution analysis for Rome, NY

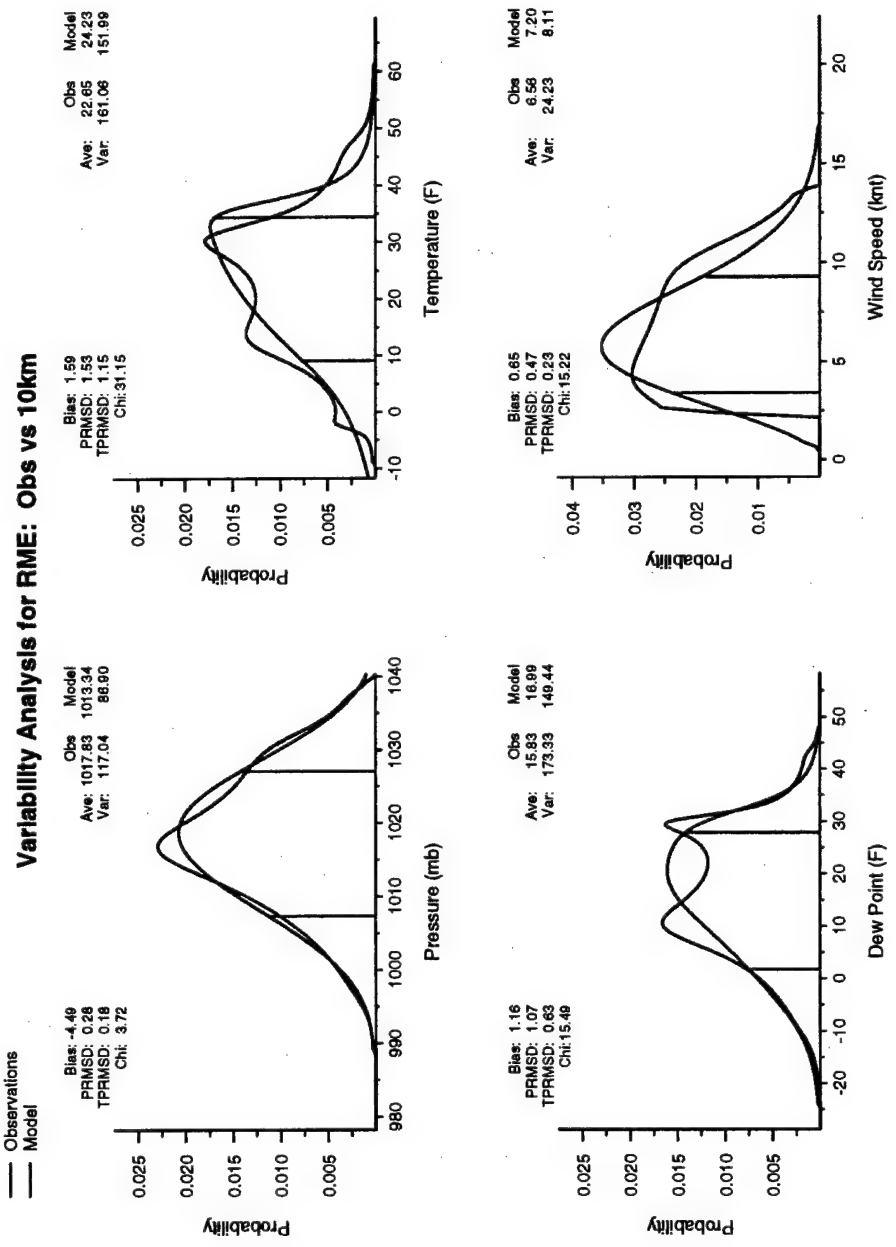

Figure 3.30: The 10 km distribution analysis for Rome, NY

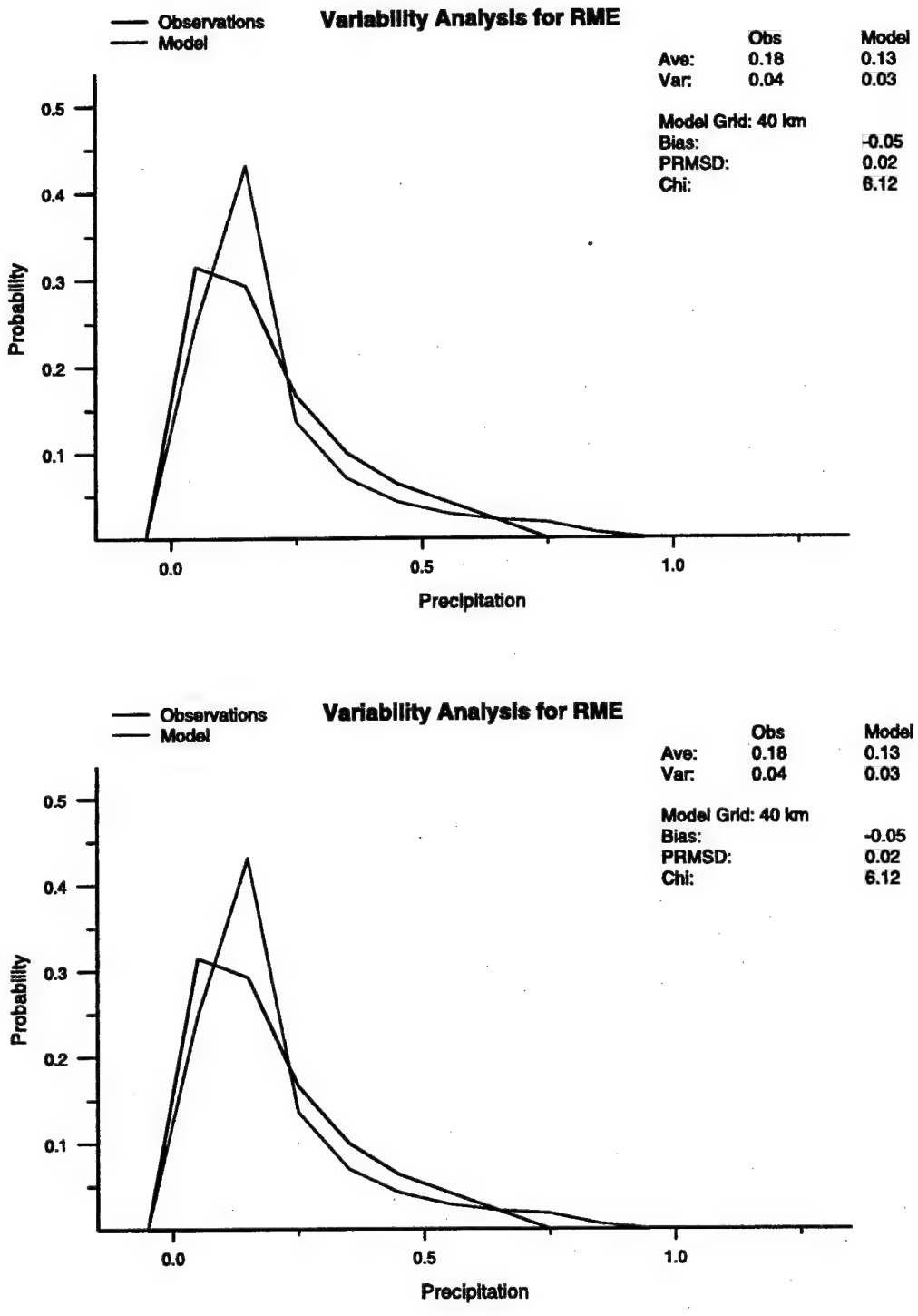

Figure 3.31: The daily precipitation distribution analysis for Rome, NY

Station Appendix: ROC - Rochester, NY

	Pressure	Temperature	Dew Point	Wind Speed
	(mb)	(F)	(F)	(knot)
Obs. Mean	**1018.186**	**25.791**	**18.276**	**9.296**
40 km Mean	1014.152	27.175	20.959	12.293
10 km Mean	1013.857	29.395	20.188	12.090
Obs Std Dev.	**9.969**	**11.379**	**11.631**	**4.906**
40 km Std Dev.	9.906	9.155	9.375	4.932
10 km Std Dev.	8.562	9.710	10.280	5.076

Table 3.8: The long term means and standard deviations for the observations, the 10 km and the 40 km simulations at Rochester, NY. The observed values are in bold type.

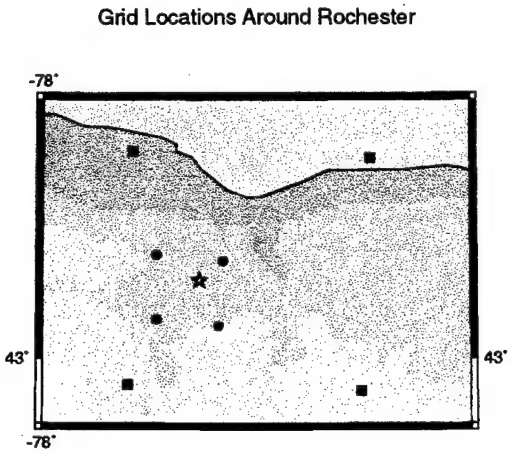

Figure 3.32: Grid point locations around Rochester. The squares are the 40 km grid points the circles are the 10 km grid points and the star indicates the station location. Brown grid points are designated as land while the blue points are designated as water.

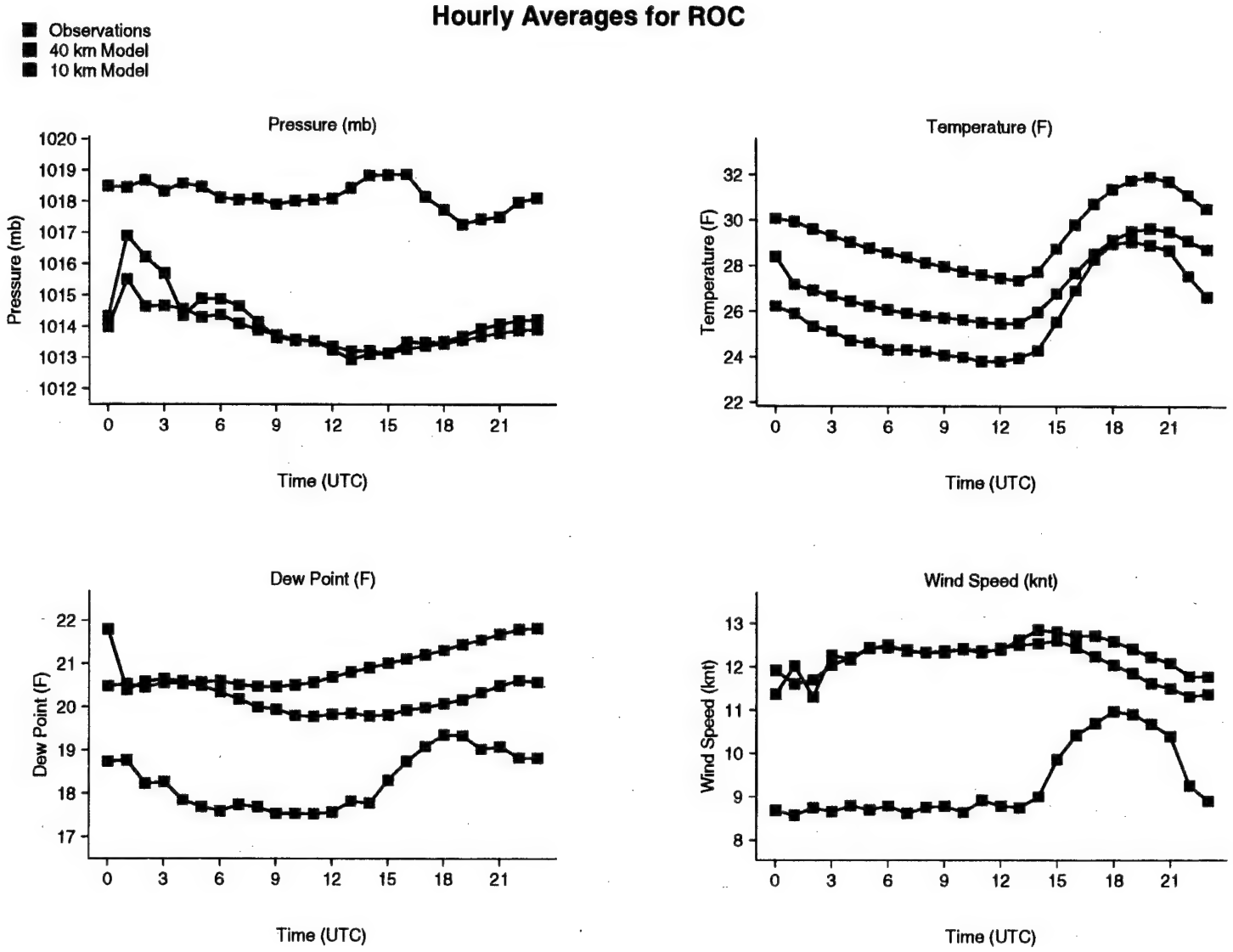

Figure 3.33: The hourly averages for Rochester, NY

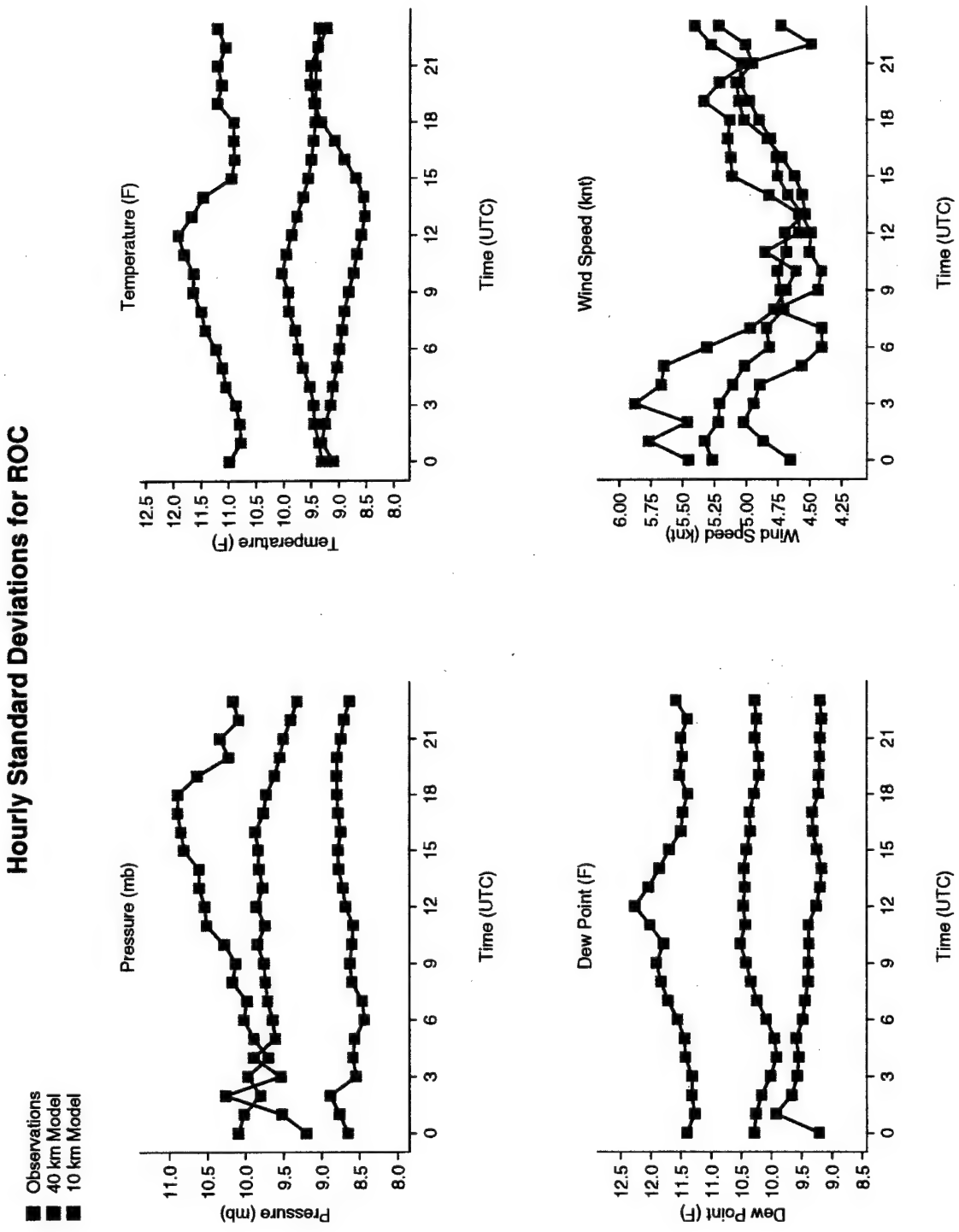

Figure 3.34: The hourly standard deviations for Rochester, NY

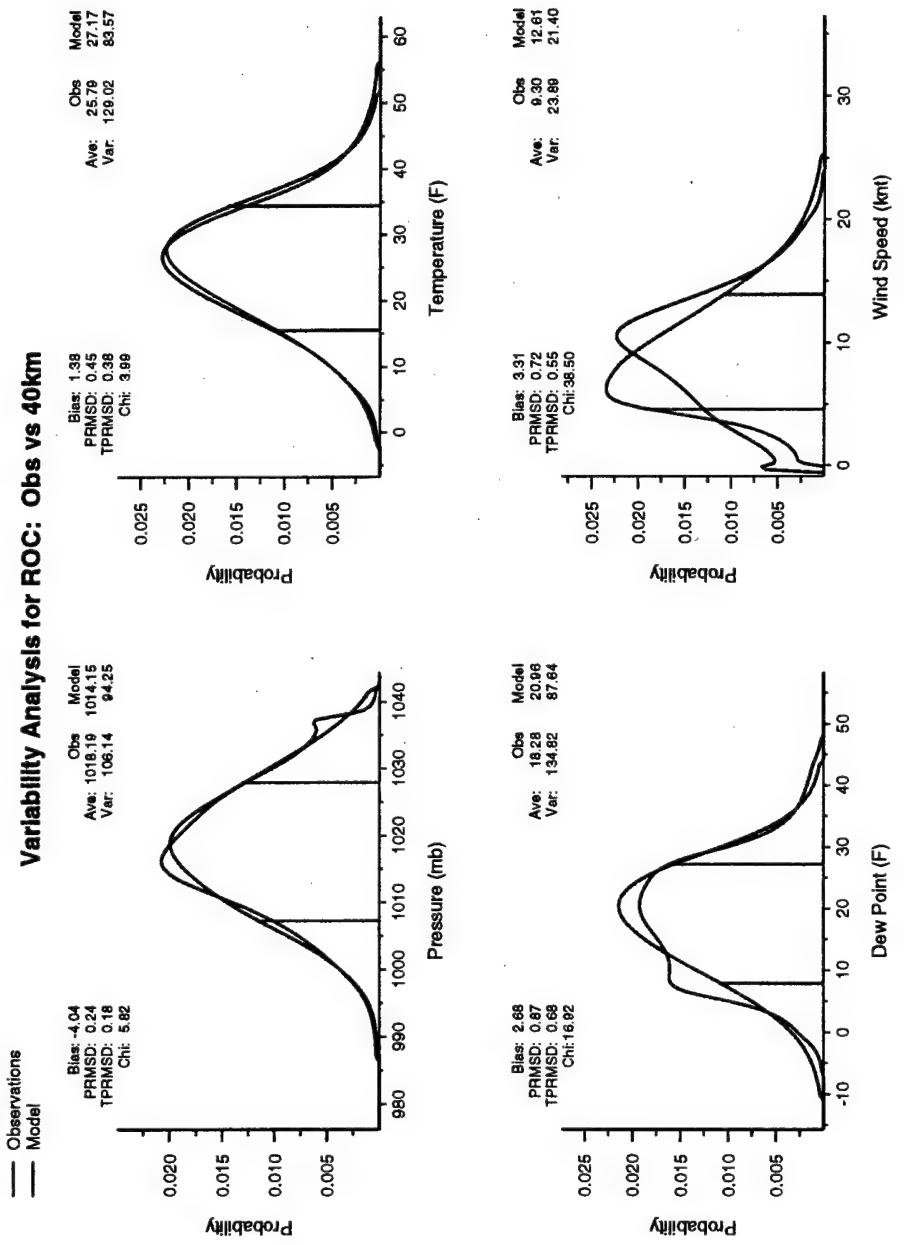

Figure 3.35: The 40 km distribution analysis for Rochester, NY

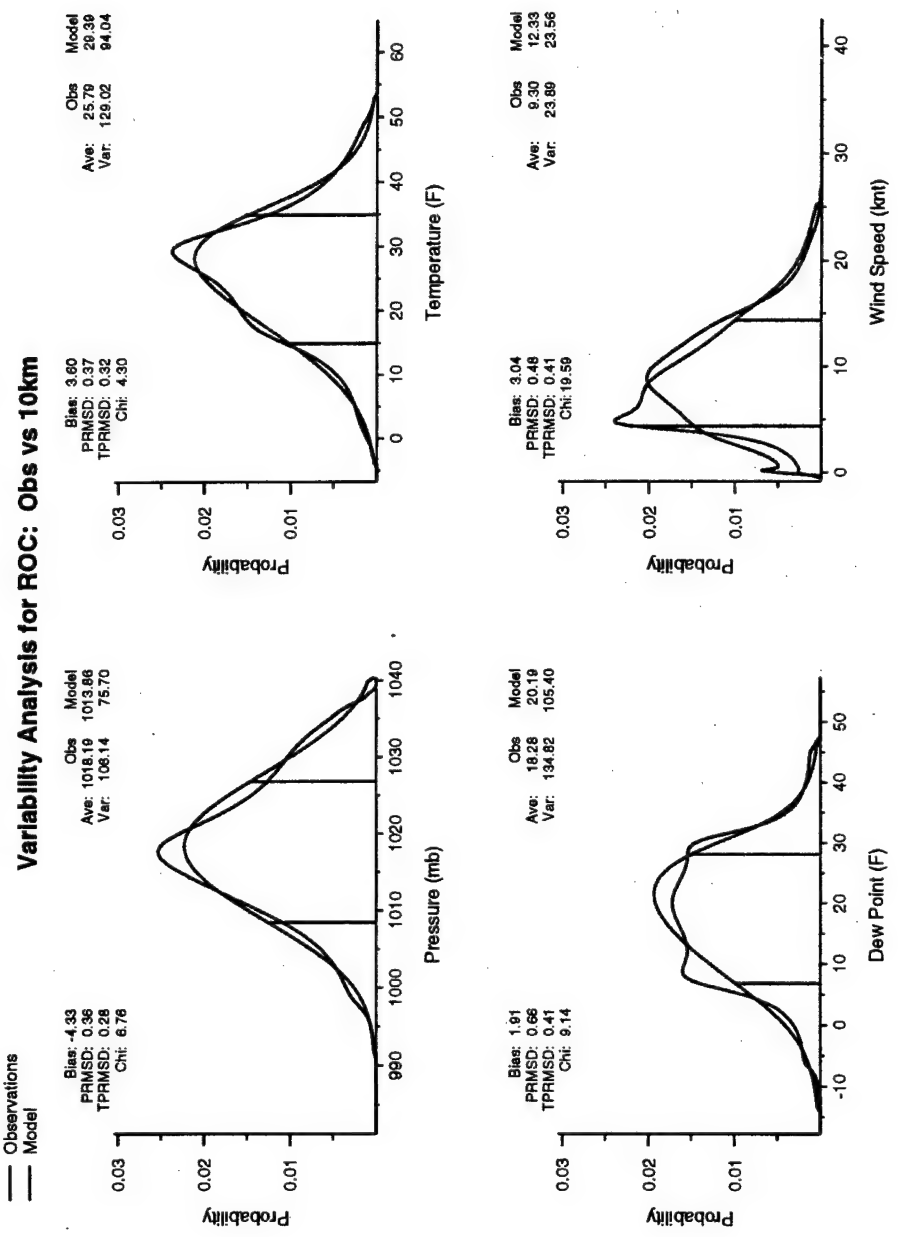

Figure 3.36: The 10 km distribution analysis for Rochester, NY

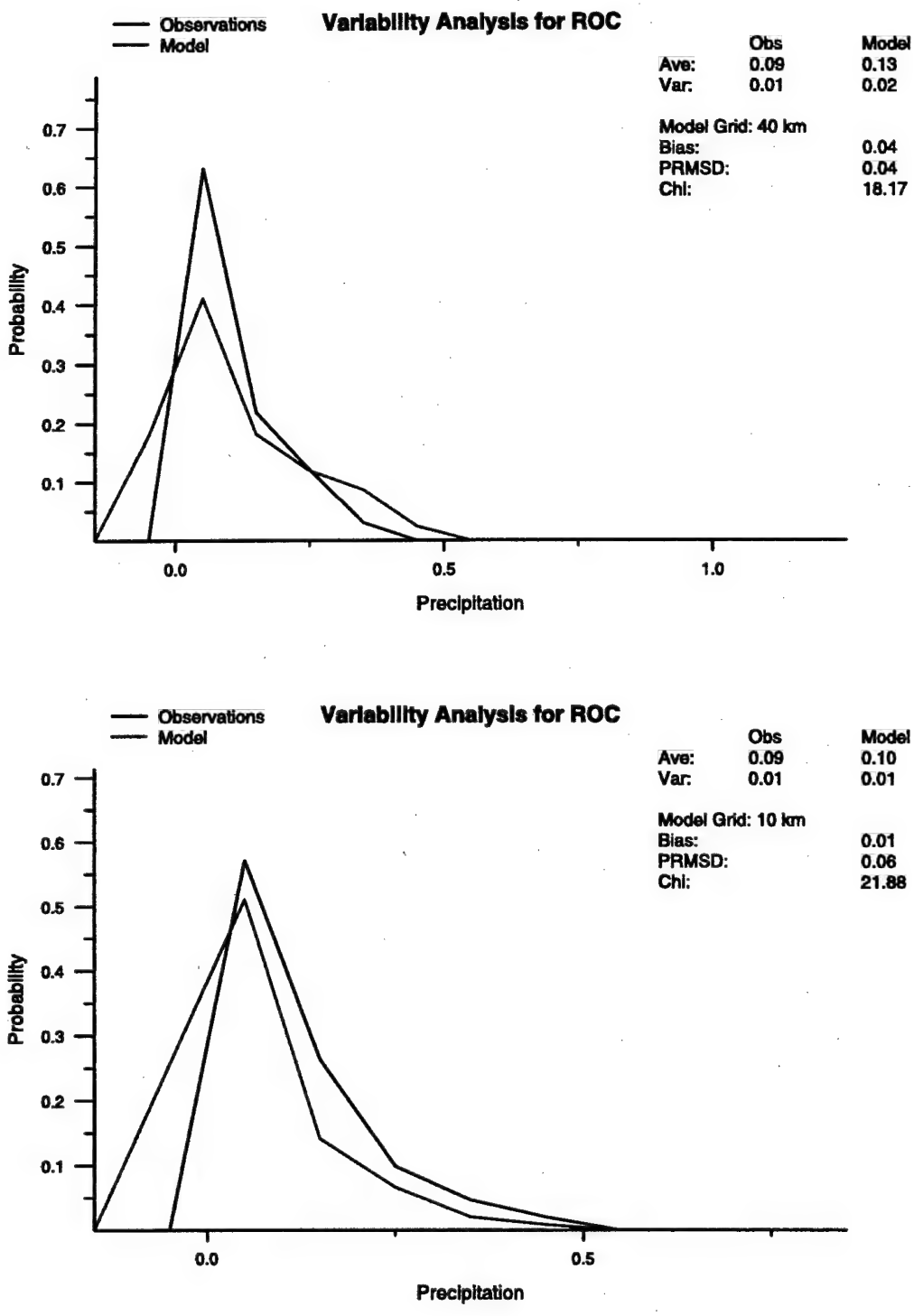

Figure 3.37: The daily precipitation distribution analysis for Rochester, NY

Station Appendix: UCA - Utica, NY

	Pressure	Temperature	Dew Point	Wind Speed
	(mb)	(F)	(F)	(knot)
Obs. Mean	**1018.025**	**22.296**	**15.444**	**9.329**
40 km Mean	1014.281	21.611	16.231	8.065
10 km Mean	1013.359	24.796	17.306	6.931
Obs Std Dev.	**10.779**	**12.206**	**12.917**	**4.085**
40 km Std Dev.	10.335	11.904	12.539	3.086
10 km Std Dev.	9.411	12.323	12.105	3.272

Table 3.9: The long term means and standard deviations for the observations, the 10 km and the 40 km simulations at Utica, NY. The observed values are in bold type.

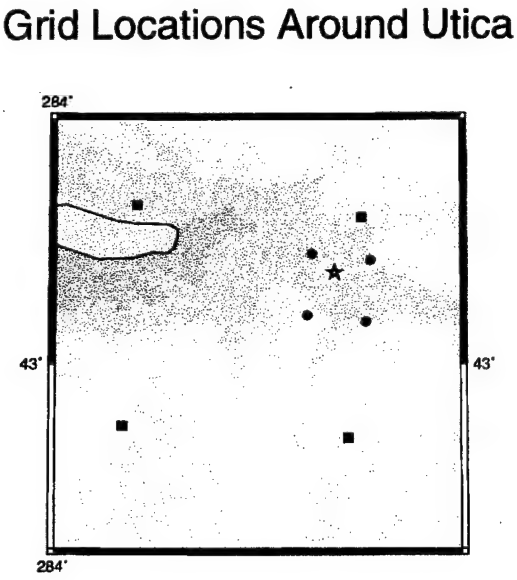

Figure 3.38: Grid point locations around Utica. The squares are the 40 km grid points the circles are the 10 km grid points and the star indicates the station location. Brown grid points are designated as land while the blue points are designated as water.

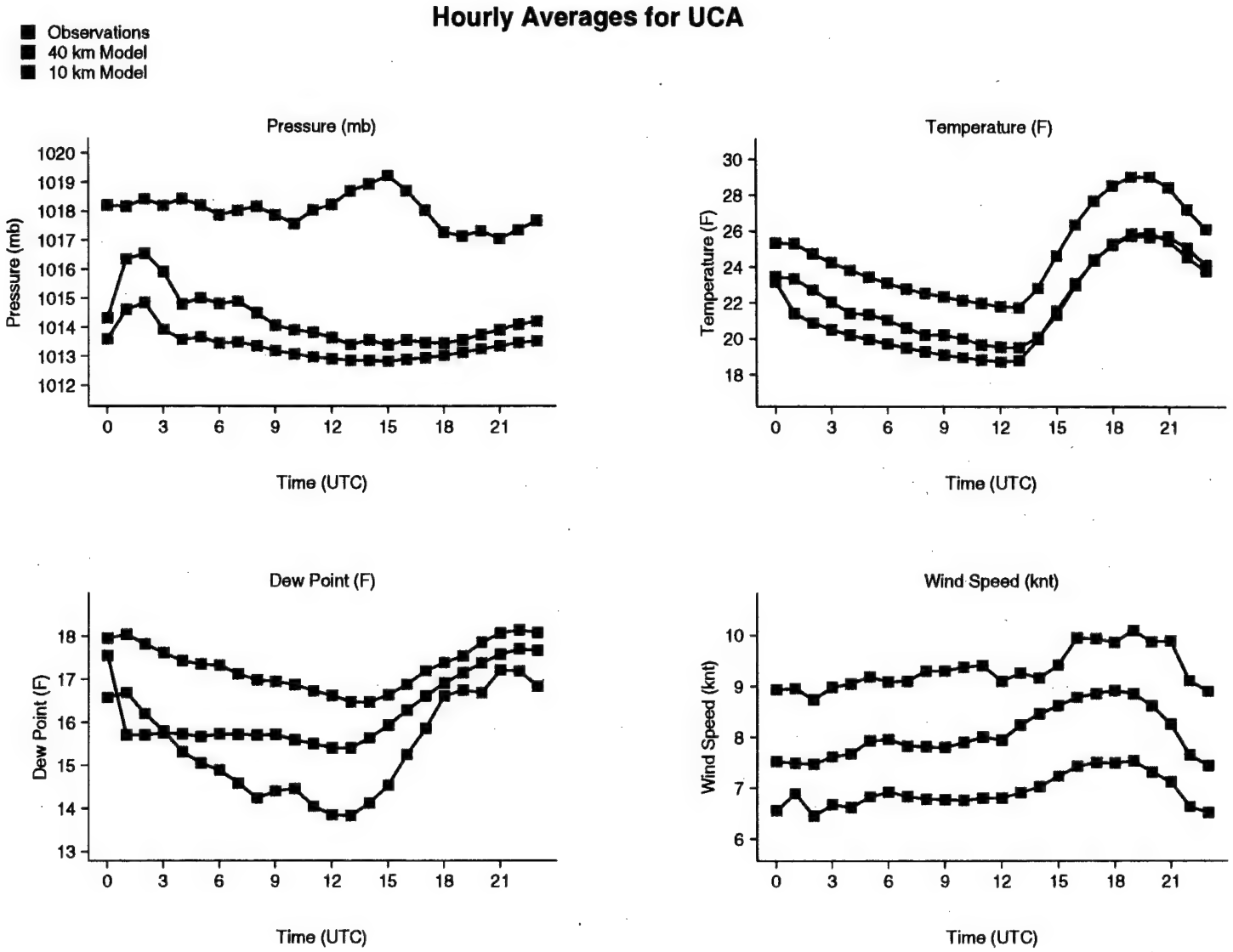

Figure 3.39: The hourly averages for Utica, NY

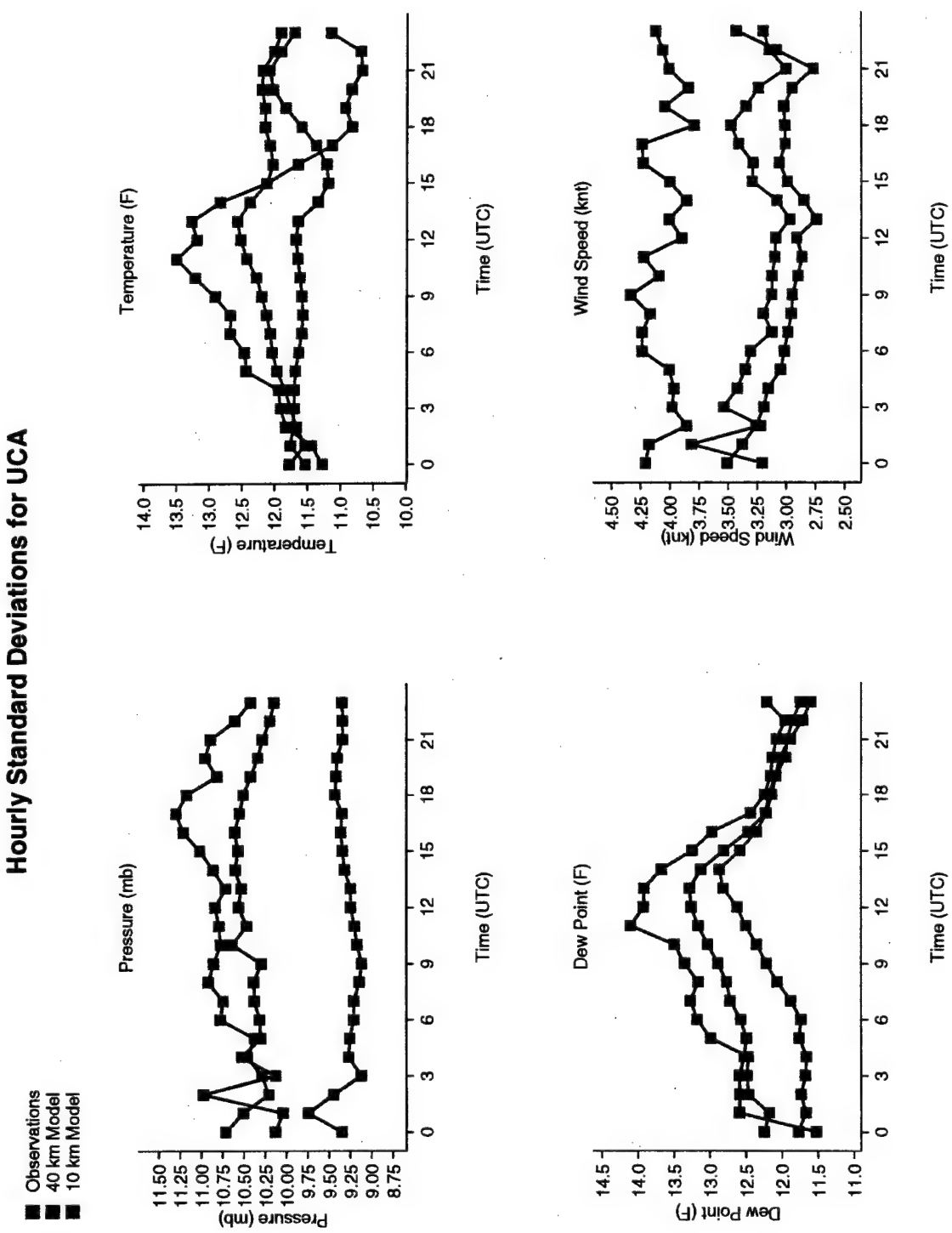

Figure 3.40: The hourly standard deviations for Utica, NY

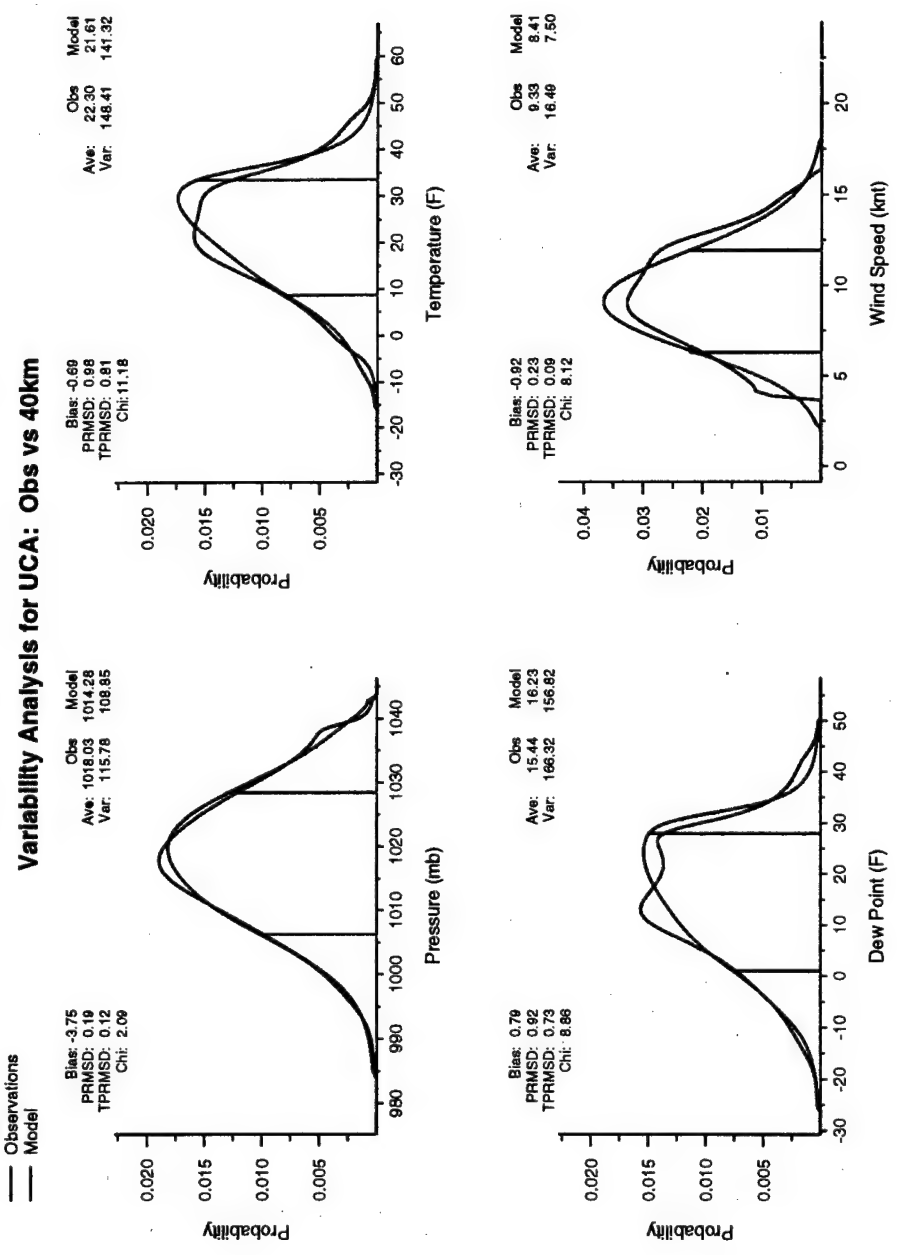

Figure 3.41: The 40 km distribution analysis for Utica, NY

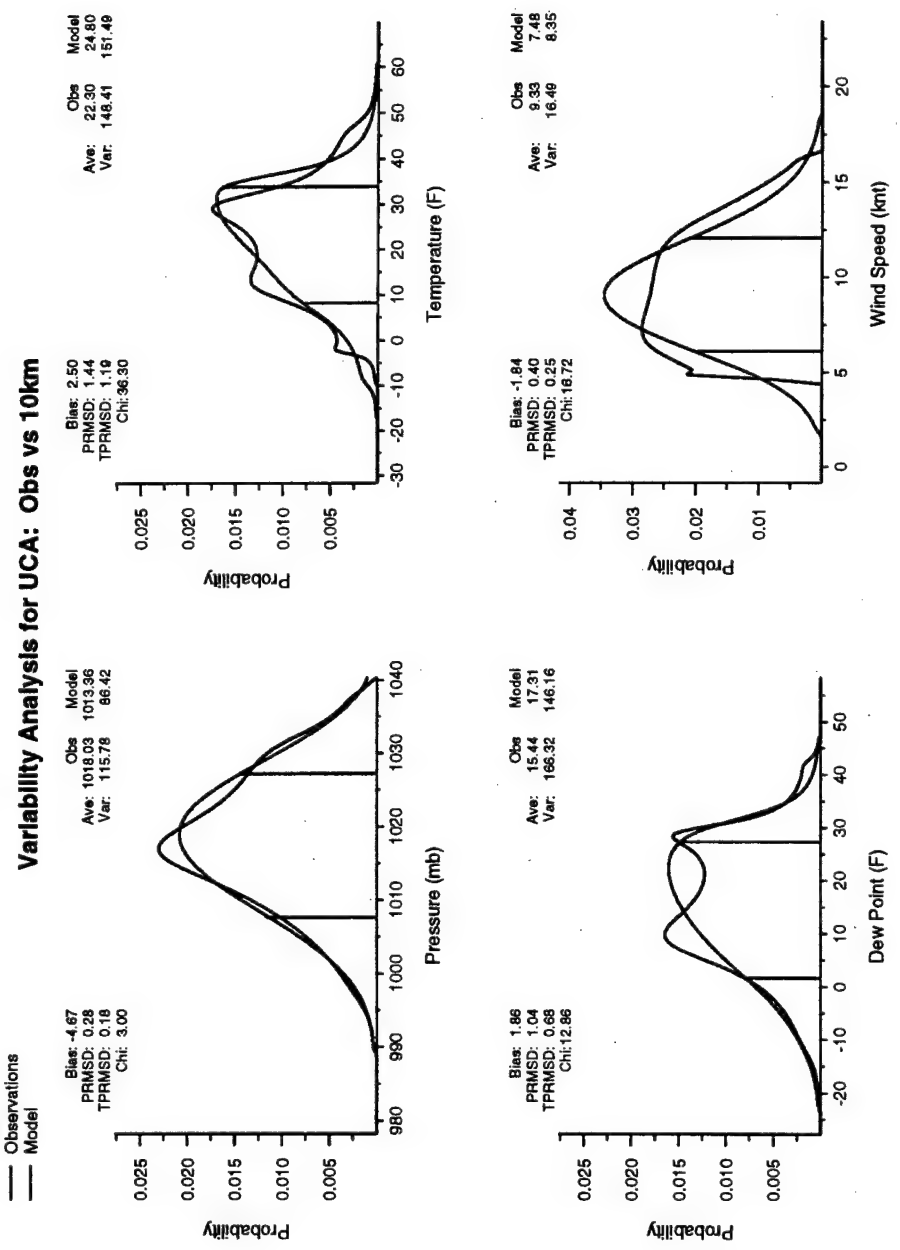

Figure 3.42: The 10 km distribution analysis for Utica, NY

Station Appendix: YTR - Trenton, Canada

	Pressure	Temperature	Dew Point	Wind Speed
	(mb)	(F)	(F)	(knot)
Obs. Mean	**1017.248**	**20.833**	**14.982**	**8.777**
40 km Mean	1013.758	23.261	16.873	9.851
10 km Mean	1013.713	22.607	14.658	8.487
Obs Std Dev.	**10.721**	**13.090**	**13.951**	**5.402**
40 km Std Dev.	9.925	11.460	13.174	4.054
10 km Std Dev.	9.470	12.845	14.292	3.984

Table 3.10: The long term means and standard deviations for the observations, the 10 km and the 40 km simulations at Trenton, Canada. The observed values are in bold type.

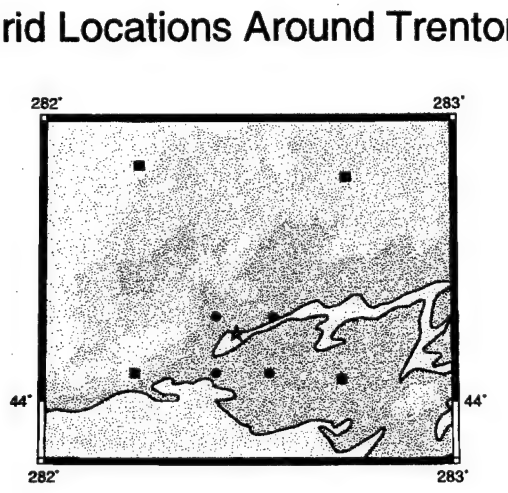

Figure 3.43: Grid point locations around Trenton. The squares are the 40 km grid points the circles are the 10 km grid points and the star indicates the station location. Brown grid points are designated as land while the blue points are designated as water.

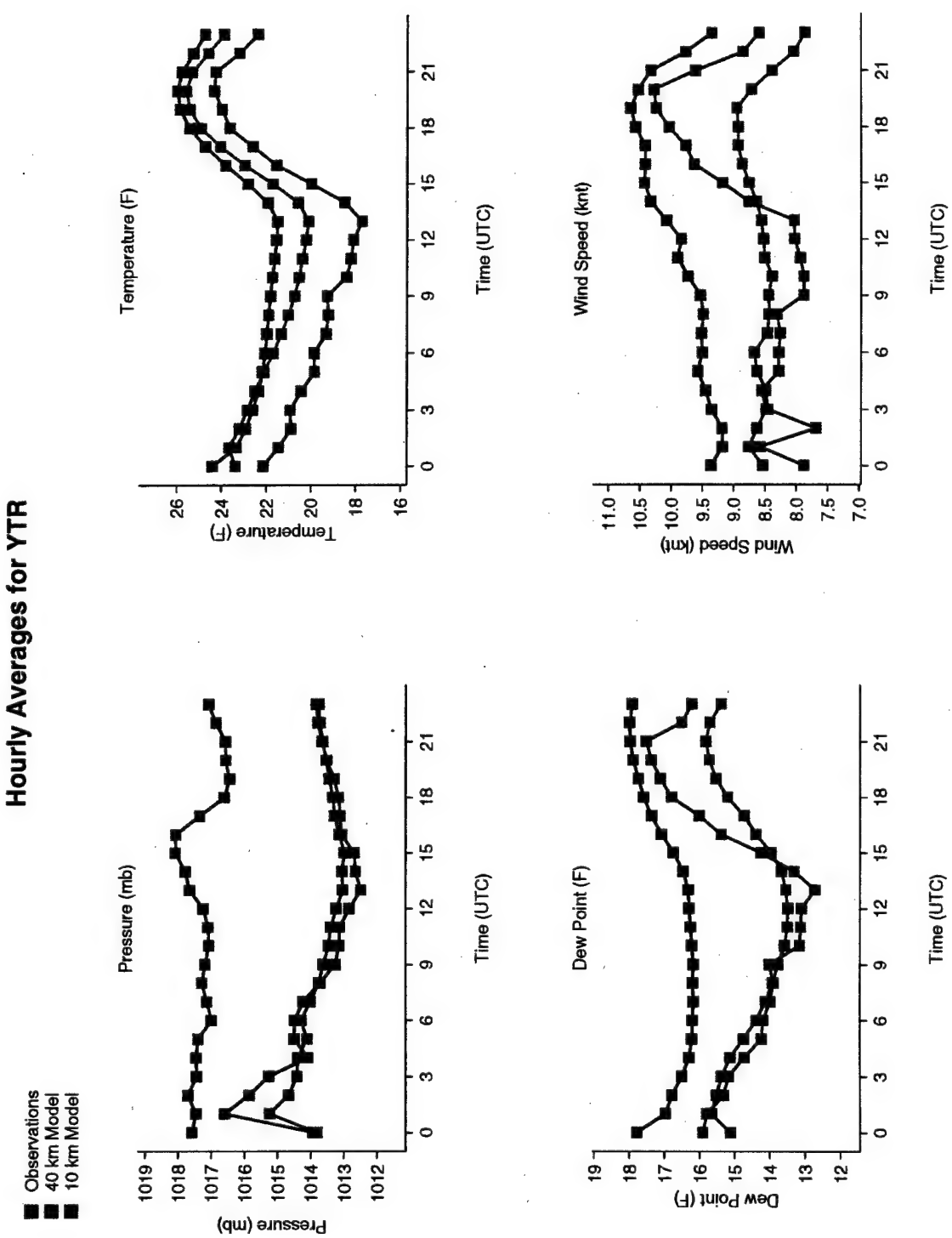

Figure 3.44: The hourly averages for Trenton, Canada

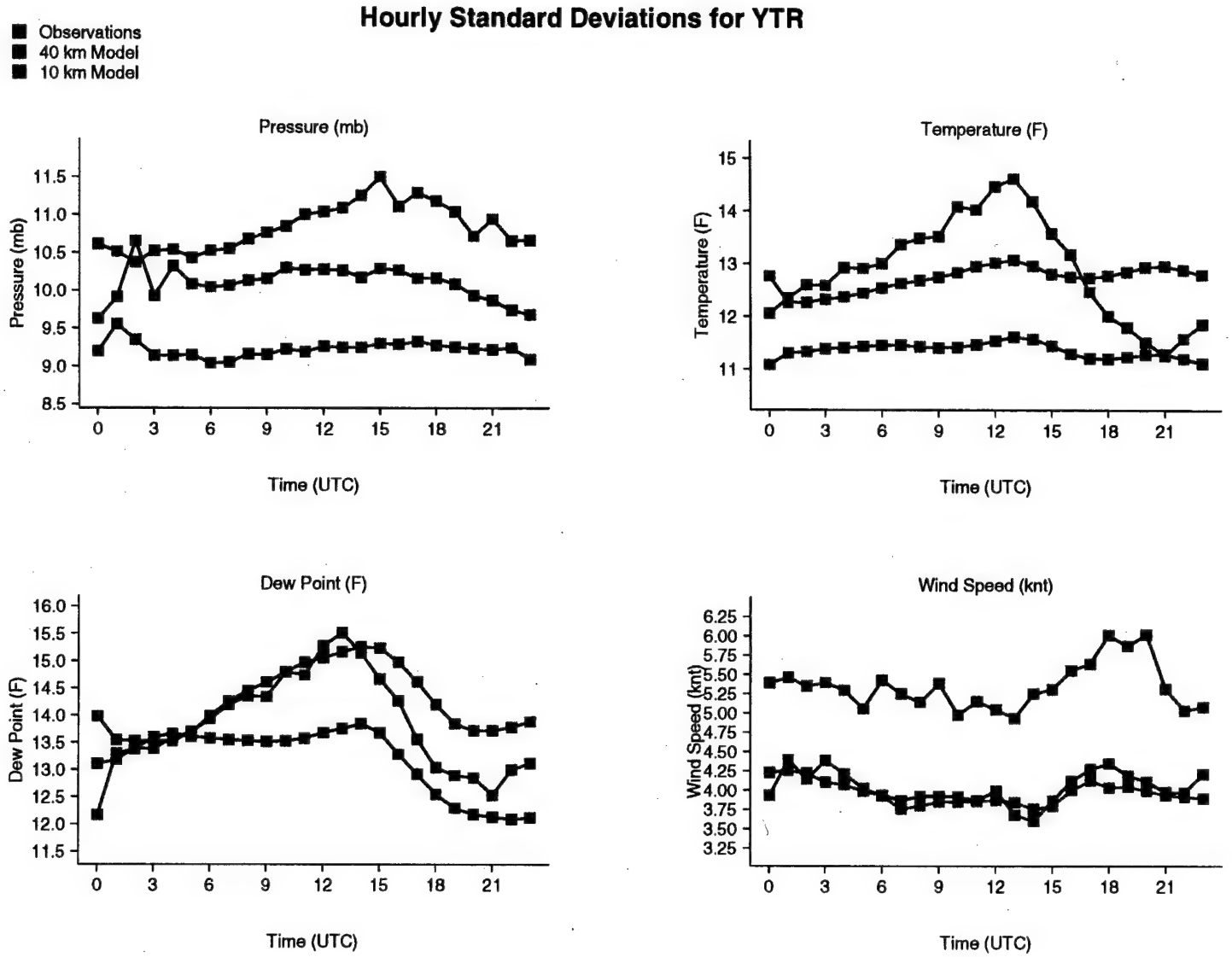

Figure 3.45: The hourly standard deviations for Trenton, Canada

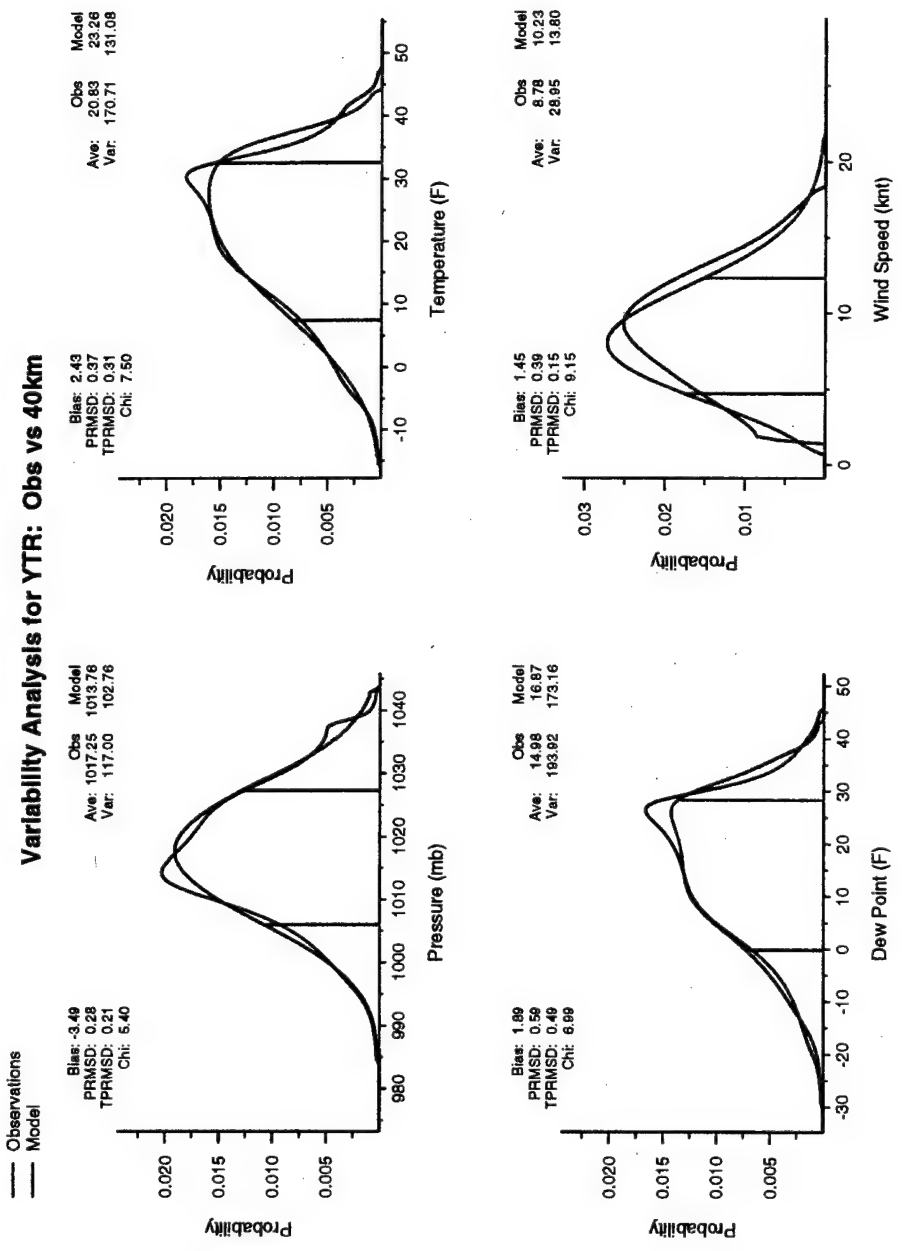

Figure 3.46: The 40 km distribution analysis for Trenton, Canada

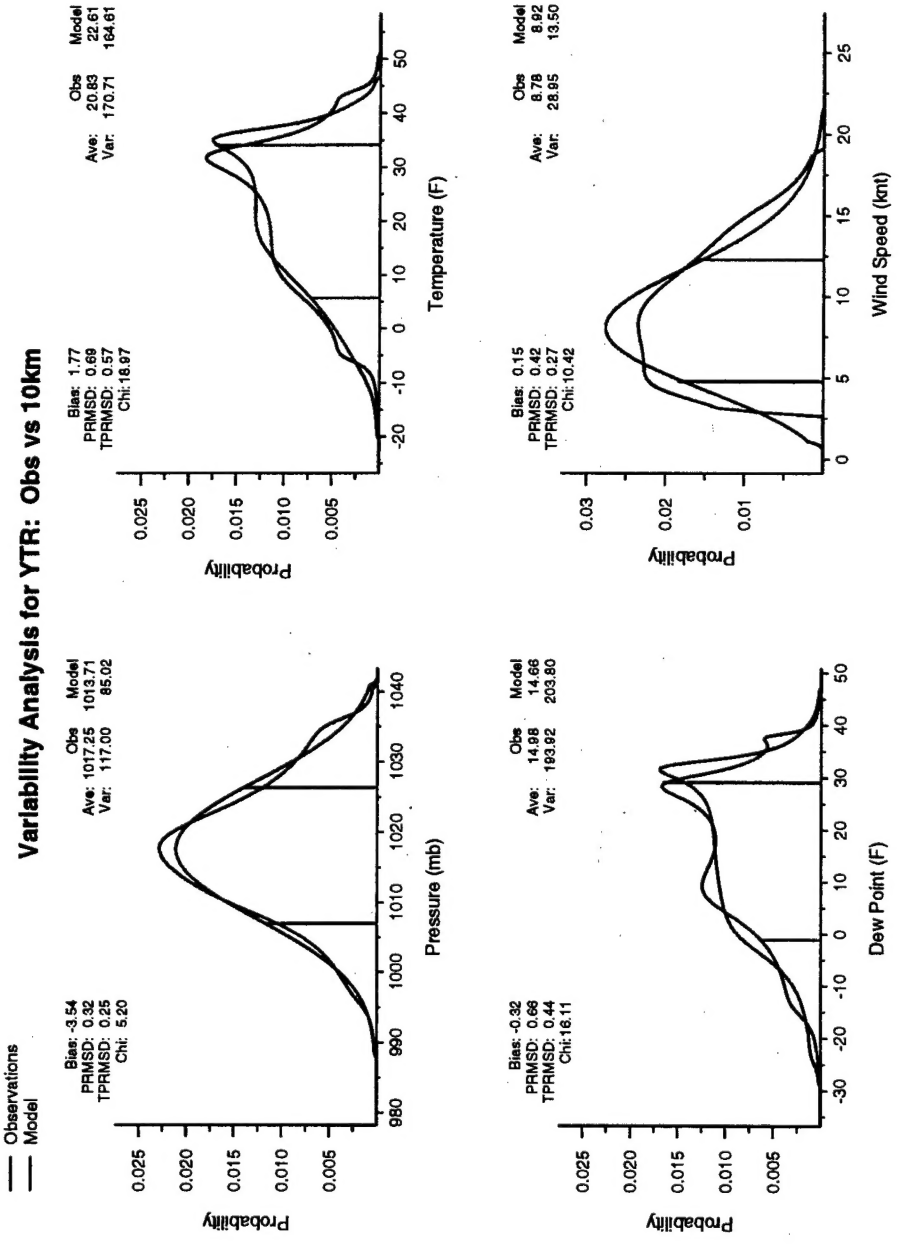

Figure 3.47: The 10 km distribution analysis for Trenton, Canada

Bibliography

Bender, E. A., 1991: *An Introduction to Mathematical Modeling.*, Krieger Publishing Company., 256 pp.

Daley, R., 1991: *Atmospheric Data Analysis.* Cambridge Atmospheric and Space Science Series. 457 pp.

Giorgi, F., and L. O. Mearns, 1991: Approaches to the simulation of regional climate change: a review. *Rev. Geophys.*, **29**, 191-216.

————, G. T. Bates, and S. T. Neiman, 1993: The multiyear surface climatology of a regional atmospheric model over the western United States. *J. Climate*, **6**, 75-95..

Gibra, I. N., 1973: *Probability and Statistical Inference for Scientists and Engineers.* Prentice-Hall, Inc., 596 pp.

Haltiner, G. J., and R. T. Williams, 1980: *Numerical Prediction and Dynamic Meteorology-Second Edition.*, John Wiley and Sons, Inc., 477 pp.

Isaaks, E. H., and R. M. Srivastava, 1989: *An Introduction to Applied Geostatistics.*, Oxford University Press, 561 pp.

Journel, A. G., C. H. J. Huijbergts, 1978: *Mining Geostatistics.*, Academic Press, 600 pp.

Kaplan, M. L., J. W. Zack, V. C. Wong, and J. J. Tuccillo, 1982: Initial results from a mesoscale atmospheric simulation system and comparison with the AVE-SESAME-I data set. *Mon. Wea. Rev.*, **110**, 1564-1590.

Manobianco, J., J. W. Zack, G. E. Taylor, 1996: Workstation based real-time mesoscale modeling designed for weather support to operations at the Kennedy Space Center and Cape Canaveral Air Station. *Bull. Amer. Meteor. Soc.*, **77**, 653-672.

McQueen, J. T., R. R. Draxler, and G. D. Rolph, 1995: Influence of grid size and terrain resolution on wind field predictions from an operational mesoscale model. *J. Appl. Meteor.*, **34**, 2166-2181.

MESO, 1995: MASS Ver. 5.6 Reference Manual, MESO, INC. Troy, NY, 12180, 118 pp.

Morrissey, M. L., 1991: Using sparse raingages to test satellite-based rainfall algorithms. *J. Geophys. Res.*, **96**, 18561-18571.

Murphy, A. H., 1995: The coefficients of correlation and determination as measures of performance in forecast verification. *Wea. Forecasting*, **10**, 681-688.

North, G. R., and S. Nakamoto, 1989: Formalism for comparing rain estimation designs. *J. Atmos. and Oceanic Tech.*, **6**, 985-992.

Pielke, R. A., 1984: *Mesoscale Meteorological Modeling.* Academic Press, 612 pp.

Ray, P. S., 1986: *Mesoscale Meteorology and Forecasting.* American Meteorological Society, 793 pp.

Trenberth, K. E., 1992: *Climate System Modeling.* Cambridge University Press., 788 pp.

Washington, W. M., and C. L. Parkinson, 1986: *An Introduction to Three Dimensional Climate Modeling.* University Science Books-Oxford University Press, 422 pp.

Zack, J. W., K. T. Waight III, M. D. Bousquet, C. E. Graves, S. Yalda, and G. E. Van Knowe, 1996: An evaluation of local climate statistics generated from the output of a 3-D mesoscale atmospheric model. Preprints, *11th Conference on Numerical Weather Prediction*, Norfolk, VA, Amer. Meteor. Soc., 379-381.

Acknowledgments

This work was completed under a Grant for the Air Force Office of Scientific Research F49620-95-1-0523. Numerous people helped in preparing and proofreading this report. In particular, Sepi Yalda and Kyle Poage of Saint Louis University were essential for much of the data analysis. Mary Bousquet and Glenn Vanknowe of MESO Inc. assisted in the simulations and Captain John Warner of the Air Force Combat Climatology Center and Don Norquist of Phillips Laboratory made many suggestions to improve the results and this report.